Applications of the Gaussian–2 and Gaussian–3 Models of Theory: A Structural and Energetics Study of Selected Chemical Systems

LAU Kai–Chi

A Thesis Submitted in Partial Fulfilment

of the Requirements for the Degree of

Master of Philosophy

in

Chemistry

July 2001

Applications of the Gaussian–2 and Gaussian–3 Models of Theory: A Structural and Energetics Study of Selected Chemical Systems

Abstract

The Gaussian–2 (G2) and Gaussian–3 (G3) levels of theory have been applied to study the dissociative mechanisms of a number of molecules. They are (i) hydrogen and methane eliminations from alkoxide anions; (ii) alkane eliminations from alkoxide anions; (iii) dissociative photoionization of dimethyl disulfide; (iv) dissociation of propylene sulfur. Besides, (v) the structural and thermochemical studies of the phosphorus fluorides and their singly charged cations and anions have also been carried out using these levels of theory.

Generally, good to excellent agreements between our calculated results and available experimental data have been obtained in our studies. Such a good agreement lends confidence and reliability to those results with no available experimental data as well as to the reaction pathways proposed.

Submitted by LAU Kai–Chi

for the degree of Master of Philosophy in Chemistry

at The Chinese University of Hong Kong in (June 2001)

利用 G2 和 G3 理論對化學體系之結構及能量的研究

摘要

本論文採用 Gaussian-2 (G2) 和 Gaussian-3 (G3) 理論系統地研究了以下的化學體系：1. 三取代甲醇陰離子中氫及甲烷的離解； 2. 三取代甲醇陰離子中烯基的離解；3. 二甲基二硫化物的光離子分解；4. 硫化丙烯的離解；5. 氟化磷及其單電荷陽離子和陰離子體系的結構與熱化學研究。

與實驗值相比較，我們的計算結果令人滿意。本論文的研究表明，對於某些缺乏實驗數據的反應和體系，可通過類似的理論計算獲取一些較可靠的信息及結果，對反應途徑的設計和熱化學數據的測量具有一定的指導作用。

Acknowledgments

I am very much indebted to my supervisor, Professor Wai–Kee Li, whose guidance and encouragement have made this thesis possible.

I also wish to thank:

Dr. See–Wing Chiu, at the University of Illinois, who suggested the project of alkoxide anions decompositions;

Dr. Fei Qi at Berkeley National Laboratory, who did the photodissociation experiments of propylene sulfide.

Table of Contents

Chapter 1
Introduction

Accurate and reliable predictions of energetics for molecular systems are the main objectives in quantum chemistry. In the past ten years, Pople and his co–workers proposed a series of ab initio methods, the Gaussian–n (Gn) models,[1–11] in order to achieve these goals. Their aim is to develop a general procedure for accurate energies applicable for a variety of molecular systems. The Gn models, based on a series of additivity approximations,[8,9] consist of a sequence of single–point calculations to provide an accurate prediction on the energetics of a given molecular system. The Gn models include: Gaussian–1 (G1),[1,2] Gaussian–2 (G2),[3,4] and Gaussian–3 (G3)[5–7] levels of theory and their less expensive variants (*vide infra*). These methods have been shown to be able to determine the energetics of the molecular systems with an average absolute deviation from experiment to be within 10 kJ mol^{-1} (or ~2 kcal mol^{-1}).

Since the G1 model yields less accurate results than G2 and G3, this method has not been applied to the projects presented in this thesis. In this thesis, we mainly employ the G3 method and its variants to study the structures and energetics of some selected chemical systems. In addition, an modified G2 method, G2++ method,[12] has also been used to study the dissociation mechanisms of the alkoxide anions.

1.1 The Gaussian–3 Method

The G3 energy is an approximation of the molecular energy at the QCISD(T)/G3large level, where G3large is a modified 6–311+G(3df,2p) basis set. In the G3 model, structures are optimized at the second–order Mϕller–Plesset theory (MP2) using the 6–31G(d) basis set with all electrons included, i.e., at the MP2(Full)/6–31G(d) level. Based on these optimized structures, single–point calculations at QCISD(T)/6–31G(d), MP4/6–31G(d), MP4/6–31+G(d), MP4/6–31G(2df,p), and MP2(Full)/G3large levels are required. Also, this model requires higher level correction (HLC) in the calculation of total electronic energies (E_e). The HLC is $-6.386 \times 10^{-3} n_\beta - 2.977 \times 10^{-3}(n_\alpha - n_\beta)$ for molecules and $-6.219 \times$

$10^{-3}n_\beta - 1.185 \times 10^{-3}(n_\alpha - n_\beta)$ for atoms, in which n_α and n_β are the number of α and β electrons, respectively, with $n_\alpha \geq n_\beta$. The MP2(Full)/6–31G(d) harmonic vibrational frequencies, scaled by 0.9661, are applied for the zero–point vibrational energy (ZPVE) correction at 0 K ($E_0 = E_e$ + ZPVE).

The G3 theory has been used to calculate molecular energies, such as atomization energies,[2–9] ionization energies,[2,10] proton affinities,[2,10] and electron affinities[2] of 125 molecules for which these quantities have been well established experimentally. The average absolute deviation is about 1.02 kcal mol^{-1} (or ~4 kJ mol^{-1}).[5] Detailed methodology of the G3 theory is given in Appendix A.

1.2 The G3 Method with Reduced Mϕller–Plesset Order and Basis Set

An economical variant of the G3 theory, G3(MP2),[6] has been introduced by Pople et al recently. The G3(MP2) model involves two single–point energy calculations at the QCISD(T)/6–31G(d) and MP2/G3MP2large levels, based on the geometry optimized at the MP2(Full)/6–31G(d) level. The G3MP2large basis set is the same as the aforementioned G3large basis set, except the core polarization functions have been removed.[6] HLC is also included to yield the E_e of the molecule, where HLC = $-9.729 \times 10^{-3}n_\beta - 4.471 \times 10^{-3}(n_\alpha - n_\beta)$. Similar to the G3 method, the MP2(Full)/6–31G(d) vibrational frequencies, scaled by 0.9661, are applied for the ZPVE correction at 0 K to give the total energy of (E_0) for the molecule.

It is noted that the G3(MP2) method is able to yield results with average absolute deviations of 1.3 kcal mol^{-1} (or ~5.4 kJ mol^{-1}), when compared with the 299 energies determined by experiments.[5]

1.3 The Gaussian–3X Method

Since the G3 theory still does poorly for some of the larger non–hydrogen systems containing second–row atoms such as the hypervalent molecules such as SF_6 and PF_5. A modification of the G3 theory, called Gaussian–3X (G3X), has been developed earlier this year.[7] This method shows an improvement for the energetics of non–hydrogen systems over the G3 theory: the G3 mean absolute deviation is 2.11 kcal mol^{-1} (or ~8.8 kJ mol^{-1})for the 47 non–hydrogen species in the G3/99 test set,[13] while the corresponding deviation for the G3X method is 1.49 kcal mol^{-1} (or

~6.2 kJ mol^{-1}).

In the G3X model, all the structures are optimized at the B3LYP/6–31G(2df,p) level. In the energy calculations, apart from the five single–points in the G3 model, one more single–point calculation, HF/G3Xlarge, is required. Comparing the G3Xlarge and the G3large basis sets, there is an additional g polarization function in the former for second–row elements Al–Cl. In other words, there is no g function for Na or Mg. HLC is also added to account for the remaining basis set deficiencies: HLC = $-6.783 \times 10^{-3} n_\beta - 3.083 \times 10^{-3} (n_\alpha - n_\beta)$. In this work, all optimized structures have been characterized by vibrational frequencies calculations at the B3LYP/6–31G(2df,p) level. A scaling factor[14] of 0.9854 was used for the ZPVE corrections. The mathematical details of the G3X theory are described in Appendix A.

1.4 The Modified G2 Method

Apart from using the conventional G3–based methods, we also employ a modified G2 method to study some anions in our projects. The modified G2 method is called G2++,[12] which has been found to be useful for organic anionic systems. In the G2++ model, all the structures are optimized at MP2(Full)/6-31++G(d) level with diffuse functions included on both heavy and hydrogen atoms. In the energy calculations, some modifications have been made on the original G2[3] single–points: QCISD(T)/6–311G(d,p), MP4/6–311G(d,p), MP4/6–311++G(d,p) [with additional diffuse functions for hydrogen atom], MP4/6–311G(2df,p), and MP2/6–311++(3df,2p) [with additional diffuse functions for hydrogen atom]. HLC is added to account for the remaining basis set deficiencies: HLC = $-5.03 \times 10^{-3} n_\beta - 0.18 \times 10^{-3} n_\alpha$. All the structures have been characterized by vibrational frequencies calculations at the MP2(Full)/6–31++G(d) level with scaling factor 0.972 applied for the ZPVE corrections.

1.5 Calculation of Thermodynamical Data

The heats of formation at temperature T (ΔH°_{fT}) in this work were calculated in the following manner. For molecule AB, its Gn ΔH°_{fT} was calculated from the corresponding heat of reaction $\Delta H^\circ_{rT}(A + B \rightarrow AB)$ and the respective experimental $\Delta H^\circ_{fT}(A)$ and $\Delta H^\circ_{fT}(B)$ for elements A and B. In the calculations of ΔH°_{rT} for anions,

we set the ΔH°_{rT} value of a free electron to be zero.

1.6 Remark on the Location of Transition Structures

In this thesis, many transition structures (TSs) were located. For each TS, the "reactant(s)" and "product(s)" were confirmed by intrinsic reaction coordinate calculations. Also, for the dissociation channels which we claim to involve only bond breaking and no TSs, we did try to locate the TS(s) for them and found none.

1.7 Scope of the Thesis

In the following chapters, the calculation results of a number of molecular systems will be discussed. In Chapters 2 and 3, the energetics and decompostion mechanisms of a variety of alkoxide anions are studied at both the G2++ and G3 levels. The dissociative photoionization and dissociation channels of dimethyl disulfide (CH_3SSCH_3) and propylene sulfide (C_3H_6S) will be discussed in Chapters 4 and 5, respectively. The method employed in these two project was the G3 model of theory. In Chapter 6, the structures and energetics of phosphorus fluorides, as well as those of their singly charged cations and anions are investigated with the G3 and G3X methods. The relative merits of these two methods are then assessed in this work as well. Finally, a conclusion will be given in Chapter 7.

Editorial Note: Each chapter of this thesis should be treated as separate entity. In other words, it has its own numbering system for molecular species, equations, tables, figures, and references.

1.8 References

1. Pople, J. A.; Head-Gordon, M.; Fox, D. J.; Raghavachari, K.; Curtiss, L. A. *J. Chem. Phys.* **1989**, *90*, 5622.
2. Curtiss, L. A.; Jones, C.; Trucks, G. W.; Raghavachari, K.; Pople, J. A. *J. Chem Phys.* **1990**, *93*, 2537.
3. Curtiss, L. A.; Raghavachari, K.; Trucks, G. W.; Pople, J. A. *J. Chem. Phys.* **1991**, *94*, 7221.
4. Curtiss, L. A.; Raghavachari, K.; Pople, J. A. *J. Chem. Phys.* **1993**, *98*, 1293.
5. Curtiss, L. A.; Raghavachari, K.; Redfern, P. C.; Rassolov, V. R.; Pople, J. A. *J.*

Chem. Phys. **1998**, *109*, 7764.

6. Curtiss, L. A.; Redfern, P. C.; Raghavachari, K.; Rassolov, V. R.; Pople, J. A. *J. Chem. Phys.* **1999**, *110*, 4703.
7. Curtiss, L. A.; Redfern, P. C.; Raghavachari, K.; Pople, J. A. *J. Chem. Phys.* **2001**, *114*, 108.
8. Curtiss, L. A.; Carpenter, J. E.; Raghavachari, K.; Pople, J. A. *J. Chem. Phys.* **1992**, *96*, 9030.
9. Curtiss, L. A.; Raghavachari, K.; Pople, J. A. *Chem. Phys. Lett.* **1993**, *214*, 183.
10. Curtiss, L. A.; Raghavachari, K.; Redfern, P. C.; Pople, J. A. *J. Chem. Phys.* **1997**, *106*, 1063.
11. Curtiss, L. A.; Raghavachari, K.; Redfern, P. C.; Pople, J. A. *J. Chem. Phys.* **1998**, *109*, 42.
12. Chiu, S.-W.; Lau, K.-C.; Li, W.-K. *J. Phys. Chem. A*. **1999**, *103*, 6003.
13. Curtiss, L. A.; Raghavachari, K.; Redfern, P. C.; Pople, J. A. *J. Chem. Phys.* **2000**, *112*, 7374.
14. Scott, A. P.; Radom, L. *J. Phys. Chem.* **1996**, *100*, 16502.

Chapter 2

A Gaussian-2 and Gaussian-3 Study of Alkoxide Anion Decompositions. I. H_2 and CH_4 Eliminations of the Methoxide, Ethoxide, *i*-Propoxide, and *t*-Butoxide Anions

Abstract

The decomposition mechanisms of four alkoxide anions: CH_3O^-, $CH_3CH_2O^-$, $(CH_3)_2CHO^-$, and $(CH_3)_3CO^-$, have been studied with a modified G2 (G2++) and G3 methods. The energy profiles for the decomposition reactions of each alkoxide anion are reported. It is found that the decompositions proceed via an anionic mechanism with a stepwise pathway. For anions $CH_3CH_2O^-$ and $(CH_3)_2CHO^-$, calculated results indicate that the H_2 elimination has a lower energy barrier than the CH_4 elimination. This result is in total agreement with the experimental data obtained in the collision activated dissociation and infrared multiple photon induced elimination studies of simple alkoxide anions.

2.1 Introduction

There have been various interests in alkoxide anions (RO^-) in the gas phase.[1-12] The gas-phase acidities of a large number of alcohols have been determined from studies of the unimolecular collision-activated dissociation (CAD) of proton-bound cluster ions $[RO\cdots H\cdots OR']^-$.[1] Extensive CAD studies of simple and complex alkoxides have been reported.[2-8] From ab initio calculations and a study of isotope effects, Bowie and co-workers[9,10] have investigated the mechanism of elimination reactions of ethoxide and *t*-butoxide. They pointed out that the two reactions should be similar and have a stepwise mechanism. The technique of infrared multiple photon (IRMP) photochemistry has also been applied to study the mechanism of decomposition of alkoxides.[11,12] Tumas et al. have studied the decompositions of 15 alkoxide anions. They reported that the decomposition should start with a heterolytic cleavage rather than a homolytic one. The charge inversion mass spectra of alkoxides have been reported.[13] Recently, a high-level theoretical study of intramolecular rearrangements and unimolecular fragmentation of ethoxide

has been described.[14] Structures, charge distributions[15,16] and fundamental vibrational frequencies[15] of selected alkoxides have also been investigated theoretically.

Loss of H_2 or CH_4 from primary alkoxide anions proceeds via a stepwise 1,2-elimination pathway involving ion-molecular complex (IMC)[17] as intermediates.[9–12] Secondary alkoxide anions, unlike the primary ones, can have more than one fragmentation pathway. *i*-Propoxide, for example, can in principle undergo both H_2 and CH_4 eliminations.[2,9] As noted by Mercer and Harrison,[2] Bowie et al.[9] also reported that CD_3H was eliminated from $(CD_3)_2CHO^-$, a result which is inconsistent with the proposed 1,2-elimination reaction. The observed products CH_3D and CD_3H, as listed in Table 1 of ref 9, would probably be due to 1,1-elimination reactions of $(CH_3)_2CDO^-$ and $(CD_3)_2CHO^-$, respectively.

In this work, we undertake the study of the following plausible 1,1- and 1,2-elimination reactions of CH_3O^-, $CH_3CH_2O^-$, $(CH_3)_2CHO^-$, and $(CH_3)_3CO^-$ at a high theoretical level:

$$CH_3O^- (\mathbf{1}) \rightarrow H_2 + HCO^- \quad (1)$$

$$CH_3CH_2O^- (\mathbf{4}) \rightarrow H_2 + CH_2{=}CHO^- \quad (2a)$$

$$CH_3CH_2O^- (\mathbf{4}) \rightarrow CH_4 + HCO^- \quad (2b)$$

$$(CH_3)_2CHO^- (\mathbf{10}) \rightarrow H_2 + CH_2{=}C(CH_3)O^- \quad (3a)$$

$$(CH_3)_2CHO^- (\mathbf{10}) \rightarrow CH_4 + CH_3CO^- \quad (3b)$$

$$(CH_3)_2CHO^- (\mathbf{10}) \rightarrow CH_4 + CH_2{=}CHO^- \quad (3c)$$

$$(CH_3)_3CO^- (\mathbf{17}) \rightarrow CH_4 + CH_2{=}C(CH_3)O^- \quad (4)$$

Such a study would lead to a better understanding of the energetics of the fragmentations of these simple alkoxide anions. In addition, there have been questions raised regarding the alkoxide anion decomposition reactions. (1) Do they proceed via a stepwise or a concerted mechanism? (2) Why is the heterolytic cleavage more favorable than the homolytic one? (3) Why does $CH_3CH_2O^-$ undergo H_2 elimination exclusively, as observed experimentally?[12] (4) Does $(CH_3)_2CHO^-$ undergo 1,2-eliminations of H_2 and CH_4, as well as 1,1-elimination of CH_4?[2,7,9,12] We will attempt to answer these questions in this work.

2.2 Methods of Calculations

All calculations were carried out on DEC 500au and SGI10000 workstations, as well as on an SGI Origin 2000 High Performance Server, using the Gaussian 94[18]

and Gaussian 98[19] packages of programs. The computational models we employed were the modified Gaussian-2 (G2++)[14] and Gaussian-3 (G3)[20] levels of theory.

2.3 Results and Discussion

In our notation, single- or double-digit numerals such as **1** and **2, etc.** refer to stable alkoxide anion structures, fragmentation intermediates, or fragments. In addition, the transition structure connecting **1** and **2** is denoted as TS(**1**→**2**), etc.

The bond dissociation energies for the homolytic versus heterolytic bond cleavage of the four alkoxide anions studied in this work, namely, the methoxide (**1**), ethoxide (**4**), *i*-propoxide (**10**), and *t*-butoxide (**17**) anions, are listed in Table 1. The G2++ and G3 results for reactions (1) to (4) are summarized in Tables 2-5, respectively; also, the energy profiles of the same reactions are schematically shown in Figures 1-4, respectively. The geometries of all the equilibrium and transition structures involved in these reactions are depicted in Figure 5. Throughout this work, G2++ energies are used for discussion unless explicitly stated otherwise.

2.3.1 Nature of ion-neutral complex. In general, the unimolecular decomposition of a variety of gaseous ions is mediated by ion-neutral complexes (INCs).[11,21-27] In this mechanism, a covalent bond cleaves in such a fashion that the charged and neutral fragments are held together by electrostatic interaction and the fragments sojourn in the vicinity of one another long enough to undergo a subsequent ion-neutral reaction.[21] Such an INC may not necessarily correspond to a local potential energy minimum.[28] The internal rotational degrees of freedom developed within the complex provide an *entropy well* in which the system tends to linger.[17] The PES of this *entropy-well* environ should be rather flat so that the lingering fragments can freely rotate relative to each other. Hence, such a complex would at most sit in a shallow potential-energy well. Chemical engagement would not take place until the fragments properly orient relative to each other.[21] It is generally accepted that a species will be considered as an INC only if its lifetime from the point of covalent bond breaking to the point of overcoming long-range electrostatic forces is long enough that a chemical reaction other than dissociation has time to occur. From entropy (density of states) consideration, INCs are stable entities and have now achieved wide acceptance as viable intermediates in unimolecular dissociations of many types of ions.[17,21,22,28]

Since the fragments of an INC show reactivities similar to those expected for the isolated species,[22,29] it is not unreasonable to expect that the character of the INC or the INC-like TS for reaction (2a), for example, is dominated by either the IMC [$H^-\cdots CH_3CHO$] or ion-radical complex (IRC) [$H\cdots CH_3CHO^-$] state if the reaction is INC-mediated. One may therefore infer the nature of an INC-mediated reaction by comparing the energetics of its two limiting (heterolytic and homolytic) pathways.[29] The stabilization energy of an INC relative to its separated fragments with a non-polar neutral is ca. 20-25 kJ mol^{-1}.[30] Stabilization energies in the range of 42–80 kJ mol^{-1} are common in INCs containing a polar neutral.[22,31] The critical energies (assuming no reverse barriers) for the formation of the two limiting states (e.g., [$H^-\cdots CH_3CHO$] and [$H\cdots CH_3CHO^-$]) of the complex can then be easily estimated from their stabilization energies (relative to their corresponding separated fragments) and the ΔH_{r0} values for the direct homolytic ($CH_3CH_2O^- \rightarrow H + CH_3CHO^-$) and heterolyic ($CH_3CH_2O^- \rightarrow H^- + CH_3CHO$) dissociations. The relative stability of the two limiting states should be the dominant factor in determining whether the INC-mediated reaction occurs by a heterolytic or homolytic mechanism. Based on the results obtained from this simple ion-dipole model, we infer that the INCs involved in the eliminations studied in this work are IMCs rather than IRCs.

In this work, we did not carry out calculations of INCs formed from the final product pair prior to dissociation. When considering the possible intermediacy of INCs in unimolecular dissociations, a distinction must be made between process in which the incipient product pair form a stable complex prior to dissociation, and process which involved INCs as intermediates before the last chemical step.[32]

2.3.2 Initial bond cleavage of alkoxide anions. There are two possible initiation steps for the elimination of H_2 or CH_4 from a simple alkoxide anion. It can start with either a homolytic or a heterolytic bond dissociation. In Table 1, it is seen that all heterolytic dissociations require less energy than the homolytic counterparts. In other words, heterolytic bond cleavage is favored over homolytic bond cleavage in the decompositions of alkoxide anions: the reaction should start with a heterolytic bond cleavage to form a ketone and a hydride ion or a carbanion rather than a homolytic bond cleavage producing a ketonic anion and a hydrogen atom or an alkyl radical.

Table 1: The Heterolytic and Homolytic Bond Dissociation Energies of Various Alkoxide Anions at the G3 level[a]

$H_2C{=}O + H^-$	←	CH_3O^- (**1**)	→	$H_2C{=}O^- + H^\bullet$
182.1		0		313.2
$(CH_3)HC{=}O + H^-$	←	$CH_3CH_2O^-$ (**4**)	→	$(CH_3)HC{=}O^- + H^\bullet$
176.8		0		322.1
$H_2C{=}O + CH_3^-$	←	$CH_3CH_2O^-$ (**4**)	→	$H_2C{=}O^- + {}^\bullet CH_3$
206.0		0		287.0
$(CH_3)_2C{=}O + H^-$	←	$(CH_3)_2CHO^-$ (**10**)	→	$(CH_3)_2C{=}O^- + H^\bullet$
175.8				319.9
$(CH_3)HC{=}O + CH_3^-$	←	$(CH_3)_2CHO^-$ (**10**)	→	$(CH_3)HC{=}O^- + {}^\bullet CH_3$
201.4		0		296.7
$(CH_3)_2C{=}O + CH_3^-$	←	$(CH_3)_3CO^-$ (**17**)	→	$(CH_3)_2C{=}O^- + {}^\bullet CH_3$
195.5		0		289.5

[a]The species shown on the first column are the products of a heterolytic cleavage of the alkoxide anions given in the middle column; those given on the last column are the products of a homolytic cleavage.

2.3.3 Dissociation of alkoxide anions. In this section, we will discuss the anionic decomposition mechanisms of each alkoxide anion studied in this work.

Dissociation of CH_3O^- (**1**). There is only one elimination pathway for this anion, namely, the 1,1-elimination of H_2. It can either be concerted or stepwise. If it occurs by a concerted mechanism, it must be a highly asynchronous one[33,34] since the synchronous and symmetrical stretching of the two C-H bonds should be symmetry forbidden. In agreement with Sheldon and Bowie's HF/6-311++G results,[6] we found no such concerted and asynchronous pathway for reaction (1) at the MP2(full)/6-31++G(d) level. The symmetry forbidden pathway is a very high-energy process[6] and is not a plausible mechanism for the occurrence of reaction (1).

On the MP2(Full)/6-31++G(d) PES, reaction (1) occurs by a stepwise mechanism:

$$CH_3O^-\ (\mathbf{1}) \rightarrow TS(\mathbf{1}\rightarrow\mathbf{2}) \rightarrow [H^- \cdots H_2CO]\ (\mathbf{2}) \rightarrow$$
$$TS(\mathbf{2}\rightarrow\mathbf{3}) \rightarrow HCO^-\ (\mathbf{3a}) + H_2\ (\mathbf{3b}) \qquad (1)$$

However, on both the G2++ and G3 PESs, the minimum energy path (MEP) of reaction (1) appears to be a single-step pathway. From Figure 1 one may notice that TS(**1**→**2**) is lower in energy than **2** by 7 kJ mol^{-1} at the G2++ level. Such an anomaly that a TS is slightly lower in energy than the local minimum to which it connects has been discussed previously.[35] Nevertheless, the deviation is somewhat

Table 2: G2++ and G3 Total Energies[a] (E_0), Enthalpies (H_{298}), and Standard Heats of Formation at 0 K (ΔH°_{f0}) and 298 K (ΔH°_{f298}) of the Species Involved in the Fragmentation Reaction of CH_3O^-

species	E_0 (hartree)	H_{298} (hartree)	ΔH°_{f0} (kJ mol^{-1})	ΔH°_{f298} (kJ mol^{-1})
1	**-114.92909**	**-114.92522**	**-132.5**	**-139.5**
	-115.01883	*-115.01499*	*–119.3*	*–126.3*
				(-139 ± 10)[b]
				(-134 ± 4.6)[c]
2	**-114.87984**	**-114.87415**	**-3.2**	**-5.4**
	-114.96853	*-114.96358*	*12.8*	*8.7*
3a + 3b	**-114.87994**	**-114.87283**		
	-114.96972	*-114.96261*		
TS(**1**→**2**)	**-114.88271**	**-114.87825**	**-10.8**	**-16.1**
	-114.96932	*-114.96483*	*10.7*	*5.4*
TS(**2**→**3**)	**-114.86822**	**-114.86340**	**27.3**	**22.9**
	-114.95862	*-114.95356*	*38.8*	*35.0*

[a]G2++ energies are shown in bold font, and G3 energies are in italic font.
[b] Experimental value, taken from ref 42, is given in bracket.
[c] Experimental value, taken from ref 43, is given in bracket.

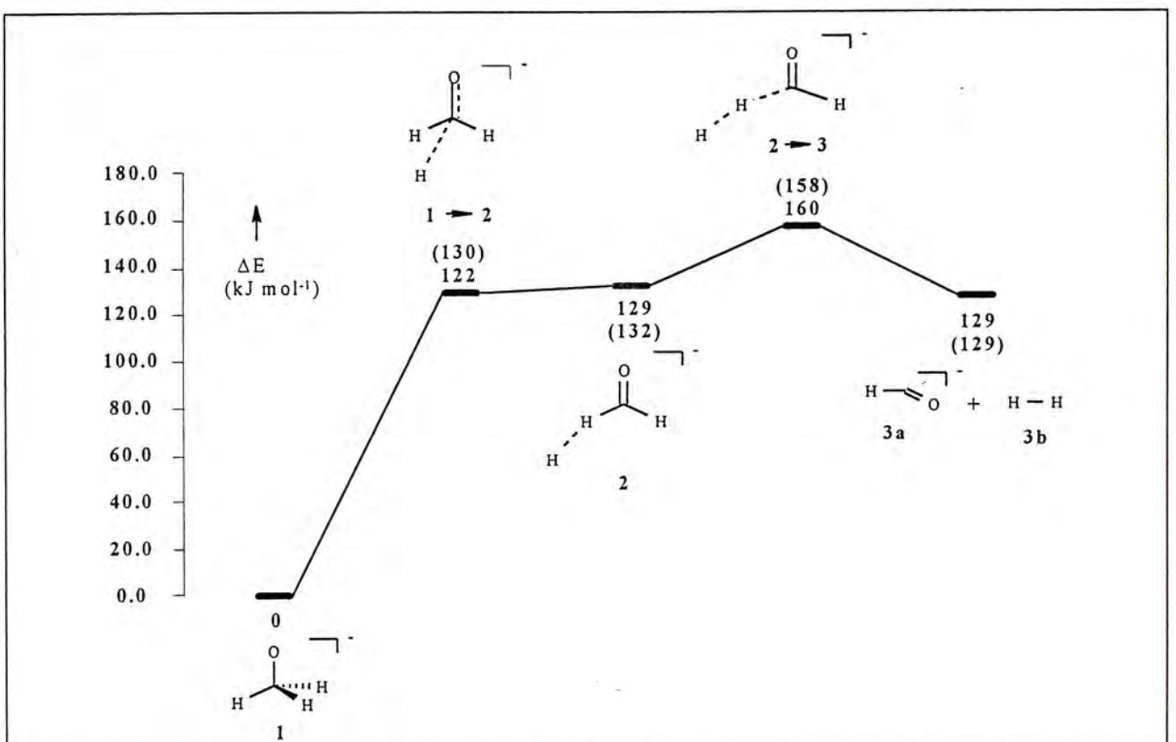

Figure 1. The G2++ energy profiles of the dissociation for CH_3O^- (**1**). The G3 relative energies are given in brackets.

too large and it suggests that optimization of the structure of TS(**1**→**2**) at the MP2(Full)/6-31++G(d) level is not adequate enough. We recalculated the G2++ energies of TS(**1**→**2**) and **2** based on their MP2(Full)/6-31++G(d,p) optimized structures and found that the former is now 3 kJ mol^{-1} lower in energy than the latter. With thermal and entropy corrections, their free energy difference at 298 K is essentially zero. Thus, initial formation of [$H^-\cdots H_2CO$] from **1** proceeds essentially without or with a very small reverse barrier. In other words, the IMC is energetically unstable. Once it is formed its fragments readily undergo association reaction to form **1**. Though an IMC is not necessary to correspond to a local minimum,[28] it may sit in an *entropy well*[17] and is *entropy stable* and its lifetime is long enough to await chemical engagement. The MEP of reaction (1) is so asynchronous that two distinct elementary processes can be clearly discerned: initial hydride anion elimination resulting the formation of [$H^-\cdots H_2CO$], followed by proton abstraction within the complex. Reaction (1) proceeds by a stepwise mechanism. It has been questioned whether any reaction can be truly concerted.[33] The barrier to the first step is 129 kJ mol^{-1} and the barrier to the proton-transfer step within the complex is 31 kJ mol^{-1}.

This reaction was studied both experimentally and computationally by Bowie and co-workers.[6] Their results are in qualitative agreement with our G2++ (or G3) data, even though there are significant quantitative differences between them. Specifically, at the HF/6-311++G level, Bowie et al obtained the following relative energies (in kJ mol^{-1}) for the species involved in reaction (1): **1** (0), TS(**1**→**2**) (142), **2** (126), TS(**2**→**3**) (335), **3a**+**3b** (177). In other words, their overall barrier is more than twice of the G2++ (or G3) counterpart. It is noted their HF/6-311++G structure[6] of TS(**2**→**3**) looks like a three-fragments complex structure [$H\cdots HCO\cdots H]^-$ and, upon checking, we found that it is not a true local TS structure at the HF/6-311++G level. Furthermore, their IMC **2** has a symmetric structure with C_{2v} symmetry, instead of the unsymmetric geometry we obtained at the MP2(Full)/6-31G(d) and MP2(Full)/6-31++G(d) levels. It appears that the structure of **2** depends on whether or not the chosen basis set has polarization functions on the non-hydrogen atoms.

Large primary isotope effect (7.5) observed in reaction (1) was assigned to be due to the first step.[6] The assignment of Bowie et al[6] was based on the calculated primary isotope effect (0.9) for the proton transfer step. The calculation[6] was based on the three-fragments complex structure which is a questionable TS for the proton-

transfer step as mentioned in the previous paragraph. One should note that the program BEBOVIB IV[36] which was used for their calculation of isotope effect gives information which is critically dependent on TS geometries.[9] As can be seen from Figure 5, the bridging C···H bond of TS(**2**→**3**) is severely extended (1.463 Å). We rationalize that there should be a significant primary isotope effect manifested by the proton-transfer step since strong primary isotope effects have been attributed to the TS for H transfer being higher in energy than that for cleavage to form the complex.[37]

Previously we investigated loss of H_2 from **4**, reaction (2a), at the G2++ level.[14] The overall energy barrier (126 kJ mol^{-1})[14] to this reaction, which is also the energy barrier to the first step, is ca. 34 kJ mol^{-1} less than that of reaction (1). This is in line with the observation[6] that loss of H_2 from **1** is several orders of magnitude less probable than from **4**. The unusally large energy barrier (ca. 31 kJ mol^{-1}) to the proton transfer step within $[H^-\cdots H_2CO]$, as compared to those found for other INC-mediated reactions investigated in this work and our previous studies,[14,29,38] suggests that this step is also rate determining.

Dissociations of $CH_3CH_2O^-$ (**4**). There are two elimination pathways to be studied, the 1,2-elimination of H_2, and 1,1-elimination of CH_4:

$$CH_3CH_2O^-\ (\mathbf{4}) \rightarrow TS(\mathbf{4}\rightarrow\mathbf{5}) \rightarrow [H^-\cdots CH_3CHO]\ (\mathbf{5}) \rightarrow TS(\mathbf{5}\rightarrow\mathbf{6})$$
$$\rightarrow [H^-\cdots H_3CCHO]\ (\mathbf{6}) \rightarrow TS(\mathbf{6}\rightarrow\mathbf{7}) \rightarrow CH_2{=}CHO^-\ (\mathbf{7a}) + H_2\ (\mathbf{7b}) \quad (2a)$$

$$CH_3CH_2O^-\ (\mathbf{4}) \rightarrow TS(\mathbf{4}\rightarrow\mathbf{8}) \rightarrow [H_3C^-\cdots H_2CO]\ (\mathbf{8})$$
$$\rightarrow TS(\mathbf{8}\rightarrow\mathbf{9})\ HCO^-\ (\mathbf{9a}) + CH_4\ (\mathbf{9b}) \quad (2b)$$

We now consider the loss of H_2 via IMC $[H^-\cdots c\text{-}CH_2CH_2O]$, i.e., **4** → $[H^-\cdots c\text{-}CH_2CH_2O]$ → H_2 + $C_2H_3O^-$ (*c*-CH_2CHO^- or $CH_2{=}CHO^-$). We found that the formation of the complex would be too energetic. Using the experimental ΔH_{f298} values[39] of **4**, H^-, H_2CO, CH_3CHO, and *c*-CH_2CH_2O as well as the stabilization energies[22,30,31] of the INCs involved, it may be concluded that $[H^-\cdots c\text{-}CH_2CH_2O]$ is higher in energy than $[H^-\cdots CH_3CHO]$ and $[H_3C^-\cdots H_2CO]$ by ca. 118 and 69 kJ mol^{-1}, respectively. Obviously, this reaction channel is energetically non-competitive to reactions (2a) and (2b). Experimentally, fragmentation of the $CH_3CD_2O^-$ anion resulted in elimination of HD only, excluding the 1,1-elimination mechanism.[2] In general, ethylene oxides are much higher in energy than their

corresponding ketonic isomers.[39] We conclude that eliminations involving IMCs containing ethylene oxide or its substituted analogs are not energetically competitive to the reactions studied in this work. Studies of their reaction pathways are therefore not carried out.

Table 3: G2++ and G3 Total Energies[a] (E_0), Enthalpies (H_{298}), and Standard Heats of Formation at 0 K (ΔH°_{f0}) and 298 K (ΔH°_{f298}) of the Species Involved in the Fragmentation Reaction of $CH_3CH_2O^-$

Species	E_0 (hartree)	H_{298} (hartree)	ΔH°_{f0} (kJ mol^{-1})	ΔH°_{f298} (kJ mol^{-1})
4	**-154.16426**	**-154.15945**	**-172.6**	**-186.1**
	-154.29930	*-154.29456*	*–159.5*	*–173.2*
				(-186 ± 10)[b]
				(-183 ± 9)[c]
5	**-154.11722**	**-154.11049**	**-49.1**	**-57.6**
	-154.25249	*-154.24580*	*-36.6*	*-45.2*
6	**-154.12021**	**-154.11362**	**-56.9**	**-65.8**
	-154.25322	*-154.24673*	*-38.5*	*-47.7*
7a + 7b	**-154.16131**	**-154.15274**		
	-154.29710	*-154.28924*		
8	**-154.10511**	**-154.09700**	**-17.3**	**-22.2**
	-154.23932	*-154.23188*	*-2.0*	*-8.7*
9a + 9b	**-154.12362**	**-154.11600**		
	-154.25834	*-154.25073*		
TS(**4**→**5**)	**-154.11627**	**-154.11080**	**-46.6**	**-58.4**
	-154.25255	*-154.24713*	*-36.8*	*-48.7*
TS(**5**→**6**)	**-154.11750**	**-154.11154**	**-49.8**	**-60.4**
	-154.25275	*-154.24682*	*-37.3*	*-47.9*
TS(**6**→**7**)	**-154.11905**	**-154.11365**	**-53.9**	**-65.9**
	-154.25579	*-154.25044*	*-45.3*	*-57.4*
TS(**4**→**8**)	**-154.10542**	**-154.09782**	**-18.1**	**-24.3**
	-154.23945	*-154.23251*	*-2.4*	*-10.3*
TS(**8**→**9**)	**-154.09981**	**-154.09270**	**-3.4**	**-10.9**
	-154.23520	*-154.22818*	*8.8*	*1.0*

[a] G2++ energies are shown in bold font, and G3 energies are in italic font.
[b] Experimental value, taken from ref 42, is given in bracket.
[c] Experimental value, taken from ref 43, is given in bracket.

It is noted that, in the G3 calculations of reaction (2a), the structures of species TS(**4**→**5**), **5**, TS(**5**→**6**), **6** and TS(**6**→**7**) were optimized at the MP2(Full)/6-31++G(d) level since only TS(**4**→**5**), but not TS(**5**→**6**) and TS(**6**→**7**), was located at the MP2(Full)/6-31G(d) level. Also, the G2++ results for these two reactions are taken directly from ref 14. From Figure 2, it is seen that the 1,2-elimination of H_2

also starts with hydride ion elimination, followed by proton abstraction on the neighboring methyl group by this anion. On the other hand, the 1,1-elimination of CH_4 starts with dissociation of a methyl carbanion, followed by proton abstraction on the carbonyl carbon by the carbanion.

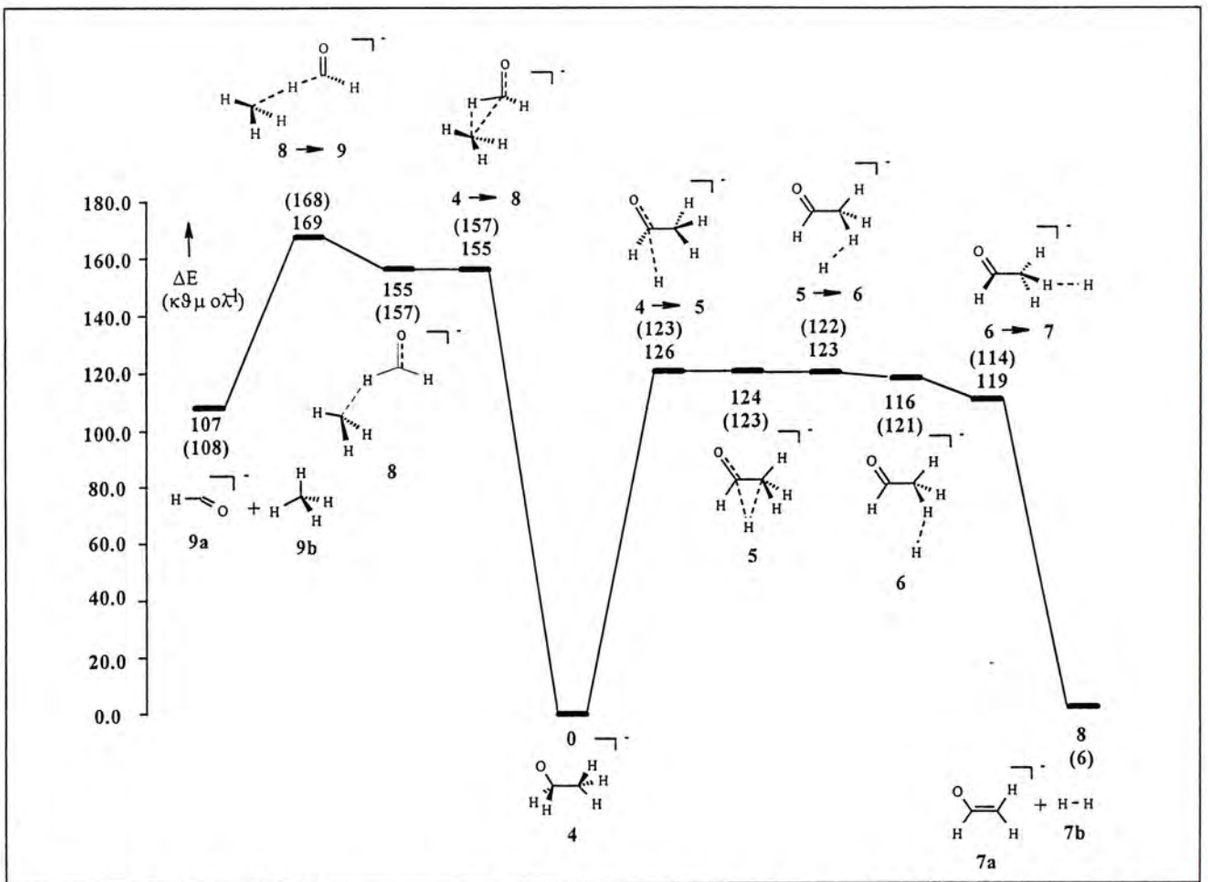

Figure 2. The G2++ energy profiles of the dissociation for $CH_3CH_2O^-$ (**4**). The G3 relative energies are given in brackets.

The G2++ PES for reaction (2a) is atypical of a stepwise reaction pathway: initial formation of intermediate **6** via TS(**4**→**5**) which becomes the TS connecting **4** and **6**, followed by proton transfer via TS(**6**→**7**). The barrier to the first step is 126 kJ mol^{-1} and that to the second step is 3 kJ mol^{-1}. The TS(**6**→**7**) is lower in energy than TS(**4**→**5**) by 7 kJ mol^{-1}. Thus the first step is rate determining. That TS(**6**→**7**) has some proton-bridged character (the bridging C–H bond is 1.262 Å) as can be seen from Figure 5 suggests the proton transfer step may have a small primary isotope effect. A large primary isotope effect for this step would require a significant lengthening the bridging C–H bond in the TS structure. This proton transfer process would proceed through a highly asymmetric TS (in term of the proton-bridged structure $[C\cdots H\cdots H]^-$) due to the large exothermicity (ca. 110 kJ mol^{-1}) of this step

and therefore should exhibit a small primary isotope effect.[40] The observed primary isotopic effect is 1.6–2.0.[9,12]

The G3 MEP of reaction (2a) essentially has an energy barrier of 123 kJ mol^{-1} over which the complex spans a wide spectrum of IMC-like structures (e.g., TS(**4**→**5**), **5**, TS(**5**→**6**), and **6**). The small energy barrier (3 kJ mol^{-}) to the proton transfer process that appears on the G2++ PES vanishes at the G3 level which is based on MP2(Full)/6-31G(d) structures. It is known[41] that use of diffuse and polarization functions centered on the H atom is significant in obtaining accurate energy of the hydride anion (H^-). Their effects on structures of IMCs consisting of a H^- fragment cannot be ignored. Obviously, the structures of $[H^-\cdots CH_3CHO]$ optimized at the MP2(Full)/6-31G(d) level are somewhat inferior to those obtained at the MP2(Full)/6-31++G(d) level. The single-barrier feature of the G3 PES is an artifact of using the MP2(Full)/6-31G(d) structures of $[H^-\cdots CH_3CHO]$. The importance of the use of polarization functions on the H atoms of $[H^-\cdots H_2CO]$ has been illustrated in the case of reaction (1).

The G2++ PES of reaction (2b) is similar to that of reaction (1). Both are 1,1-elimination and have similar overall barrier height (160 kJ mol^{-1} for reaction (1) and 169 kJ mol^{-1} for reaction (2b)). The energy barrier to the initial C–C bond cleavage leading to the formation of **8** is 155 kJ mol^{-1}. This process proceeds without a reverse barrier. The energy barrier to the proton transfer within the complex $[CH_3^-\cdots H_2CO]$ is 14 kJ mol^{-1}. Based on these results, we rationalize that 1,1-elimination of H_2 from **4** would have a similar overall energy barrier (ca. 160 kJ mol^{-1}) if it ever occurs. Thus, 1,2-H_2 elimination is energetically favored over the 1,1-eliminations for **4**. This result agrees with those of the experiments: CAD[2,9] and IRMP[11] studies on the ethoxide anion show that **4** undergoes H_2 elimination exclusively and no 1,1-elimination[2,9] of H_2 occurs.

Dissociation of $(CH_3)_2CHO^-$ (**10**). There are three elimination pathways to be studied:

$$(CH_3)_2CHO^- (\mathbf{10}) \rightarrow TS(\mathbf{10}\rightarrow\mathbf{11}) \rightarrow [H^-\cdots CH_3COCH_3] (\mathbf{11})$$
$$\rightarrow TS(\mathbf{11}\rightarrow\mathbf{12}) \rightarrow CH_2{=}C(CH_3)O^- (\mathbf{12a}) + H_2 (\mathbf{12b}) \quad (3a)$$
$$(CH_3)_2CHO^- (\mathbf{10}) \rightarrow TS(\mathbf{10}\rightarrow\mathbf{13}) \rightarrow [H_3C^-\cdots HCOCH_3] (\mathbf{13})$$
$$\rightarrow TS(\mathbf{13}\rightarrow\mathbf{14}) \rightarrow CH_3CO^- (\mathbf{14a}) + CH_4 (\mathbf{14b}) \quad (3b)$$

$(CH_3)_2CHO^-$ (**10**) → TS(**10**→**15**) → **15** → TS_1(**15**→**16**) → TS_2(**15**→**16**)
→ CH_2=CHO^- (**16a**) + CH_4 (**16b**) (3c)

Table 4: G2++ and G3 Total Energies[a] (E_0), Enthalpies (H_{298}), and Standard Heats of Formation at 0 K (ΔH°_{f0}) and 298 K (ΔH°_{f298}) of the Species Involved in the Fragmentation Reaction of $(CH_3)_2CHO^-$

Species	E_0 (hartree)	H_{298} (hartree)	ΔH°_{f0} (kJ mol^{-1})	ΔH°_{f298} (kJ mol^{-1})
10	**-193.39936**	**-193.39333**	**-212.5**	**-231.9**
	-193.58006	*-193.57408*	*-200.5*	*-220.1*
				(-232 ± 10)[b]
				(-231 ± 9)[c]
11	**-193.35794**	**-193.35030**	**-103.7**	**-118.9**
	-193.53751	*-193.53078*	*-88.8*	*-106.4*
12a + 12b	**-193.39338**	**-193.38408**		
	-193.57428	*-193.56521*		
13	**-193.34318**	**-193.33412**	**-65.0**	**-76.4**
	-193.52179	*-193.51261*	*-47.5*	*-58.7*
14a + 14b	**-193.36495**	**-193.35614**		
	-193.54281	*-193.53390*		
15	**-193.34318**	**-193.33413**	**-64.8**	**-76.6**
	-193.52179	*-193.51261*	*-47.5*	*-58.7*
16a + 16b	**-193.40497**	**-193.39589**		
	-193.58572	*-193.57736*		
TS(**10**→**11**)	**-193.35068**	**-193.34398**	**-84.6**	**-102.3**
	-193.52930	*-193.52265*	*-67.2*	*-85.1*
TS(**11**→**12**)	**-193.35595**	**-193.34920**	**-98.5**	**-116.0**
	-193.53659	*-193.53041*	*-86.4*	*-105.4*
TS(**10**→**13**)	**-193.34268**	**-193.33493**	**-63.7**	**-78.6**
	-193.52114	*-193.51304*	*-45.8*	*-59.8*
TS(**13**→**14**)	**-193.33572**	**-193.32691**	**-45.4**	**-57.5**
	-193.51527	*-193.50680*	*-30.4*	*-43.4*
TS(**10**→**15**)	**-193.34269**	**-193.33494**	**-63.5**	**-78.7**
	-193.52111	*-193.51302*	*-45.7*	*-59.8*
TS_1(**15**→**16**)	**-193.34288**	**-193.33469**	**-64.0**	**-78.0**
	-193.52111	*-193.51302*	*-45.7*	*-59.8*
TS_2(**15**→**16**)	**-193.34178**	**-193.33330**	**-61.1**	**-74.4**
	-193.52114	*-193.51289*	*-45.8*	*-59.4*

[a] G2++ energies are shown in bold font, and G3 energies are in italic font.
[b] Experimental value, taken from ref 42, is given in bracket.
[c] Experimental value, taken from ref 43, is given in bracket.

The G2++ barriers for reaction (3a) are 128 (first step) and 5 (second step) kJ mol^{-1} similar to those for reaction (2a). The TS(**11**→**12**) has some proton-bridged character; however, the bridging C–H bond (1.290 Å) is still quite intact. Thus small

primary isotope effect would be manifested in the proton transfer step as in the case of reaction (2a). This is in line with the measured value (2.0)[9].

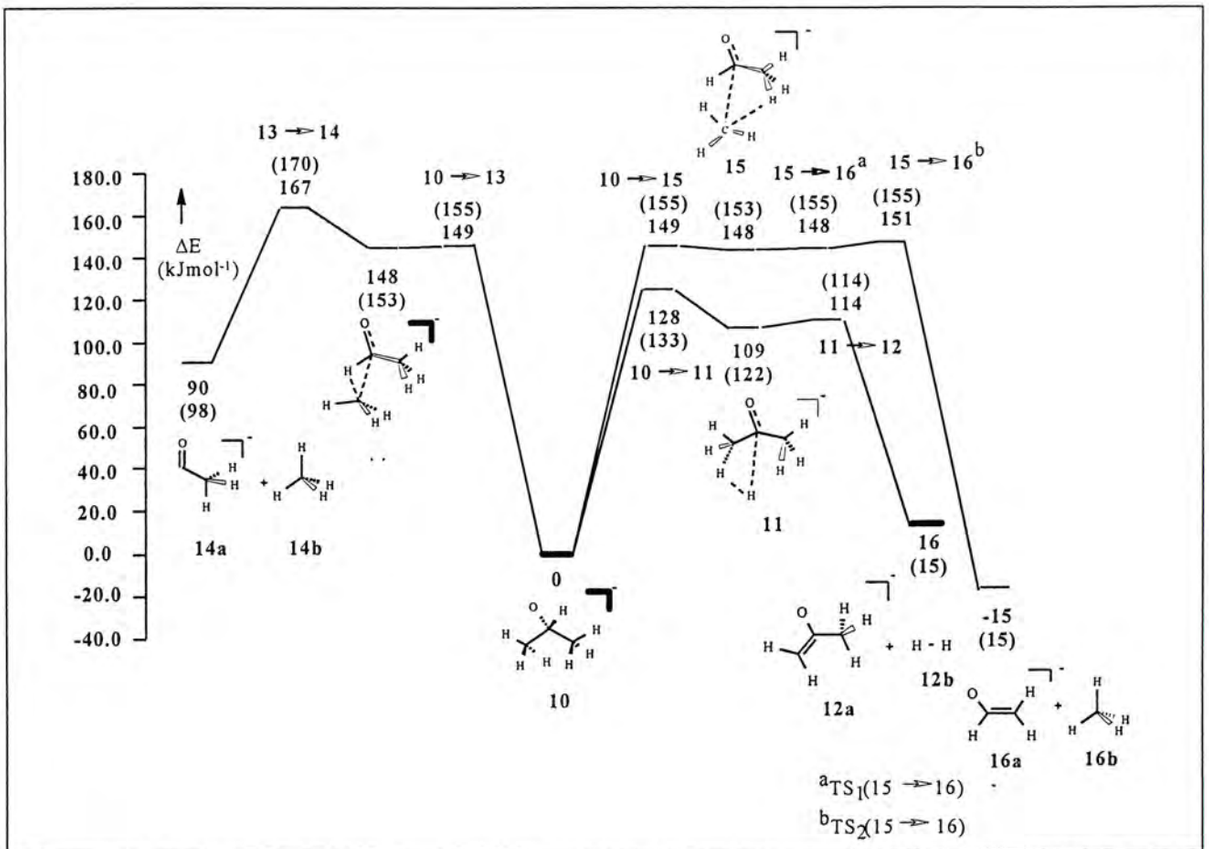

Figure 3. The G2++ energy profiles of the dissociation for $(CH_3)_2CHO^-$ (**10**). The G3 relative energies are given in brackets.

Both the 1,1-elimination (reaction (3b)) and 1,2-elimination (reaction (3c)) of CH_4 start with the dissociation of methyl carbanion, followed by proton abstraction on the carbonyl and methyl carbon, respectively. The energy barriers to the first steps of reactions (3b) and (3c) are essentially the same, ca. 149 kJ mol^{-1}. However, the energy barrier to the proton transfer step in reaction (3b) is ca. 16 kJ mol^{-1} higher than that in reaction (3c). In addition, **16a** is lower in energy than **14a** by 105 kJ mol^{-1}. Hence, reaction (3c) is thermodynamically and kinetically more favorable than reaction (3b).

Among reactions (3a), (3b), and (3c), the first one has the lowest critical energy. In other words, H_2 elimination is again energetically favored over CH_4 eliminations for **10**. This is consistent with the CAD result[2] that at the lowest collision energies elimination of H_2 is the dominant fragmentation reaction. This indicates that this reaction has the lower critical reaction energy and will be the channel observed when threshold reactions are probed by multiphoton activation.

Indeed, Brauman and co-workers[7,11] have reported that the infrared multiphoton photodissociation of **10** results in elimination of H_2 only. The rapid rise in importance of the 1,2-elimination of CH_4, reaction (3c), with increasing collision energy suggests that the critical energy for 1,2-CH_4 elimination should be slightly greater than that for H_2 elimination and there may be entropy effects which favors CH_4 elimination.[2] The calculated overall energy barrier to reaction (3c) is ca. 23 kJ mol^{-1} higher than that to reaction (3a), in line with the conclusion inferred from the experimental result.[2]

While Mercer and Harrison[2] observed elimination of CD_4 and HD from $(CD_3)_2CHO^-$, Bowie et al[9] reported that CD_3H, CH_3D, and CH_4 were also eliminated from $(CD_3)_2CHO^-$, $(CH_3)_2CDO^-$, and $CH_3(CD_3)CHO^-$, respectively, reactions consistent with a 1,1-elimination. Energetically, reaction (3b) is competitive to reaction (3c) since the overall energy barrier of the former is only 16 kJ mol^{-1} higher than the latter. However, reaction (3b) is 105 kJ mol^{-1} less exothermic than reaction (3c). The occurrence of reaction (3b) is less probable than that of reaction (3c). 1,1-Elimination of H_2 from **1**, reaction (1), is plausible but is several magnitude of order less probable than reaction (2a), a 1,2-elimination reaction. Our calculated results suggest that 1,1-CH_4 elimination is energetically plausible in fragmentation of **10**. However, it is less probable than 1,2-elimination of CH_4 and would be several magnitude of order less probable than 1,2-H_2 loss from **10**. In conclusion, reactions (3a) and (3c) are the dominant channels in the fragmentation of **10**. If reaction (3b) ever occurs, its elimination products would be in an insignificant amount.

Dissociation of $(CH_3)_3CO^-$ (**17**). There is only one pathway to be studied, the 1,2-elimination of CH_4 other than loss of H_2 via $[H^-\cdots c\text{-}CH_2OC(CH_3)_2]$:

$$(CH_3)_3CO^- (\mathbf{17}) \rightarrow TS(\mathbf{17}\rightarrow\mathbf{18}) \rightarrow [H_3C^-\cdots CH_3COCH_3]\ (\mathbf{18})$$
$$\rightarrow TS(\mathbf{18}\rightarrow\mathbf{19}) \rightarrow CH_2{=}C(CH_3)O^-\ (\mathbf{19a}) + CH_4\ (\mathbf{19b}). \qquad (4)$$

From Figure 4, it is seen that the G2++ barrier for the elimination of CH_4 is 146 kJ mol^{-1} (the G3 result is quite similar). This barrier height is close to that (151 kJ mol^{-1}) of reaction (3c). This CH_4 dissociation involves the methyl carbanion elimination, followed by proton abstraction on the neighboring methyl group by this carbanion. There exists no energy barrier to the proton transfer process. The structure of TS(**18**→**19**) is IMC-like, suggesting the primary isotope effect for the proton transfer step would be small. The measured values[9,12] range from 1.6 to 2.1.

Table 5: G2++ and G3 Total Energies[a] (E_0), Enthalpies (H_{298}), and Standard Heats of Formation at 0 K (ΔH°_{f0}) and 298 K (ΔH°_{f298}) of the Species Involved in the Fragmentation Reaction of $(CH_3)_3CO^-$

Species	E_0 (hartree)	H_{298} (hartree)	ΔH°_{f0} (kJ mol^{-1})	ΔH°_{f298} (kJ mol^{-1})
17	**-232.63238**	**-232.62499**	**-246.9**	**-271.8**
	-232.85894	*-232.85160*	*-236.6*	*-261.7*
				(-275 ± 12)[b]
				(-277 ± 9)[c]
18	**-232.58353**	**-232.57339**	**-118.6**	**-136.4**
	-232.80870	*-232.79908*	*-104.7*	*-123.8*
19a + 19b	**-232.63704**	**-232.62723**		
	-232.86292	*-232.85334*		
TS(**17→18**)	**-232.57681**	**-232.56737**	**-101.0**	**-120.6**
	-232.80139	*-232.79198*	*-85.5*	*-105.1*
TS(**18→ 19**)	**-232.58401**	**-232.57463**	**-119.9**	**-139.6**
	-232.80862	*-232.79991*	*-104.5*	*-126.0*

[a]G2++ energies are shown in bold font, and G3 energies are in italic font.
[b] Experimental value, taken from ref 42, is given in bracket.
[c] Experimental value, taken from ref 43, is given in bracket.

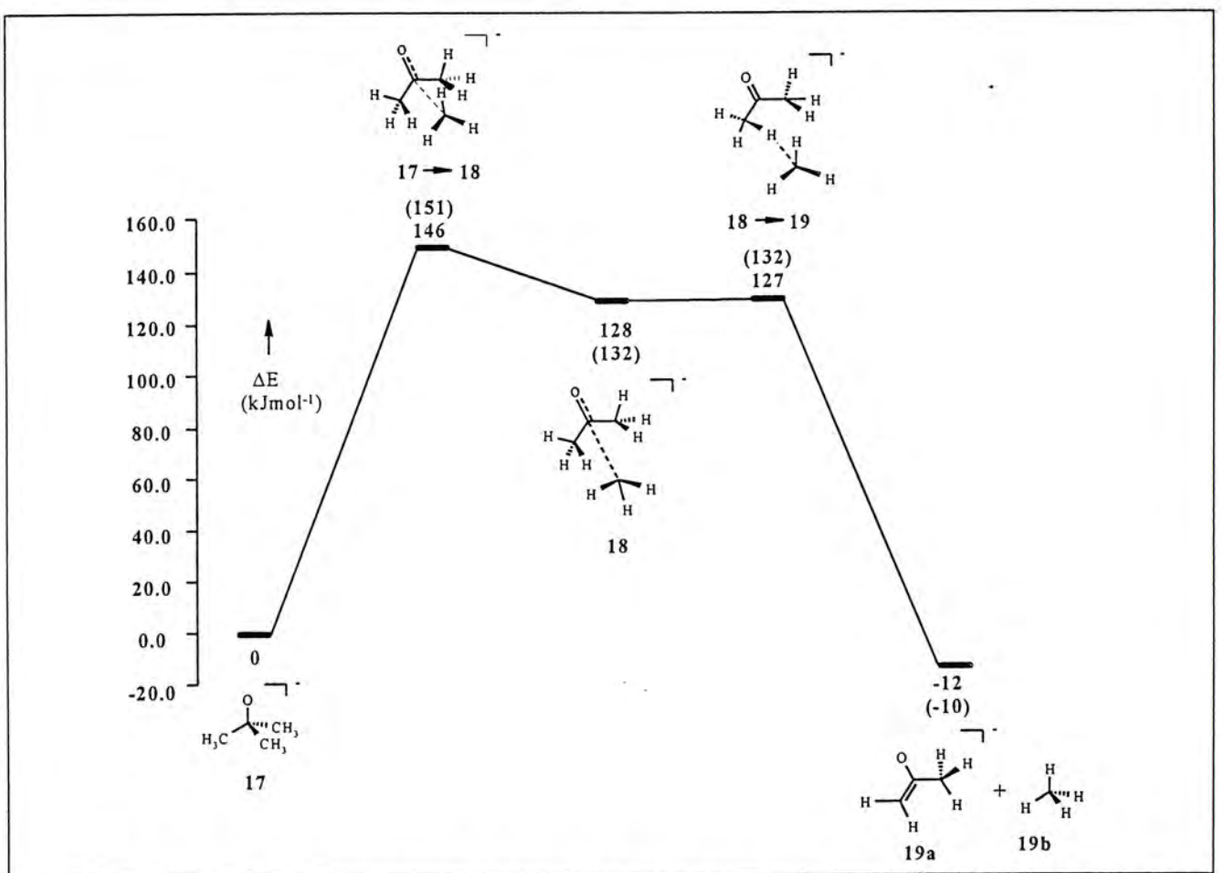

Figure 4. The G2++ energy profiles of the dissociation for $(CH_3)_3CO^-$ (**17**). The G3 relative energies are given in brackets.

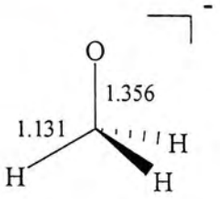

1, C_{3v}

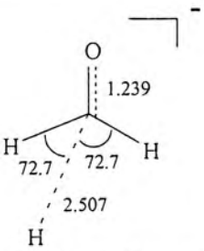

TS(**1** → **2**), C_s

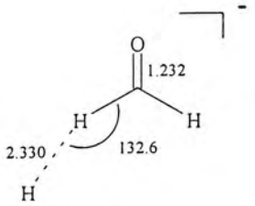

2, C_s

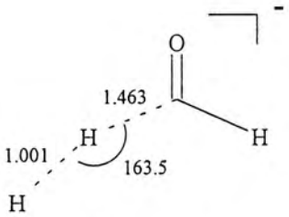

TS(**2** → **3**), C_s

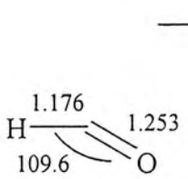

3a, C_s + 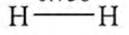

3b, $D_{\infty h}$

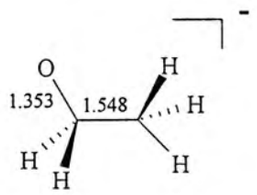

4, C_s

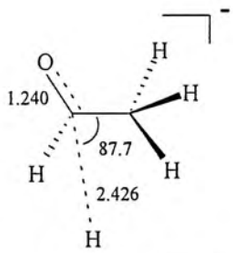

TS(**4** → **5**), C_1

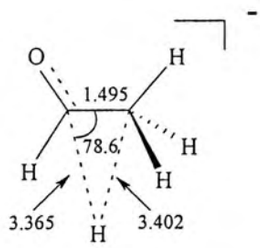

5, C_1

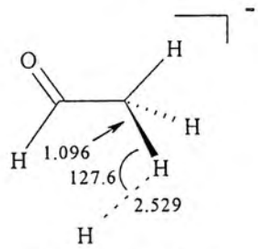

TS(**5** → **6**), C_1

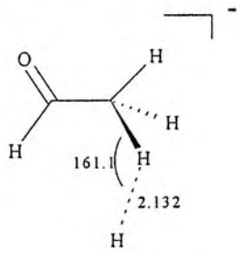

6, C_1

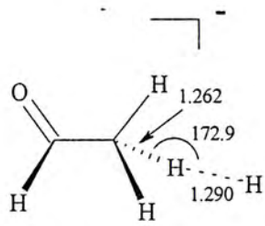

TS(**6** → **7**), C_1

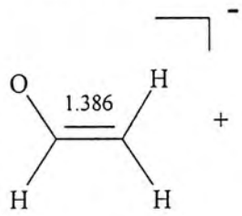

7a, C_s + 

7b, $D_{\infty h}$

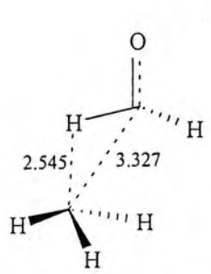

TS(**4** → **8**), C_1

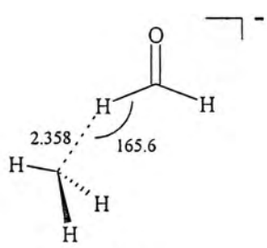

8, C_1

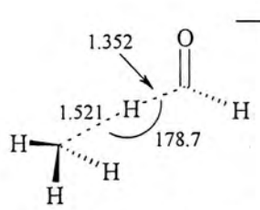

TS(**8** → **9**), C_1

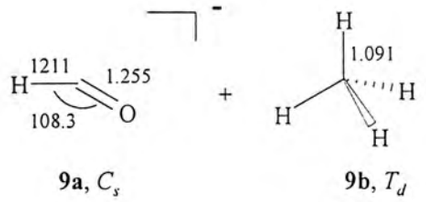

9a, C_s **9b**, T_d

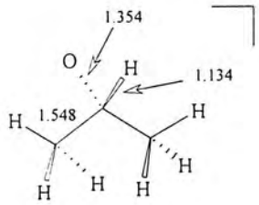

10, C_s

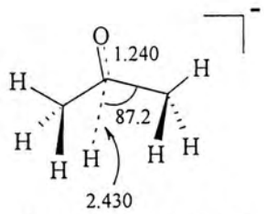

TS(**10** → **11**), C_1

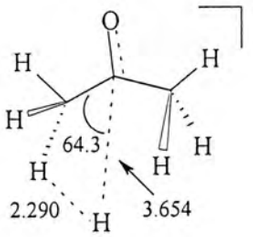

11, C_1

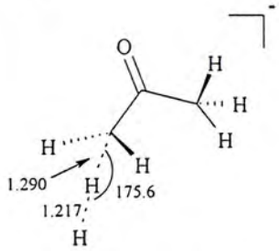

TS(**11** → **12**), C_1

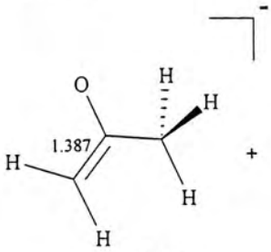

12a, C_s **12b**, $D_{\infty h}$

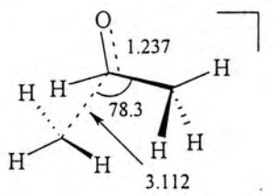

TS(**10** → **13**), C_1

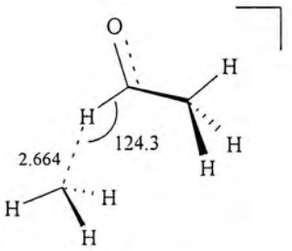

13, C_1

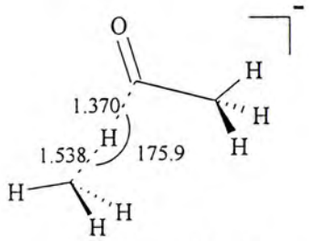

TS(**13** → **14**), C_1

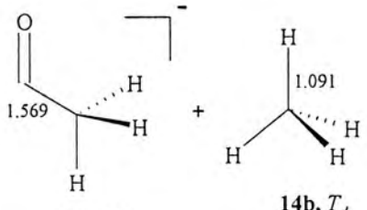

14a, C_s **14b**, T_d

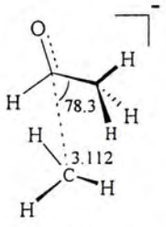

TS(**10** → **15**), C_1

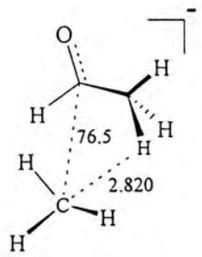

15, C_1

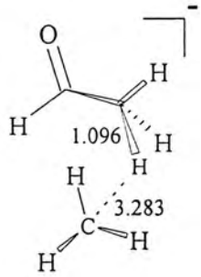

TS$_1$(**15** → **16**), C_1

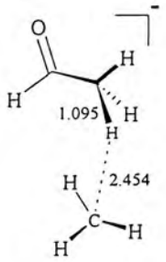

TS$_2$(**15** → **16**), C_1

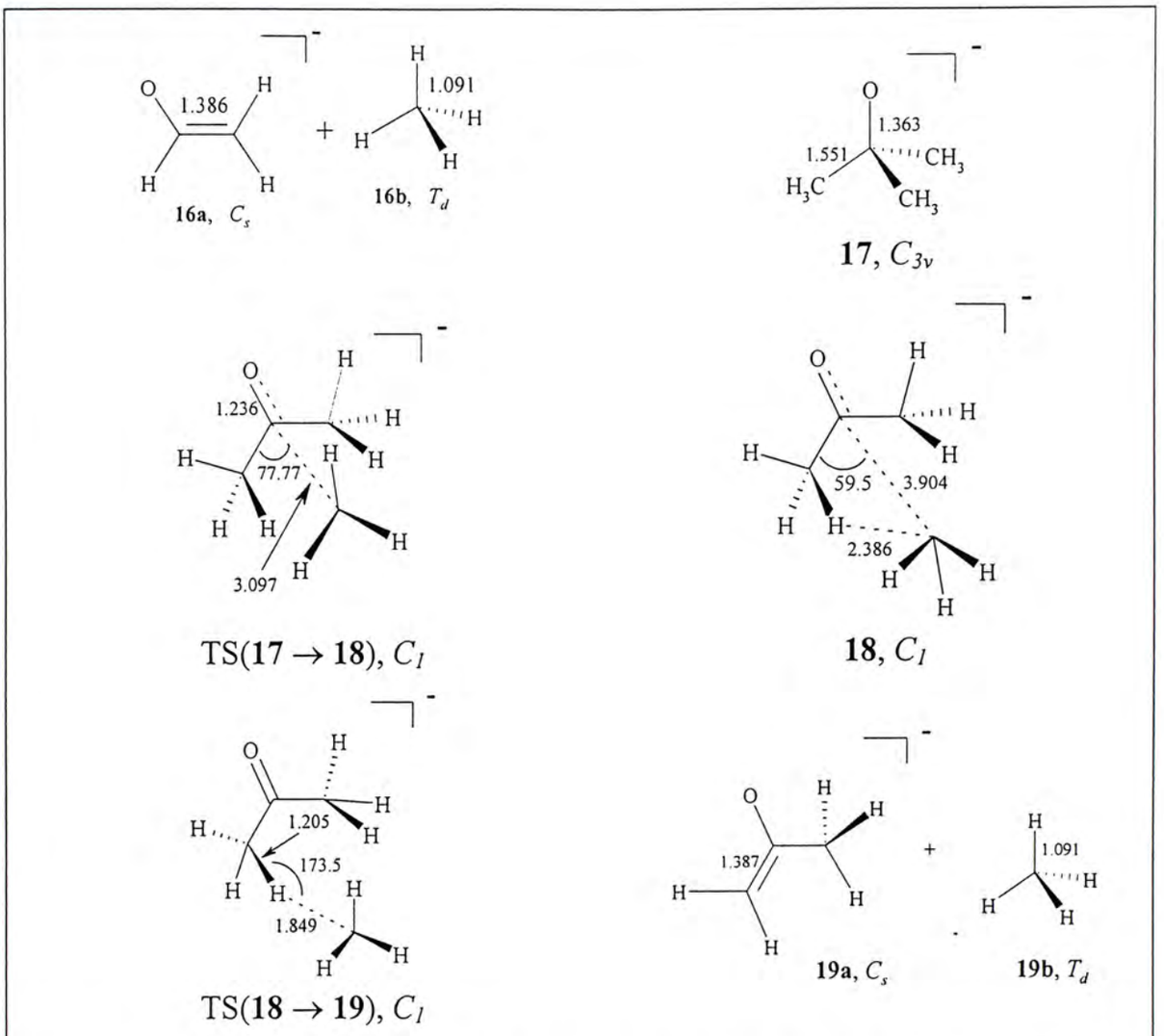

Figure 5. Optimized structures of all the species involved in the fragmentation reactions of the four alkoxide anions studied in this work. All the structures were optimized at the MP2(Full)/6-31++G(d) level.

In passing, it is noted that the calculated G2++/G3 heats of formation for the four alkoxide anions studied (**1**, **4**, **10**, and **17**) are in very good accord with the experimental data available in the literature. In particular, the excellent agreement between the G2++ and the experimental results is especially noticeable. Such an agreement should give credence to the other reported energies such as the energies and activation barriers of the reactions studied in this work.

2.4 Conclusions

The dissociation mechanisms of four simple alkoxide anions, CH_3O^- (**1**), $CH_3CH_2O^-$ (**4**), $(CH_3)_2CHO^-$ (**10**), and $(CH_3)_3CO^-$ (**17**), were studied by the ab initio G2++ and G3 methods. For each anion, the calculated heat of reaction for the heterolytic dissociation was found to be smaller than that of the homolytic one. This

result shows that the decomposition reactions should start with heterolytic bond cleavage.

Based on our calculated results, it is concluded that the dissociation of these alkoxide anions should proceed via a stepwise mechanism: H_2 dissociation from an alkoixde anion starts with hydride anion elimination, followed by proton abstraction by the hydride anion. Similarly, CH_4 dissociation from an alkoxide anion starts with methyl carbanion elimination, followed by proton abstraction by the carbanion. Between the hydride/carbanion elimination and proton abstraction, an IMC intermediate is formed.

For the fragmentation pathways of (**4**) and of (**10**), 1,2-H_2 elimination has a lower energy barrier than 1,1- or 1,2-CH_4 eliminations. The overall energy barriers of 1,1-elimination reactions studied range from 160 to 170 kJ mol^{-1}. 1,2-H_2 eliminations have barrier range of 126 to 128 kJ mol^{-1} and 1,2-CH_4 eliminations have barrier height (146-151 kJ mol^{-1}) in between those of 1,1-CH_4 and 1,2-H_2 eliminations. These results are in accord with the CAD[2,9] and IRMP[11] studies of **4** that only H_2 elimination is observed. The calculated results are also in line with the low-energy CAD study[2] of **10** that 1,2-H_2 elimination is the dominant channel observed among its fragmentation pathways. Elimination of CH_4 from **10** increases as collision energy increases.[2] It has two plausible pathways: 1,1- and 1,2-elimination mechanisms. Our calculated results suggest that the occurrence of the 1,2-elimination pathway should be dominant over the 1,1-elimination pathway, in accord with the experimental results[2] that CD_4 and HD are observed from CAD study of $(CD_3)_2CHO^-$.

In addition, the calculated G2++/G3 heats of formation of these alkoxide anions, (**1**), (**4**), (**10**), and (**17**) are in excellent agreement with available experimental data. The use of the basis set 6-31G(d) may be inadequate in characterizing IMC structures having a H^- fragment. Overall, the G3 results, which are based on MP2(full)/6-31G(d) structures, are qualitatively comparable to the G2++ results although the PES landscape calculated at the G3 level for reaction (2a) is qualitatively different from that obtained at the G2++ level.

If an alkoxide anion is represented by the general formula $(R^1)(R^2)(R^3)CO^-$, the anions studied in this work are the special cases with R^1, R^2, R^3 = H or CH_3. Currently under investigation are the anions with R^1, R^2, R^3 = CH_3, C_2H_5, or *i*-Pr.

With these systems, steric effects as well as electronic effects will be the controlling factors for their decomposition reactions.

2.5 Publication Note

An article based on the results reported in this Chapter has now appeared *in J. Phys. Chem. A* **2001**, *105*, 432.

2.6 References

1. Hass, J. M.; Harrison, A.G. *Int. J. Mass Spectrom. Ion Proc.* **1993**, *124*, 115.
2. Mercer, R. S.; Harrison, A.G. *Can. J. Chem.* **1988**, *66*, 2947.
3. Raftery, M. J.; Bowie, J. H.; Sheldon, J. C. *J. Chem. Soc., Perkin Trans. 2* **1988**, 563.
4. Eichinger, P. C. H.; Bowie, J. H. *J. Chem. Soc., Perkin Trans. 2* **1988**, 497.
5. Eichinger, P. C. H.; Bowie, J. H.; Blumenthal, T. *J. Org. Chem.* **1986**, *51*, 5078.
6. Sheldon, J. C.; Bowie, J. H.; Lewis, D. E. *New. J. Chem.* **1988**, *12*, 269.
7. Tumas, W.; Foster, R. F.; Pellerite, M. J.; Brauman, J. I. *J. Am. Chem. Soc.* **1984**, *106*, 4053.
8. Tumas, W.; Foster, R. F.; Pellerite, M. J.; Brauman, J. I. *J. Am. Chem. Soc.* **1983**, *105*, 7464.
9. Hayes, R. N.; Sheldon, J. C.; Bowie, J. H.; Lewis, D. E. *Aust. J. Chem.* **1985**, *38*, 1197.
10. Hayes, R. N.; Sheldon, J. C.; Bowie, J. H.; Lewis, D. E. *J. Chem. Soc., Chem. Commun.* **1984**, 1431.
11. Tumas, W.; Foster, R. F.; Brauman, J. I. *J. Am. Chem. Soc.* **1988**, *110*, 2714.
12. Tumas, W.; Foster, R. F.; Pellerite, M. J.; Brauman, J. I. *J. Am. Chem. Soc.* **1987**, *109*, 961.
13. Mercer, R. S.; Harrison, A. G. *Org. Mass Spectrom.* **1987**, *22*, 710.
14. Chiu, S.-W.; Lau, K.-C.; Li, W.-K. *J. Phys. Chem. A.* **1999**, *103*, 6003.
15. Mestres, J.; Duran, M.; Bertran, J.; Csizmadia, I. G. *J. Mol. Struct.(Theochem)* **1995**, *358*, 229.
16. Wiberg, K. B. *J. Am. Chem. Soc.* **1990**, *112*, 3379.
17. McAdoo, D. J. *Mass Spectrom. Rev.* **1988**, *7*, 363.
18. Frisch, M. J.; Trucks, G. W.; Schlegel, H. B.; Gill, P. M. W.; Johnson, B. J.; Robb, M. A.; Cheeseman, J. R.; Keith, T. A.; Petersson, G. A.; Montgomery, J.

A.; Raghavachari, K.; Al-Laham, M. A.; Zarkrewski, V. G.; Ortiz, J. V.; Foresman, J. B.; Cioslowski, J.; Stefanov, B. B.; Nanayakkara, A.; Challacombe, M.; Peng, C. Y.; Ayala, P. Y.; Chen, W.; Wong, M. W.; Andres, J. L.; Replogle, E. S.; Gomperts, R.; Martin, R. L.; Fox, D. J.; Binkley, J. S.; Defrees, D. J.; Baker, J.; Stewart, J. J. P.; Head-Gordon, M.; Gonzalez, C.; Pople, J. A. *GAUSSIAN* 94, Revision D4; Gaussian, Inc., Pittsburgh, PA, 1995.

19. Frisch, M. J.; Trucks, G. W.; Schlegel, H. B.; Scuseria, G. E.; Robb, M. A.; Cheeseman, J. R.; Zakrzewski, V. G.; Montgogery, J. A.; Jr.; Stratmann, R.E.; Burant, J. C.; Dapprich, S.; Millam, J. M.; Daniels, A. D.; Kudin, K. N.; Strain, M. C.; Farkas, O.; Tomasi, J.; Barone, V.; Cossi, M.; Cammi, R.; Mennucci, B.; Pomelli, C.; Adamo, C.; Clifford, S.; Ochterski, J.; Petersson, G. A.; Ayala, P. Y.; Cui, Q.; Morokuma, K.; Malick, D. K.; Rabuck, A. D.; Raghavachari, K.; Foresman, J. B.; Cioslowski, J.; Ortiz, J. V.; Baboul, A. G.; Stefanov, B. B.; Liu, G.; Liashenko, A.; Piskorz, P.; Komaromi, I.; Gomperts, R.; Martin, R. L.; Fox, D. J.; Keith, T.; Al-Laham, M. A.; Peng, C. Y.; Nanayakkara, A.; Gonzalez, C.; Challacombe, M.; Gill, P. M. W.; Johnson, B.; Chen, W.; Wong, M. W.; Andres, J. L.; Gonzalez, C.; Head-Gordon, M.; Replogle, E. S.; Pople, J. A. *GAUSSIAN 98*, Revision A.7; Gaussian, Inc., Pittsburgh PA, 1998.
20. Curtiss, L. A.; Raghavachari, K.; Redfern, P. C.; Redfern V.; Pople, J. A. *J. Chem. Phys.* **1998**, *109*, 7764.
21. Morton, T. H. *Org. Mass Spectrom.* **1992**, *27*, 353.
22. Bowen, R. D. *Acc. Chem. Res.* **1991**, *24*, 364.
23. Moylan, C. R.; Brauman, J. I.; *J. Am. Chem. Soc.* **1985**, *107*, 761.
24. Audier, H. E.; Bouchoux, G.; McMahon, T. B.; Milliet, A.; Vulpius, T. *Org. Mass Spectrom.* **1994**, *29*, 176.
25. Nguyen, M. T.; Bouchoux, G. *J. Phys. Chem.* **1996**, *100*, 2089.
26. Wang, D.; Squires, R. B. *Int. J. Mass Spectrom. Ion Processes Rev.* **1991**, *107*, 7.
27. Heinrich,N.; Louage, F.; Lifshitz, C.; Schwarz, H. *J. Am. Chem. Soc.* **1988**, *110*, 8183.
28. Chronister E. L.; Morton, T. H. *J. Am. Chem. Soc.* **1990**, *112*, 133.

29. Chiu, S. W.; Cheung, Y. S.; Ma, N. L.; Li, W. K.; Ng, C. Y. *J. Molec. Structure (Theochem)* **1999**, *468*, 21.

30. McAdoo, D. J.; Traeger, J. C.; Hudson, C. E.; Griffin, L. L. *J. Chem. Phys.* **1988**, *92*, 9524.

31. Kebarle, P. *Ann. Rev. Phys. Chem.* **1977**, *28*, 445.

32. Hammerum, I. S.; Hansen, M. M.; Audier, H. E. *Int. J. Mass Spectrom.* **1977**, *160*. 183.

33. Dewar, M. J. S. *J. Am. Chem. Soc.* **1984**, *106*, 209.

34. Gajewsk, J. *Acc. Chem. Res.* **1980**, *13*, 142.

35. Cheung, Y.-S.; Li, W.-K.; Ng, C. Y. *J. Mol. Struct. (THEOCHEM)* **1995**, *339*, 25.

36. Sims, L. B.; Burton, B. W.; Lewis, D. W. *Quant. Chem. Program Exch.* No. 337, **1977**.

37. Hudson, C. E.; McAdoo, D. J. *Int. J. Mass Spectrom. Ion Processes* **1984**, *59*, 325.

38. Chiu, S.-W.; Lau, K.-C.; Li, W.-K.; Ma, N. L.; Cheung, Y.-S.; Ng, C.Y.; *J. Molec. Structure (Theochem)* **1999**, *490*, 109.

39. **NIST Chemistry WebBook, NIST Standard Reference Database Number 69**, Eds. W. G. Mallard and P.J. Linstrom, November 1998, National Institute of Standards and Technology, Gaithersburg MD, 20899 (http://webbook.nist.gov).

40. Melander, L.;Saunders, W. H. *Reactions of Isotopic Molecules*, Wiley, New Yord, **1980**.

41. Li, W.-K. *J. Chem. Educ.* **1994**, *71*, 1094.

42. Lias, S. G.; Bartmess, J. E.; Liebman, J. F.; Holmes, J. L.; Levin, R. D.; Mallard, W. G. *J. Phys. Chem. Ref. Data* **1988**, *17* (Suppl.1).

43. Haas, M. J.; Harrison, A. G. *Int. J. Mass Spectrom. Ion. Processes* **1993**, *124*, 115.

Chapter 3

A Gaussian–2 and Gaussian–3 Study of Alkoxide Anion Decompositions. II. Alkane Eliminations of $(CH_3)_2(C_2H_5)CO^-$ and $(i\text{-Pr})(C_2H_5)_2CO^-$

Abstract

The energetics and decomposition mechanisms of $(CH_3)_2(C_2H_5)CO^-$ and $(i\text{–Pr})(C_2H_5)_2CO^-$ have been studied at the G2++, G3, and G3(MP2) levels of theory. It is found that the energies require for methane elimination of $(CH_3)_2(C_2H_5)CO^-$ is less than that for ethane elimination, in agreement with experiment. On the other hand, the energies require for ethane and propane eliminations of $(i\text{–Pr})(C_2H_5)_2CO^-$ are comparable. So both eliminations are equally likely, again in accord with experiment.

The alkane dissociation mechanism of the tertiary alkoxide anions is similar to the methane elimination of primary and secondary alkoxides. It starts with dissociation of a carbanion, followed by proton abstraction to form an alkane molecule. An ion-molecular complex is formed as intermediate.

3.1 Introduction

The decomposition of alkoxide anions have been studied to a fairly extensive extent both experimentally[1-9] and theoretically.[10-12] The dissociation mechanism of simple alkoxide anions have been investigated by collision-activated dissociation (CAD) which showed that the elimination of alkoxide anions should proceed via a stepwise pathway.[1-7] Besides, the technique of infrared multiple photon (IRMP) photodissociation has also been applied to study these dissociations.[8,9] Brauman and his co-workers further suggested that the initial bond breaking involved in the dissociation of alkoxide anions should be heterolytic rather than homolytic.[8] On the other hand, different levels of theory have also been employed to study the energetics and mechanisms on the hydrogen and methane eliminations of alkoxide anions.[10-12] Bowie et al[10,11] have studied the mechanism of elimination reaction of ethoxide and *tert*-butoxide anions. Also, we have recently reported[12] the energy barriers and

reaction mechanisms of hydrogen and methane elimination of several simple alkoxide anions at the G2++[13] and G3[14] levels of theory. All of these findings are consistent with the results reported from experiments. However, it appears that there is a lack of theoretical study on the methane, ethane, and propane eliminations from tertiary alkoxide anions, and this is the subject we take up in this work.

Here we study the following alkane eliminations of $(CH_3)_2(C_2H_5)CO^-$ and $(i\text{–Pr})(C_2H_5)_2CO^-$ at a high theoretical level:

$$(CH_3)_2(C_2H_5)CO^- \rightarrow CH_3CH{=}C(CH_3)O^- + CH_4 \quad (1a)$$

$$(CH_3)_2(C_2H_5)CO^- \rightarrow CH_2{=}C(C_2H_5)O^- + CH_4 \quad (1b)$$

$$(CH_3)_2(C_2H_5)CO^- \rightarrow CH_2{=}C(CH_3)O^- + C_2H_6 \quad (1c)$$

$$(i\text{–Pr})(C_2H_5)_2CO^- \rightarrow CH_3CH{=}C(C_2H_5)O^- + C_3H_8 \quad (2a)$$

$$(i\text{–Pr})(C_2H_5)_2CO^- \rightarrow (CH_3)_2C{=}C(C_2H_5)O^- + C_2H_6 \quad (2b)$$

This study attempts to answer some of the questions raised in our previous paper[12] regarding alkoxide anion dissociations: (1) When the anions are tertiary alkoxides, do their dissociations proceed via a stepwise or a concerted mechanism? (2) Why is the heterolytic cleavage more favorable than the homolytic one, as deduced from experimental results? Also, we will attempt to draw a conclusion on the dissociation mechanisms of primary, secondary, and tertiary alkoxide anions. Besides, the relative reactivities of leaving groups, including H, CH_3, C_2H_5, and *i*-Pr, in the alkoxide anions are also discussed.

3.2 Methods of Calculations

All the calculations were carried out on DEC 500au, XP900, XP1000, as well as on an SGI Origin 2000 High-Performance Server, using he Gaussian 94[15] and Gaussian 98[16] packages of programs. The computational models we employed for $(CH_3)_2(C_2H_5)CO^-$ were the modified Gaussian–2 (G2++)[13] and Gaussian–3 (G3)[14] levels of theory. Due to the large size of the $(i\text{–Pr})(C_2H_5)_2CO^-$ system, a less expensive derivative of the G3 method, G3(MP2),[17] was employed for all the stable and transition structures involved in the dissociation channels.

3.3 Results and Discussion

The heterolytic and homolytic bond dissociation energies of the alkoxide anions $(CH_3)_2(C_2H_5)CO^-$ (**1**) and $(i\text{–Pr})(C_2H_5)_2CO^-$ (**7**) are summarized in Table 1.

The G2++ and G3 standard heats of formation for the species involved in reactions (1a), (1b), and (1c) at 0 and 298 K are listed in Table 2, while the G3(MP2) results for the species involved in reactions (2a) and (2b) are given in Table 3. Also, the energy profiles for these four dissociation reactions are displayed in Figures 1 and 2. The equilibrium geometries for all the stable and transition structures are illustrated in Figure 3. Throughout this work, G2++ and G3MP2 energies are used for discussion unless explicitly stated otherwise.

TABLE 1: Heterolytic and Homolytic Bond Dissociation Energies of Various Alkoxide Anions at the G3 Level[a,b]

$(C_2H_5)(CH_3)C{=}O + CH_3^-$	←	$(CH_3)_2(C_2H_5)CO^-$ (**1**)	→	$(C_2H_5)(CH_3)C{=}O^- + {}^\bullet CH_3$
200.4		0		287.2
$(CH_3)_2C{=}O + C_2H_5^-$	←	$(CH_3)_2(C_2H_5)CO^-$ (**1**)	→	$(CH_3)_2C{=}O^- + {}^\bullet C_2H_5$
224.3		0		296.0
$(i\text{-Pr})(C_2H_5)C{=}O + C_2H_5^-$	←	$(i\text{-Pr})(C_2H_5)_2CO^-$ (**7**)	→	$(i\text{-Pr})(C_2H_5)C{=}O^- + {}^\bullet C_2H_5$
209.5		0		264.1
$(C_2H_5)_2C{=}O^- + i\text{-Pr}^-$	←	$(i\text{-Pr})(C_2H_5)_2CO^-$ (**7**)	→	$(C_2H_5)_2C{=}O^- + {}^\bullet i\text{-Pr}$
197.8		0		263.4

[a]The species shown in the first column re the products of a heterolytic cleavage of the alkoxide anions given in the middle column; those given in the last column are the products of a homolytic cleavage.
[b]The values for **7** and all the related species are calculated at the G3(MP2) level.

3.3.1 Initial bond cleavage of alkoxide anions. As mentioned in our previous paper,[12] the dissociation of alkoxide anions are mediated by ion–neutral complexes (INCs). We can determine whether the reaction is dominated by ion–molecular complexes (IMCs) or ion–radical complexes (IRCs) when we compare the energetics for the heterolytic and homolytic pathways. From Table 1, it is seen that all the heterolytic cleavages require less energies than their homolytic counterparts. So, we can simply conclude that, for alkoxide anion dissociations, the heterolytic bond cleavage is more favorable than the homolytic one. In other words, the reaction starts with heterolytic bond cleavage to form the carbanion rather than homolytic bond cleavage to form the alkyl radical. Based on these results, we infer that the INCs involved in the dissociations studied in this work are IMCs rather than IRCs. These results are consistent with our previous study. In the homolytic bond cleavage process, two open–shell species, i.e. radicals, are formed, while the

heterolytic cleavage forms two close–shell species. It is generally held that close–shell species should be more stable than the open–shell ones. So, it is not surprising that the heterolytic cleavage is more favorable than the homolytic one in the dissociation of an alkoxide anion.

TABLE 2: G2++ and G3 Total Energies[a] (E_0), Enthalpies ($H298$), and Standard Heats of Formation at 0 K ($\Delta H_f^\circ{}_0$) and 298 K ($\Delta H_f^\circ{}_{298}$) of the Species Involved in the Fragmentation Reaction of $(CH_3)_2(C_2H_5)CO^-$ (1)

species	E_0 (hartree)	H_{298} (hartree)	ΔH°_{f0} (kJ mol^{-1})	ΔH°_{f298} (kJ mol^{-1})
1	**-271.86028**	**-271.85153**	**-267.9**	**-298.3**
	-272.13111	*-272.12251*	*-255.0*	*-285.9*
				(-300 ± 13)[b]
				(-300 ± 8.8)[c]
2	**-271.80964**	**-271.79810**	**-134.9**	**-158.0**
	-272.08140	*-272.06997*	*-124.5*	*-148.0*
3a + 3b	**-271.86296**	**-271.85155**		
	-272.13394	*-272.12288*		
4a + 4b	**271.86325**	**271.85233**		
	-272.13418	*-272.12345*		
5	**-271.80172**	**-271.79083**	**-114.1**	**-139.0**
	-272.07025	*-272.05961*	*-95.3*	*-120.8*
6a + 6b	**-271.85653**	**-271.84608**		
	-272.12743	*-272.11725*		
TS(**1**→**2**)	**-271.80523**	**-271.79423**	**-123.3**	**-147.9**
	-272.07684	*-272.06594*	*-112.6*	*-137.4*
TS(**2**→**3**)	**-271.81082**	**-271.79976**	**-138.0**	**-162.4**
	-272.08309	*-272.07213*	*-129.0*	*-153.6*
TS(**2**→**4**)	**-271.80999**	**-271.79922**	**-135.8**	**-161.0**
	-272.08229	*-272.07162*	*-126.9*	*-152.3*
TS(**1**→**5**)	**-271.79507**	**-271.78446**	**-96.6**	**-122.2**
	-272.06365	*-272.05326*	*-77.9*	*-104.1*
TS(**5**→**6**)	**-271.80230**	**-271.79212**	**-115.6**	**-142.3**
	-272.07082	*-272.06105*	*-96.7*	*-124.5*

[a] G2++ energies are shown in bold font, and G3 energies are in italic font.
[b] Experimental value, taken from ref 19, is given in brackets.
[c] Experimental value, taken from ref 20, is given in brackets.

3.3.2 Dissociation of alkoxide anions.

Dissociation of $(CH_3)_2(C_2H_5)CO^-$ (1). As shown in Figure 1, there are three possible dissociations for **1**. They are the 1,2–elimination of methane and 1,2–elimination of ethane:

$$(CH_3)_2(C_2H_5)CO^- \text{ (1)} \rightarrow \text{TS(1}\rightarrow\text{2)} \rightarrow [H_3C^- \cdots (CH_3)(C_2H_5)CO] \text{ (2)}$$

$\rightarrow$ TS(**2**$\rightarrow$**3**) $\rightarrow$ $CH_3CH{=}C(CH_3)O^-$ (**3a**) + CH_4 (**3b**) (1a)

$(CH_3)_2(C_2H_5)CO^-$ (**1**) $\rightarrow$ TS(**1**$\rightarrow$**2**) $\rightarrow$ [$H_3C^-\cdots(CH_3)(C_2H_5)CO$] (**2**)

$\rightarrow$ TS(**2**$\rightarrow$**4**) $\rightarrow$ $CH_2{=}C(C_2H_5)O^-$ (**4a**) + CH_4 (**4b**) (1b)

$(CH_3)_2(C_2H_5)CO^-$ (**1**) $\rightarrow$ TS(**1**$\rightarrow$**5**) $\rightarrow$ [$H_5C_2^-\cdots(CH_3)_2CO$] (**5**)

$\rightarrow$ TS(**5**$\rightarrow$**6**) $\rightarrow$ $CH_2{=}C(CH_3)O^-$ (**6a**) + C_2H_6 (**6b**) (1c)

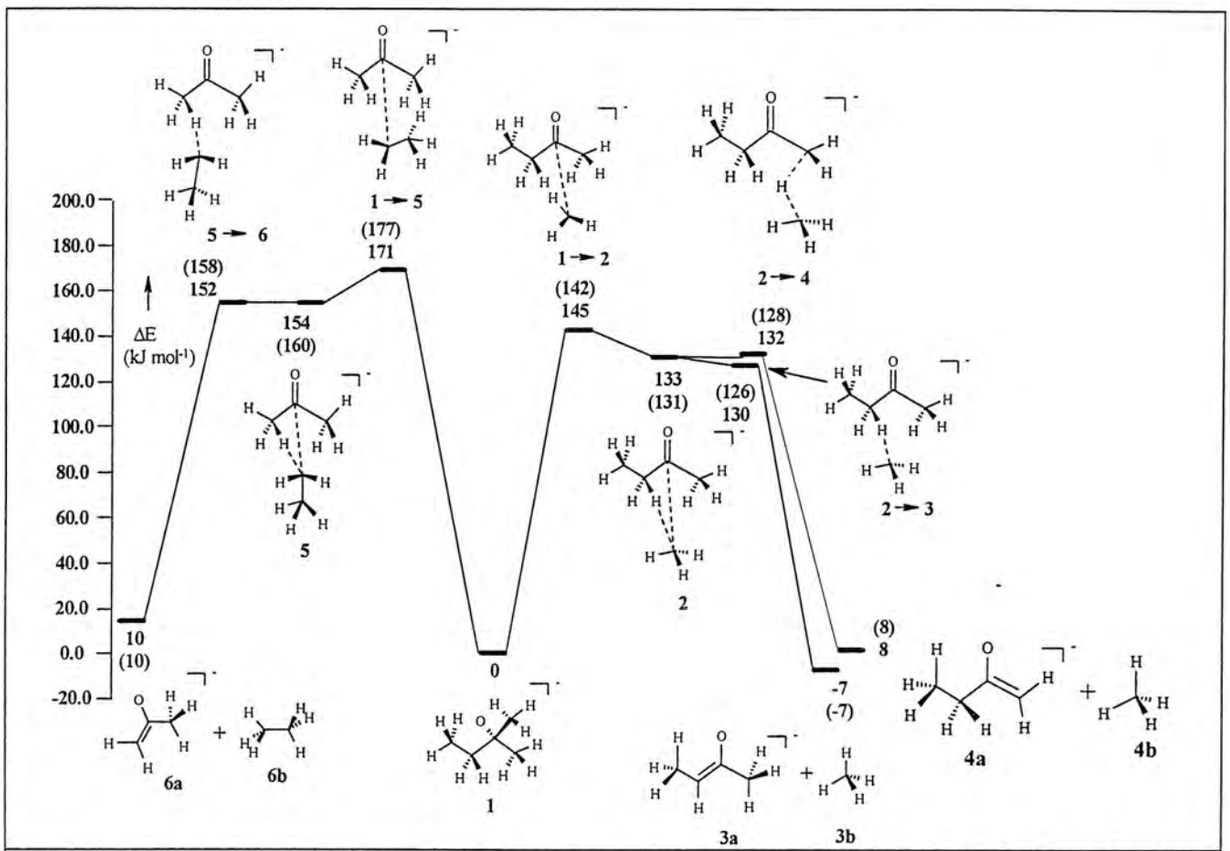

Figure 1. G2++ energy profiles of the dissociations for $(CH_3)_2(C_2H_5)CO^-$ (**1**). The G3 relative energies are given in parentheses.

It is noted that, in the G3 calculations of reactions (1a) and (1b), the structures of TS(**1**$\rightarrow$**2**), **2**, TS(**2**$\rightarrow$**3**), and TS(**2**$\rightarrow$**4**) were optimized at the MP2(Full)/6-31++G(d) level since only TS(**1**$\rightarrow$**2**) but no **2**, TS(**2**$\rightarrow$**3**), and TS(**2**$\rightarrow$**4**) were located in the MP2(Full)/6-31G(d) level. It is known that the use of diffuse functions is very important in the geometry optimization and energy calculations for the anions. Although **1** is a tertiary alkoxide anion, it is still possible for it to undergo hydrogen elimination via IMC [$H^-\cdots c$-$CH_2C(C_2H_5)(CH_3)O$], i.e., **1** $\rightarrow$ [$H^-\cdots c$–$CH_2C(C_2H_5)(CH_3)O$] $\rightarrow$ H_2 + $C_5H_9O^-$ [c-$CHC(C_2H_5)(CH_3)O^-$ or $(C_2H_5)(CH_3)C{=}CHO^-$]. However, as we discussed in our previous paper,[12] we have concluded that this kind of reaction is energetically noncompetitive to reactions

studied in this work. From Figure 1, it is seen that the 1,2–elimination of methane starts with methyl anion dissociation, followed by proton abstraction to form the methane molecule. On the other hand, the 1,2–elimination of ethane starts with ethyl anion dissociation, followed by proton abstraction to form the ethane molecule. Both of these pathways involve the formation of IMC intermediates. In other words, the dissociations proceed through stepwise pathways.

From the G2++ potential energy curves for reactions (1a), (1b), and (1c), the overall barrier for either of the two CH_4 eliminations is 145 kJ mol^{-1}, while that for the elimination of ethane is 171 kJ mol^{-1}. In other words, the eliminations of methane are more favorable by 26 kJ mol^{-1} (the G3 results are similar). This is indeed consistent with the results reported by Brauman and his co-workers,[8] where only methane was observed in their experiments. The G2++ (or G3) results are also in line with the low-energy CAD study[1] of **1**: methane elimination is the dominant channel observed among its dissociation pathways and elimination of ethane from **1** increases as collision energy increases.[1]

The energy barriers of reactions (1a) and (1b) are the same (145 kJ mol^{-1}). However, fragment **3a** is more stable than **4a** by 15 kJ mol^{-1}. Hence, reaction (1a) is thermodynamically more favorable than reaction (1b). In other words, among the three dissociation pathways of **1**, the elimination of methane leading to the formation of **3a** and **3b** is the most favorable.

Dissociation of (i-Pr)$(C_2H_5)_2CO^-$ (**7**). There are also two dissociations to be studied, the 1,2–elimination of ethane and 1,2–elimination of propane, as shown in Figure 2:

(i-Pr)$(C_2H_5)_2CO^-$ (**7**) → TS(**7**→**8**) →[$(CH_3)_2HC^-\cdots(C_2H_5)_2CO$] (**8**)

→ TS(**8**→**9**) → $CH_3CH{=}C(C_2H_5)O^-$ (**9a**) + C_3H_8 (**9b**) (2a)

(i-Pr)$(C_2H_5)_2CO^-$ (**7**) → TS(**7**→**10**) →[$H_5C_2^-\cdots$(i-Pr)$(C_2H_5)CO$] (**10**)

→ TS(**10**→**11**) → $(CH_3)_2C{=}C(C_2H_5)O^-$ (**11a**) + C_2H_6 (**11b**) (2b)

The dissociation mechanisms for **7** are very similar to those of **1**: elimination of ethane starts with ethyl anion elimination, followed by proton abstraction on the neighboring *iso*-propyl group. On the other hand, the elimination of propane starts with propyl anion elimination, followed by proton abstraction on the neighboring ethyl group. Both reactions involve the formation of IMC intermediates. From Figure 2, the G3(MP2) potential energy curve shows that the energy barrier for the elimination of ethane is 147 kJ mol^{-1}, while the barrier for the elimination of propane

TABLE 3: G3(MP2) Total Energies (E_0), Enthalpies ($H298$), and Standard Heats of Formation at 0 K ($\Delta H_f^\circ{}_0$) and 298 K ($\Delta H_f^\circ{}_{298}$) of the Species Involved in the Fragmentation Reaction of (i-Pr)$(C_2H_5)_2CO^-$ (6)

species	E_0 (hartree)	H_{298} (hartree)	ΔH°_{f0} (kJ mol^{-1})	ΔH°_{f298} (kJ mol^{-1})
7	-389.60248	-389.58989	-281.1	-328.7
8	-389.55188	-389.53710	-148.2	-190.1
9a + 9b	-389.60502	-389.59111		
10	-389.55481	-389.53964	-155.9	-196.8
11a + 11b	-389.60424	-389.58983		
TS(**7**→**8**)	-389.54730	-389.53318	-136.2	-179.9
TS(**8**→**9**)	-389.55099	-389.53714	-145.9	-190.2
TS(**7**→**10**)	-389.54633	-389.53205	-133.7	-176.9
TS(**10**→**11**)	-389.55667	-389.54247	-160.8	-204.2

is 145 kJ mol^{-1}. The small difference in the energy barriers suggests that both the ethane and propane eliminations of **7** are equally likely. Again, this conclusion is consistent with the results obtained by Brauman et al.[8], which indicate that almost equal amounts of ethane (45%) and propane (55%) are detected as products in the dissociation of **7**. It is worth mentioning that we have also investigated the reaction (i–Pr)$(C_2H_5)_2CO^-$ (7) → $CH_3CH{=}C(i\text{–Pr})O^-$ + C_2H_6. However, the TS involved can only be located at the HF/6–31+G(d) level, i.e. no TS is found at the MP2 level. In any event, this investigation is still on-going.

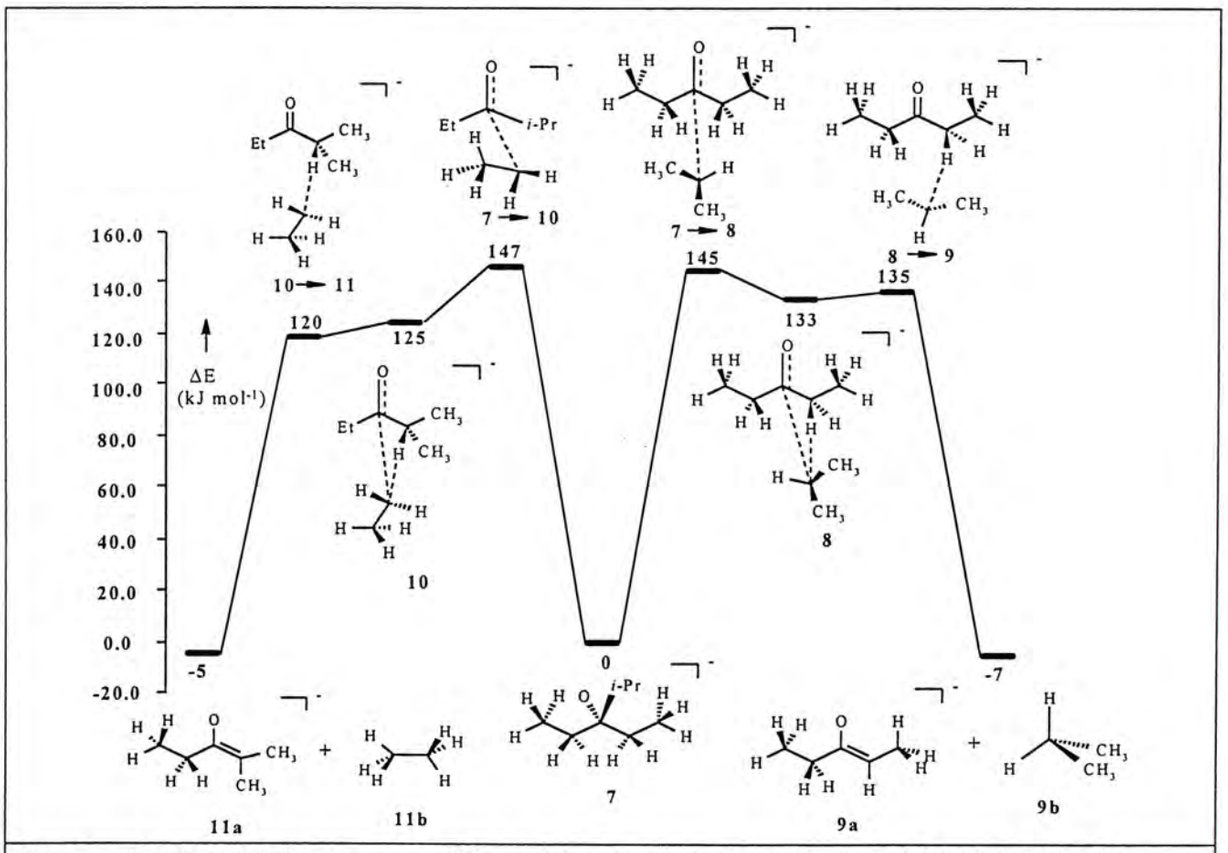

Figure 2. G3(MP2) energy profiles of the dissociations for (i-Pr)$(C_2H_5)_2CO^-$ (**6**).

3.3.3 General dissociation mechanism of alkoxide anions. In the previous work[12] and the present one, the dissociations of six alkoxide anions, CH_3O^-, $CH_3CH_2O^-$, $(CH_3)_2CHO^-$, $(CH_3)_3CO^-$, $(CH_3)_2(C_2H_5)CO^-$, and $(i\text{-Pr})(C_2H_5)_2CO^-$, have been studied at the G2++, G3, and G3(MP2) levels of theory. Based on the calculated results, it is found that the mechanisms of hydrogen and alkane eliminations are very similar. They proceed through stepwise pathways and the initial bond cleavage should be heterolytic rather than homolytic, i.e. hydride ions or carbanions are first formed in the dissociations. For the hydrogen elimination from an alkoxide anion, the reaction starts with hydride ion dissociation. Then an IMC intermediate is formed. Finally, this intermediate abstracts a proton to form a hydrogen molecule. On the other hand, alkane eliminations start with alkyl anion dissociation, followed by formation of an IMC intermediate. This intermediate then abstracts a proton to form an alkane molecule. In other words, the mechanisms for methane, ethane, and propane eliminations are very similar. It is noted that the charged (hydride ions or alkyl anions) and neutral fragments are held together by electrostatic interaction and the fragments sojourn in the vicinity of one another long enough to undergo a subsequent ion-neutral reaction.[18]

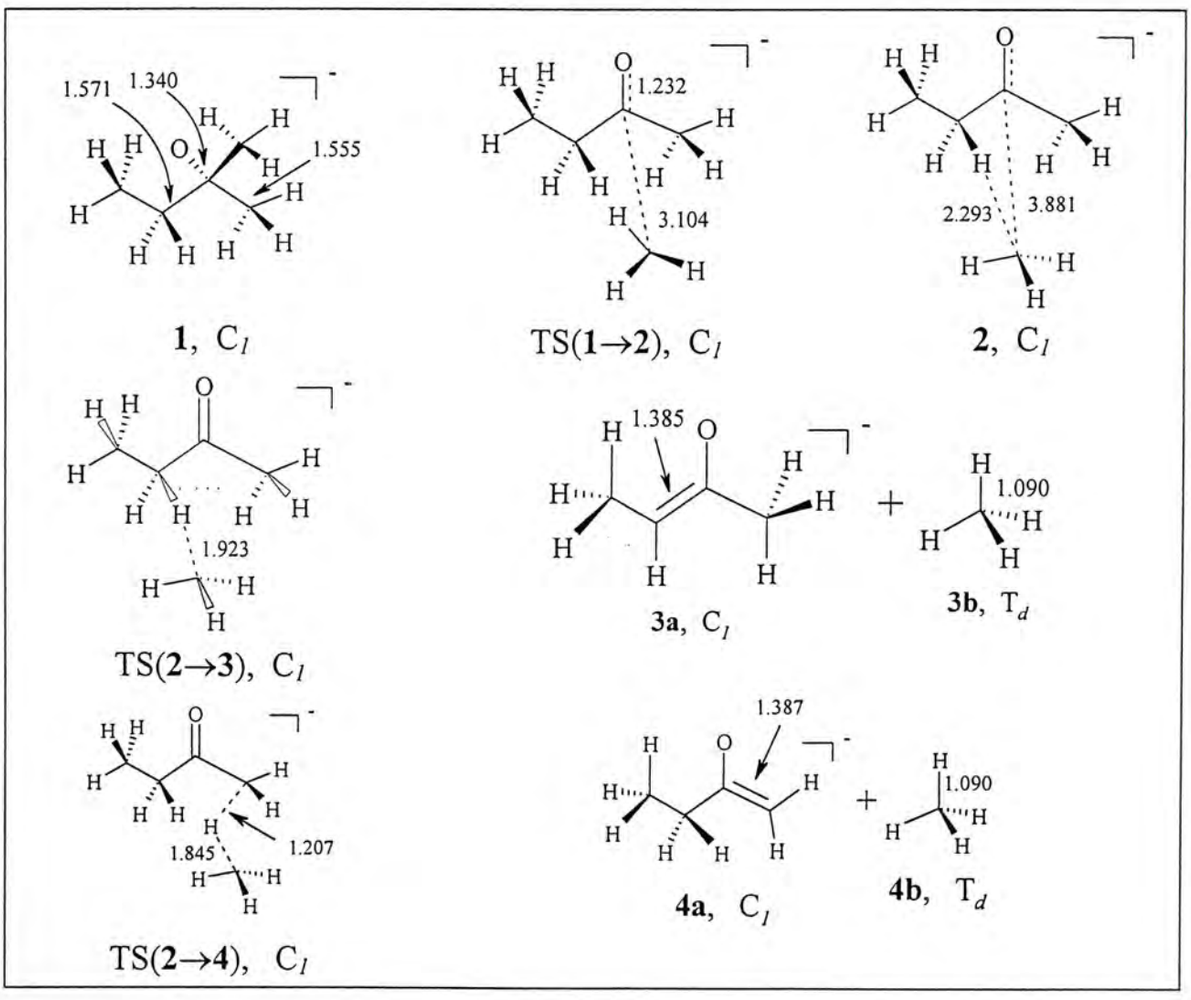

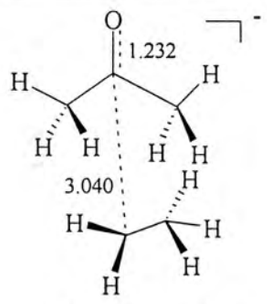

TS(**1**→**5**), C_1

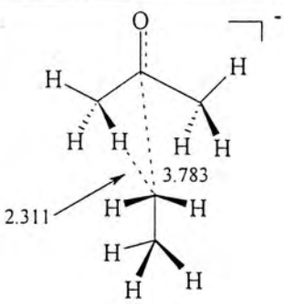

5, C_1

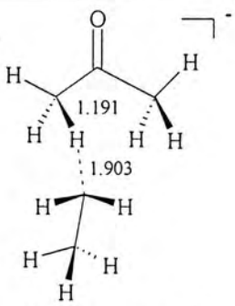

TS(**5**→**6**), C_1

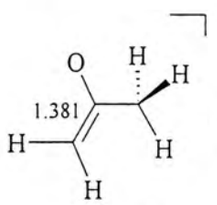

6a, C_s +

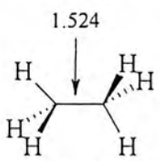

6b, D_{3d}

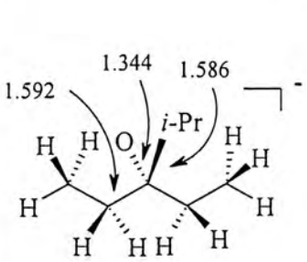

7, C_s

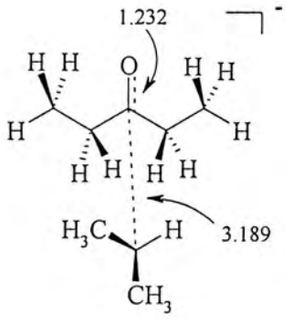

TS(**7**→**8**), C_1

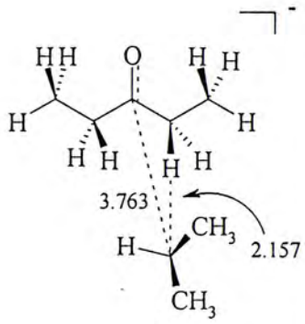

8, C_1

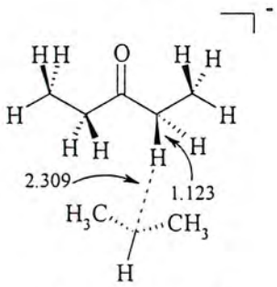

TS(**8**→**9**), C_1

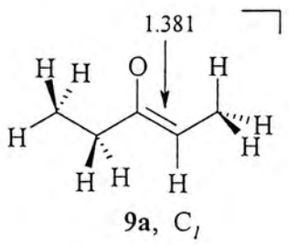

9a, C_1 +

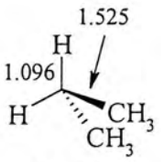

9b, C_s

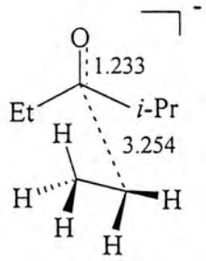

TS(**7**→**10**), C_1

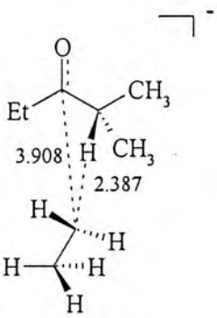

10, C_1

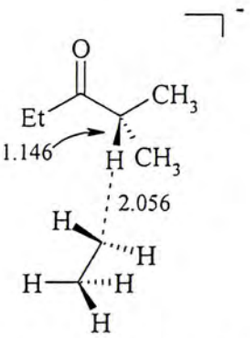

TS(**10**→**11**), C_1

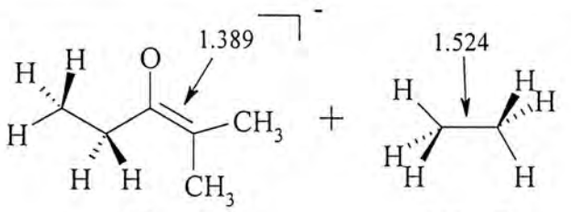

11a, C_1 **11b**, D_{3d}

Figure 3. Optimized structures of all the species involved in the fragmentation reactions of $(CH_3)_2(C_2H_5)CO^-$ (**1**) and $(i\text{-Pr})(C_2H_5)_2CO^-$ (**7**). All the structures involved with the reactions of **1** were optimized at the MP2(Full)/6–31++G(d) level. Those involved with the reactions of **7** were determined at the MP2(Full)/6–31G(d) level.

3.4 Conclusions

The dissociation mechanisms of $(CH_3)_2(C_2H_5)CO^-$ (**1**) and $(i\text{-Pr})(C_2H_5)_2CO^-$ (**7**) have been studied using the G2++, G3, and G3(MP2) levels of theory. Based on our calculated results, we found that methane elimination is more favorable than ethane elimination for **1**. On the other hand, both ethane and propane eliminations are equally likely for **7**. The dissociations of alkoxide anions proceed through a stepwise pathway and the initial bond breaking should be heterolytic rather than homolytic. The ethane elimination starts with ethyl anion elimination, followed by proton abstraction to form the ethane molecule. The propane elimination starts with propyl anion elimination, followed by proton abstraction to form the propane molecule.

The dissociation mechanisms of the primary, secondary and tertiary alkoxide anions are similar. Hydrogen elimination starts with hydride ion elimination, followed by proton abstraction to form a hydrogen molecule. Alkane elimination starts with alkyl anion elimination, followed by proton abstraction to from alkane molecule. Both of the dissociation pathways involved IMC intermediates.

3.5 References

1. Mercer, R. S.; Harrison, A.G. *Can. J. Chem.* **1988**, *66*, 2947.
2. Raftery, M. J.; Bowie, J. H.; Sheldon, J. C. *J. Chem. Soc., Perkin Trans. 2* **1988**, 563.
3. Eichinger, P. C. H.; Bowie, J. H. *J. Chem. Soc., Perkin Trans. 2* **1988**, 497.
4. Eichinger, P. C. H.; Bowie, J. H.; Blumenthal, T. *J. Org. Chem.* **1986**, *51*, 5078.
5. Sheldon, J. C.; Bowie, J. H.; Lewis, D. E. *New. J. Chem.* **1988**, *12*, 269.

6. Tumas, W.; Foster, R. F.; Pellerite, M. J.; Brauman, J. I. *J. Am. Chem. Soc.* **1984**, *106*, 4053.
7. Tumas, W.; Foster, R. F.; Pellerite, M. J.; Brauman, J. I. *J. Am. Chem. Soc.* **1983**, *105*, 7464.
8. Tumas, W.; Foster, R. F.; Brauman, J. I. *J. Am. Chem. Soc.* **1988**, *110*, 2714.
9. Tumas, W.; Foster, R. F.; Pellerite, M. J.; Brauman, J. I. *J. Am. Chem. Soc.* **1987**, *109*, 961.
10. Hayes, R. N.; Sheldon, J. C.; Bowie, J. H.; Lewis, D. E. *Aust. J. Chem.* **1985**, *38*, 1197.
11. Hayes, R. N.; Sheldon, J. C.; Bowie, J. H.; Lewis, D. E. *J. Chem. Soc., Chem. Commun.* **1984**, 1431.
12. Chiu, S.-W.; Lau, J. K.-C.; Li, W.-K. *J. Phys. Chem.* **2001**, *105*, 432.
13. Chiu, S.-W.; Lau, K.-C.; Li, W.-K. *J. Phys. Chem. A.* **1999**, *103*, 6003.
14. Curtiss, L. A.; Raghavachari, K.; Redfern, P. C.; Rassolov V.; Pople, J. A. *J. Chem. Phys.* **1998**, *109*, 7764.
15. Frisch, M. J.; Trucks, G. W.; Schlegel, H. B.; Gill, P. M. W.; Johnson, B. J.; Robb, M. A.; Cheeseman, J. R.; Keith, T. A.; Petersson, G. A.; Montgomery, J. A.; Raghavachari, K.; Al-Laham, M. A.; Zarkrewski, V. G.; Ortiz, J. V.; Foresman, J. B.; Cioslowski, J.; Stefanov, B. B.; Nanayakkara, A.; Challacombe, M.; Peng, C. Y.; Ayala, P. Y.; Chen, W.; Wong, M. W.; Andres, J. L.; Replogle, E. S.; Gomperts, R.; Martin, R. L.; Fox, D. J.; Binkley, J. S.; Defrees, D. J.; Baker, J.; Stewart, J. J. P.; Head-Gordon, M.; Gonzalez, C.; Pople, J. A. *GAUSSIAN* 94, Revision D4; Gaussian, Inc., Pittsburgh, PA, 1995.
16. Frisch, M. J.; Trucks, G. W.; Schlegel, H. B.; Scuseria, G. E.; Robb, M. A.; Cheeseman, J. R.; Zakrzewski, V. G.; Montgogery, J. A.; Jr.; Stratmann, R.E.; Burant, J. C.; Dapprich, S.; Millam, J. M.; Daniels, A. D.; Kudin, K. N.; Strain, M. C.; Farkas, O.; Tomasi, J.; Barone, V.; Cossi, M.; Cammi, R.; Mennucci, B.; Pomelli, C.; Adamo, C.; Clifford, S.; Ochterski, J.; Petersson, G. A.; Ayala, P. Y.; Cui, Q.; Morokuma, K.; Malick, D. K.; Rabuck, A. D.; Raghavachari, K.; Foresman, J. B.; Cioslowski, J.; Ortiz, J. V.; Baboul, A. G.; Stefanov, B. B.; Liu, G.; Liashenko, A.; Piskorz, P.; Komaromi, I.; Gomperts, R.; Martin, R. L.; Fox, D. J.; Keith, T.; Al-Laham, M. A.; Peng, C. Y.; Nanayakkara, A.; Gonzalez, C.; Challacombe, M.; Gill, P. M. W.; Johnson, B.; Chen, W.; Wong, M. W.; Andres,

J. L.; Gonzalez, C.; Head-Gordon, M.; Replogle, E. S.; Pople, J. A. *GAUSSIAN 98*, Revision A.7; Gaussian, Inc., Pittsburgh PA, 1998.

17. Curtiss, L. A.; Redfern, P. C.; Raghavachari, K.; Rassolov, V.; Pople, J. A. *J. Chem. Phys.* **1999**, *110*, 4703.
18. Morton, T. H. *Org. Mass Spectrom.* **1992**, *27*, 353.
19. Lias, S. G.; Bartmess, J. E.; Liebman, J. F.; Holmes, J. L.; Levin, R. D.; Mallard, W. G. *J. Phys. Chem. Ref. Data* **1988**, *17* (Suppl.1).
20. **NIST Chemistry WebBook, NIST Standard Reference Database Number 69**, Eds. W. G. Mallard and P.J. Linstrom, November 1998, National Institute of Standards and Technology, Gaithersburg MD, 20899 (http://webbook.nist.gov).

Chapter 4

A Gaussian–3 Study of the Photoionization and Dissociative Photoionization Channels of Dimethyl Disulfide

Abstract

We have carried out the Gaussian–3 (G3) calculations on the energetics of dissociative photoionizations of dimethyl disulfide. Combining the G3 results with the experimental appearance energies for the photodissociation fragment ions CH_3^+, $C_2H_3^+$, SH_3^+, HCS^+, CH_2S^+, CH_2SH^+, CH_3SH^+, $CH_3SH_2^+$, $CH_3SCH_2^+$, S_2^+, $CH_2S_2^+$, and $CH_2S_2H^+$, we have established the dissociation channels of dimethyl disulfide. Among all the dissociation channels, our calculated results are generally in good agreement with the experimental results. However, there is a large deviation between the G3 results and experimental values in four of the dissociation channels. We believe the deviation arises from the kinetic shift of the experiment.

4.1 Introduction

Organosulfur molecules are among the sources of acid rain.[1–4] Radicals formed in the atmospheric ultraviolet breakdown of organosulfur pollutants are intermediates in the atmospheric sulfur cycles and have the effect of accelerating the oxidation of organosulfur molecules, leading to the formation of SO_2.[5–7] Sulfur containing compounds including SO_2 will form acid rain when they are removed in the atmosphere by rain or snow. Dimethyl disulfide (CH_3SSCH_3) has been found to be an important precursor in the formation of the acid rain.[5–10]

In order to understand the structures and energetics of photoionization products of dimethyl disulfide, Butler et al[11] have studied the dissociation of $CH_3SSCH_3^+$ in the photon energy range of 8–12 eV. The appearance energies (AEs) of six major fragment ions, CH_3SS^+, $C_2H_5S^+$, $CH_3SH_2^+$, CH_3SH^+, CH_3S^+, and CH_2S^+, were reported. Ma and co-workers have re-examined the dissociative photoionization process, $CH_3SSCH_3 + h\nu(193\ nm) \rightarrow CH_3S_2^+ + CH_3 + e^-$, both theoretically and experimentally.[12] They found that there should be a kinetic shift at 0.2 eV for this channel. Besides, the most stable isomer for $CH_3S_2^+$ should be CH_2SSH^+, instead of CH_3SS^+, so CH_2SSH^+ was proposed to be the cationic fragment for the above

dissociation channel. Recently, Chiang and his co-workers[13] have again investigated the photoionization of CH_3SSCH_3 in the photon energy region of 8–25 eV. Apart from the six products reported by Butler et al,[11] six more fragments as well as their AEs were measured. In this work, we use the Gaussian-3 (G3)[14] method to study the structures and energetics of these twelve fragments, CH_3^+, $C_2H_3^+$, SH_3^+, HCS^+, CH_2S^+, CH_2SH^+, CH_3SH^+, $CH_3SH_2^+$, $CH_3SCH_2^+$, S_2^+, $CH_2S_2^+$, and $CH_2S_2H^+$, as well as their possible dissociation mechanisms based on the result obtained by Chiang et al.[13] Such a study would lead to a better understanding of the photodissociative processes of dimethyl disulfide.

4.2 Methods of Calculation

All calculations were carried out on DEC 500au, XP900 and XP1000 workstations using the Gaussian 98[15] packages of program. The computational model we employed was the aforementioned G3 level of theory.

4.3 Results and Discussion

The AEs of the fragments CH_3^+, $C_2H_3^+$, SH_3^+, HCS^+, CH_2S^+, CH_2SH^+, CH_3SH^+, $CH_3SH_2^+$, $CH_3SCH_2^+$, S_2^+, $CH_2S_2^+$, and $CH_2S_2H^+$, measured from experiment,[13] for the photoionization and dissociative photoionizations of dimethyl disulfide, are listed in Table 1. The structural formulas of the species involved in this work, along with their symmetry point groups, are displayed in Figure 1. The G3 standard heats of formation of various species involved in the dissociations of CH_3SSCH_3 (**1**) and its cation (**2**) are summarized in Table 2.

TABLE 1. Appearance Energies (eV) Measured in the Dissociative Photoionizations of Dimethyl Disulfide

m/e	ion	AE	m/e	ion	AE
15	CH_3^+	12.85±0.05	49	$CH_3SH_2^+$	10.90±0.04
27	$C_2H_3^+$	13.32±0.05	61	$CH_3SCH_2^+$	10.50±0.05
35	SH_3^+	12.84±0.05	64	S_2^+	14.12±0.05
45	HCS^+	13.24±0.05	78	$CH_2S_2^+$	12.29±0.10
46	CH_2S^+	10.73±0.04	79	$CH_2S_2H^+$	11.12±0.05
47	CH_2SH^+	10.82±0.04	94	$CH_3SSCH_3^+$	8.20±0.04
48	CH_3SH^+	10.78±0.04			

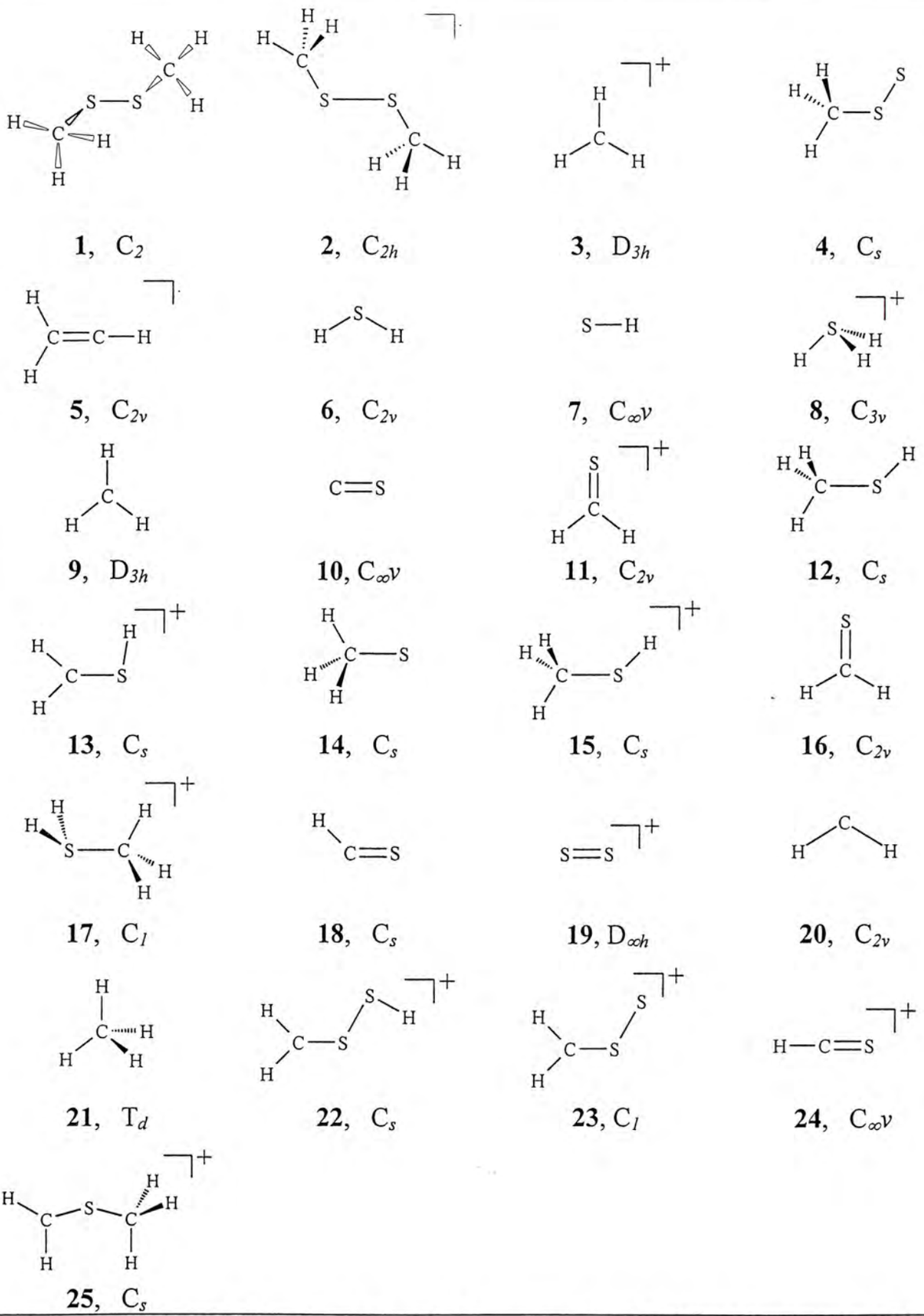

Figure 1. Structural formula of the stable species involved in the dissociation of dimethyl disulfide, along with their symmetry point groups.

TABLE 2: G3 Total Energies (E_0), Enthalpies (H_{298}), and Standard Heats of formation at 0 K (ΔH°_{f0}) and 298 K (ΔH°_{f298}) of the Species Involved in the Dissociation of Dimethyl Disulfide and its Cation

species	E_0 (hartree)	H_{298} (hartree)	ΔH°_{f0} (kJ mol^{-1})	ΔH°_{f298} (kJ mol^{-1})
CH_3SSCH_3 (**1**)	-875.82710	-875.81974	3.1	-11.9
$CH_3SSCH_3^+$ (**2**)	-875.52816	-875.52057	788.0	773.6
CH_3^+ (**3**)	-39.42928	-39.42548	1100.4	1097.1
CH_3S_2 (**4**)	-835.94575	-835.94045	89.6	82.5
$C_2H_3^+$ (**5**)	-77.51349	-77.50897	1138.2	1136.1
H_2S (**6**)	-399.23786	-399.23407	-14.7	-17.0
SH (**7**)	-398.59510	-398.59180	141.5	142.1
SH_3^+ (**8**)	-399.50386	-399.50003	818.3	811.9
CH_3 (**9**)	-39.79144	-39.78733	149.6	147.1
CS (**10**)	-436.06070	-436.05738	272.1	276.2
CH_2S^+ (**11**)	-436.94044	-436.93654	1025.1	1022.4
CH_3SH (**12**)	-438.49974	-438.49524	-6.1	-15.7
CH_2SH^+ (**13**)	-437.57454	-437.57055	891.6	884.9
CH_3S (**14**)	-437.86373	-437.85963	132.4	126.0
CH_3SH^+ (**15**)	-438.15253	-438.14794	905.5	896.2
CH_2S (**16**)	-437.28505	-437.28117	120.3	117.5
$CH_3SH_2^+$ (**17**)	-438.79245	-438.78780	756.8	743.4
HCS (**18**)	-436.63686	-436.63302	290.8	292.1
S_2^+ (**19**)	-795.73686	-795.73344	1036.1	1037.2
CH_2 (**20**)	-39.11718	-39.11339	388.5	389.3
CH_4 (**21**)	-40.45548	-40.45167	-62.5	-70.0
$CH_2S_2H^+$ (**22**)	-835.64134	-835.63580	888.9	882.3
$CH_2S_2^+$ (**23**)	-834.99594	-834.99118	1052.0	1047.6
HCS^+ (**24**)	-436.36208	-436.35857	1012.2	1012.6
$CH_3SCH_2^+$ (**25**)	-476.86463	-476.85923	826.1	814.1
26	-875.50623	-875.49910	845.6	830.0
27	-834.95827	-834.95272	1150.9	1148.6
28	-875.48017	-875.47231	914.0	900.3
$\mathbf{TS_a}$	-875.44336	-875.43603	1010.7	995.5
$\mathbf{TS_b}$	-875.40248	-875.39470	1118.0	1104.1
$\mathbf{TS_c}$	-834.92225	-834.91776	1245.5	1240.4
$\mathbf{TS_d}$	-834.95875	-834.95331	1149.6	1147.0
$\mathbf{TS_e}$	-875.44836	-875.44171	997.5	980.6
$\mathbf{TS_f}$	-875.46476	-875.45725	954.5	939.8

The G3 ionization energies (IE) of **1** is calculated to be 8.13 eV, which is in a good agreement with the experimental value (8.20 eV).[13] With the aid of Table 2, we can establish the bond dissociation energies (ΔE) of each reaction (ΔE = AE – IE). Based on our calculated results, two types of dissociation channels are found: simple bond cleavage reactions and reactions involving transition structures (TSs) and reaction barriers.

4.3.1 Bond cleavage reactions. Dissociations of the dimethyl disulfide cation (**2**), which involve only the cleavage of bond(s), are summarized in this section.

$$CH_3SSCH_3^+ (\mathbf{2}) \xrightarrow{\Delta E_1} CH_3^+ (\mathbf{3}) + CH_3S_2 (\mathbf{4}) \quad (1)$$

$$\Delta E_1 = AE(CH_3^+) - IE(CH_3SSCH_3) = 4.65 \text{ eV}$$

$$CH_3SSCH_3^+ (\mathbf{2}) \xrightarrow{\Delta E_2} C_2H_3^+ (\mathbf{5}) + H_2S (\mathbf{6}) + SH (\mathbf{7}) \quad (2)$$

$$\Delta E_2 = AE(C_2H_3^+) - IE(CH_3SSCH_3) = 5.12 \text{ eV}$$

$$CH_3SSCH_3^+ (\mathbf{2}) \xrightarrow{\Delta E_3} SH_3^+ (\mathbf{8}) + CH_3 (\mathbf{9}) + CS (\mathbf{10}) \quad (3)$$

$$\Delta E_3 = AE(SH_3^+) - IE(CH_3SSCH_3) = 4.64 \text{ eV}$$

$$CH_3SSCH_3^+ (\mathbf{2}) \xrightarrow{\Delta E_2} CH_2S^+ (\mathbf{11}) + CH_3SH (\mathbf{12}) \quad (4)$$

$$\Delta E_4 = AE(CH_2S^+) - IE(CH_3SSCH_3) = 2.53 \text{ eV}$$

$$CH_3SSCH_3^+ (\mathbf{2}) \xrightarrow{\Delta E_5} CH_2SH^+ (\mathbf{13}) + CH_3S (\mathbf{14}) \quad (5)$$

$$\Delta E_5 = AE(CH_2SH^+) - IE(CH_3SSCH_3) = 2.62 \text{ eV}$$

$$CH_3SSCH_3^+ (\mathbf{2}) \xrightarrow{\Delta E_6} CH_3SH^+ (\mathbf{15}) + CH_2S (\mathbf{16}) \quad (6)$$

$$\Delta E_6 = AE(CH_3SH^+) - IE(CH_3SSCH_3) = 2.58 \text{ eV}$$

$$CH_3SSCH_3^+ (\mathbf{2}) \xrightarrow{\Delta E_7} CH_3SH_2^+ (\mathbf{17}) + HCS (\mathbf{18}) \quad (7)$$

$$\Delta E_7 = AE(CH_3SH_2^+) - IE(CH_3SSCH_3) = 2.70 \text{ eV}$$

$$CH_3SSCH_3^+ (\mathbf{2}) \xrightarrow{\Delta E_8} S_2^+ (\mathbf{19}) + CH_2 (\mathbf{20}) + CH_4 (\mathbf{21}) \quad (8)$$

$$\Delta E_8 = AE(S_2^+) - IE(CH_3SSCH_3) = 5.92 \text{ eV}$$

$$CH_3SSCH_3^+ (\mathbf{2}) \xrightarrow{\Delta E_9} CH_2S_2H^+ (\mathbf{22}) + CH_3 (\mathbf{9}) \quad (9)$$

$$\Delta E_9 = AE(CH_2S_2H^+) - IE(CH_3SSCH_3) = 2.92 \text{ eV}$$

The above experimental dissociation energies, along with those calculated by the G3 method, are tabulated in Table 3 for easy comparison. From Table 3, it is seen that the G3 results are in very good agreement with the experimental values, except reactions (1) and (9). We believe that these errors arise from kinetic shifts, as suggested by Ma et al [12] and Chiang and co-workers.[13] Take reaction (9) as an example, the measured and G3 ΔE's are 2.92 and 2.60 eV, respectively. The kinetic

shift for this reaction was estimated to be 0.20 eV by Ma et al, [12] which would close the gap between experimental and G3 ΔE's to 0.12 eV.

TABLE 3: Experimental and Calculated Energies (eV) of the Dissociation of the Dimethyl Disulfide

dissociation reaction	ΔE (expt)	ΔE (G3) or reaction barrier
Simple bond cleavage reactions		
(1) $CH_3SSCH_3^+$ (**2**) → CH_3^+ (**3**) + CH_3S_2 (**4**)	4.65	4.17
(2) $CH_3SSCH_3^+$ (**2**) → $C_2H_3^+$ (**5**) + H_2S (**6**) + SH (**7**)	5.12	4.94
(3) $CH_3SSCH_3^+$ (**2**) → SH_3^+ (**8**) + CH_3 (**9**) + CS (**10**)	4.64	4.68
(4) $CH_3SSCH_3^+$ (**2**) → CH_2S^+ (**11**) + CH_3SH (**12**)	2.53	2.39
(5) $CH_3SSCH_3^+$ (**2**) → CH_2SH^+ (**13**) + CH_3S (**14**)	2.62	2.45
(6) $CH_3SSCH_3^+$ (**2**) → CH_3SH^+ (**15**) + CH_2S (**16**)	2.58	2.46
(7) $CH_3SSCH_3^+$ (**2**) → $CH_3SH_2^+$ (**17**) + HCS (**18**)	2.70	2.69
(8) $CH_3SSCH_3^+$ (**2**) → S_2^+ (**19**) + CH_2 (**20**) + CH_4 (**21**)	5.92	5.95
(9) $CH_3SSCH_3^+$ (**2**) → $CH_3S_2H^+$ (**22**) + CH_3 (**9**)	2.92	2.60
reactions involving reaction barriers		
(10) $CH_3SSCH_3^+$ (**2**) → $CH_2S_2^+$ (**23**) + CH_4 (**21**)	4.09	3.42
(11) $CH_3SSCH_3^+$ (**2**) → HCS^+ (**24**) + CH_4 (**21**) + SH (**7**)	5.04	4.09
(12) $CH_3SSCH_3^+$ (**2**) → $CH_3SCH_2^+$ (**25**) + SH (**7**)	2.30	2.31

4.3.2 Dissociation channels involving transition structures. In this section, we consider the dissociation of the dimethyl disulfide cation which involve TSs.

$$CH_3SSCH_3^+ (\mathbf{2}) \xrightarrow{\Delta E_{10}} CH_2S_2^+ (\mathbf{23}) + CH_4 (\mathbf{21}) \qquad (10)$$

$$\Delta E_{10} = AE(CH_2S_2^+) - IE(CH_3SSCH_3) = 4.09 \text{ eV}$$

From Figure 2, it is seen that the elimination of methane (**21**) starts with **2** undergoing methyl shift to form intermediate **26**. This intermediate then abstracts the neighboring hydrogen atom to form $CH_2S_2^+$ (**23**) and CH_4 (**21**). The overall G3 barrier for this reaction is calculated to be 3.42 eV, which is much lower than the experimental result (4.09 eV). We have tried to investigate this reaction by forming different kinds of neutral products like $CH_2 + H_2$ (ΔE = 6.75 eV) or $CH_3 + H$ (ΔE = 6.52 eV). However, the energies required for these kind of dissociations are higher than the experimental value, so these dissociations are not possible. Again, we believe the large deviation between our calculated result and the experimental value arises from the kinetic shift of the experiment.

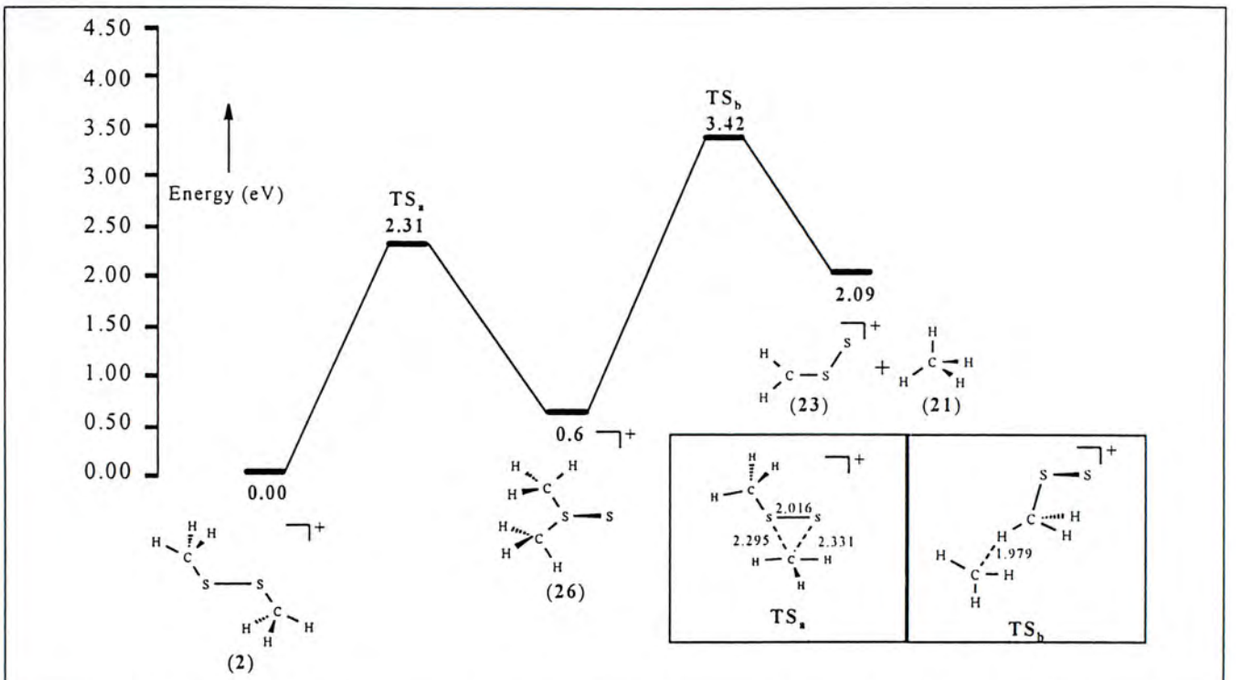

Figure 2. Potential energy surface showing the possible mechanism for dissociation $CH_3SSCH_3^+ \rightarrow CH_2S_2^+ + CH_4$.

$$CH_3SSCH_3^+ \text{ (2)} \xrightarrow{\Delta E_{11}} HCS^+ \text{ (24)} + CH_4 \text{ (21)} + SH \text{ (7)} \qquad (11)$$

$$\Delta E_{11} = AE(HCS^+) - IE(CH_3SSCH_3) = 5.04 \text{ eV}$$

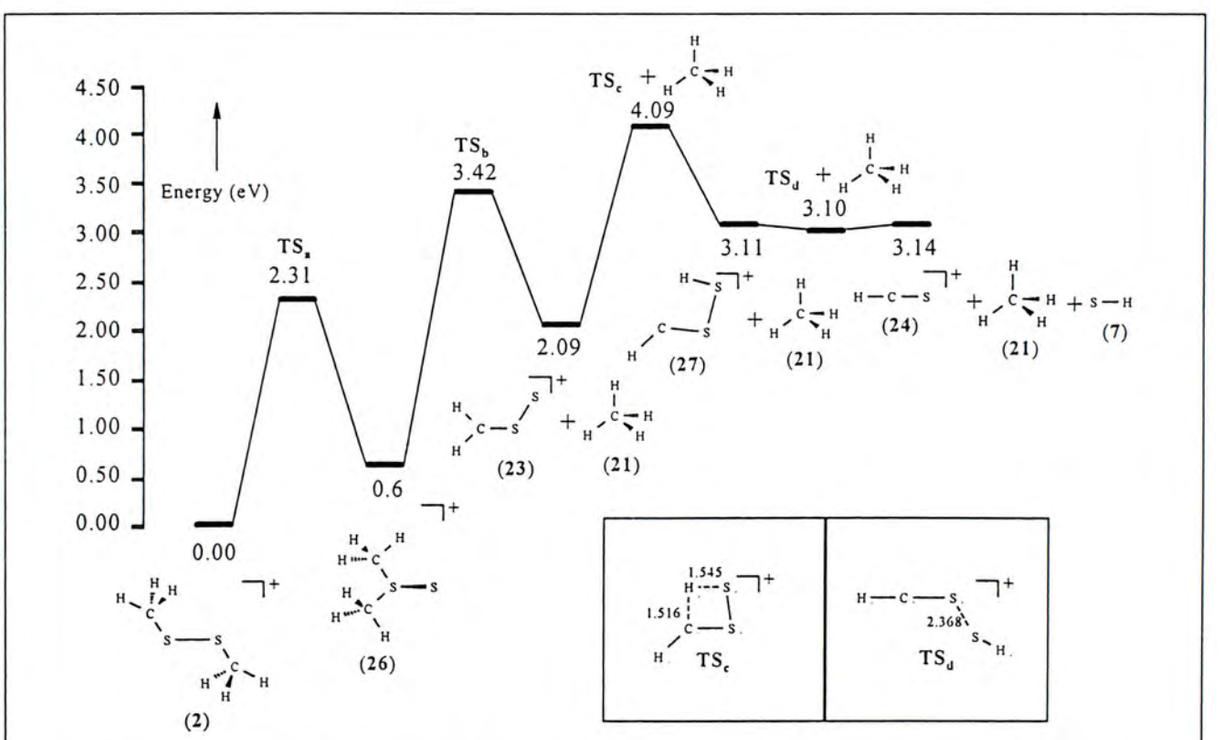

Figure 3. Potential energy surface showing the possible mechanism for dissociation $CH_3SSCH_3^+ \rightarrow HCS^+ + CH_4 + SH$.

The energy profile for this dissociation is summarized in Figure 3. The reaction starts with **2** undergoing methane elimination to form $CH_2S_2^+$ (**23**) and CH_4 (**21**). Cation **23** then undergoes hydrogen shift to form intermediate **27**. Finally, cleavage of S–S bond leads to the formation of HCS^+ (**24**) and SH (**7**). The G3 energy barrier for this dissociation is 4.09 eV which is not consistent with the experimental value of 5.04 eV. Apart from forming CH_4 + SH, CH_3 + H_2S and HCS + $2H_2$ are also possible to be the neutral fragments of this reaction. However, they are thermodynamically less stable (ΔH_f for CH_3 + H_2S = 134.9 kJ mol^{-1} while ΔH_f for HCS + $2H_2$ = 289.2 kJ mol^{-1}) than CH_4 + SH (ΔH_f = 79.0 kJ mol^{-1}). So, these dissociations are not considered. Once more, we believe the large deviation between the G3 and experimental ΔE's value arises from the kinetic shift of the experiment.

$$CH_3SSCH_3^+ \text{ (2)} \xrightarrow{\Delta E_{12}} CH_3SCH_2^+ \text{ (25)} + SH \text{ (7)} \qquad (12)$$

$$\Delta E_{12} = AE(HCS^+) - IE(CH_3SSCH_3) = 2.30 \text{ eV}$$

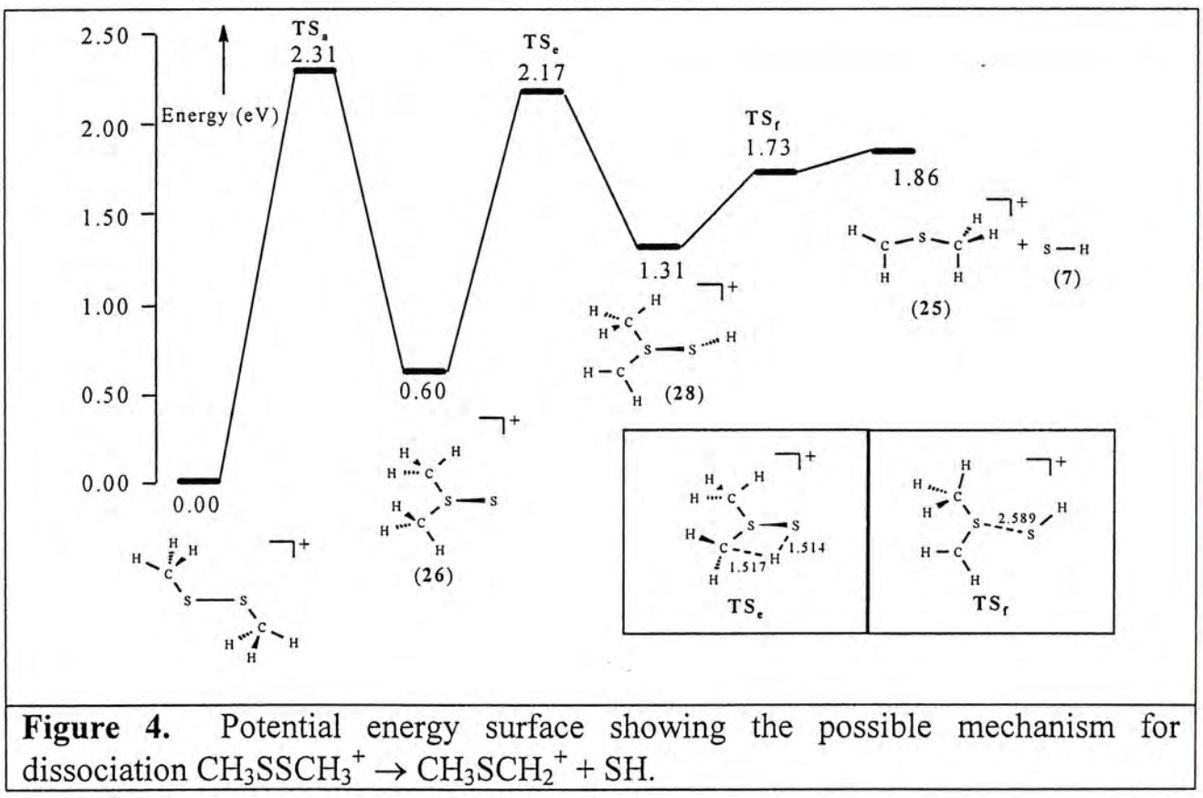

Figure 4. Potential energy surface showing the possible mechanism for dissociation $CH_3SSCH_3^+ \rightarrow CH_3SCH_2^+ + SH$.

The energy profile for this dissociation is shown in Figure 4. The reaction starts with **2** undergoing methyl shift to form intermediate **26**, which then undergoes hydrogen shift via $\mathbf{TS_e}$ to form cation **28**. Finally, the cleavage of C–S bond produces

$CH_3SCH_2^+$ (**25**) + SH (**7**). The G3 energy barrier for this reaction is 2.31 eV, which is in very good agreement with the experimental result of 2.30 eV.

The bond dissociation energies and our G3 barriers for reactions (10)–(12) are also included in Table 3. Since there is a large kinetic shift in the experiment, significant deviations between the calculated and experimental results are found for some dissociations. However, it is noted that our proposed dissociation channels have the most thermodynamically stable products.

4.4 Conclusions

The energetics for the dissociative photoionizations of dimethyl disulfide have been carried out by the G3 method. Combining these results with the experimental photoionization spectra of various fragments reported by Chiang et al, we are able to establish the dissociation channels for the formation of the following ions: CH_3^+, $C_2H_3^+$, SH_3^+, HCS^+, CH_2S^+, CH_2SH^+, CH_3SH^+, $CH_3SH_2^+$, $CH_3SCH_2^+$, S_2^+, $CH_2S_2^+$, and $CH_2S_2H^+$. The G3 results are in good accord with the experimental values in most cases. However, there is a large deviation between the calculated and experimental values in four dissociation channels. We believe the deviation arises from the kinetic shift of the experiments.

4.5 References

1. Graedel, T. E. *Rev. Geophys. Space Phys.* **1977**, *15*, 421.
2. Benson, S. W. *Chem Rev.* **1978**, *78*, 23.
3. Burnett, W. E. *Environ. Sci. Technol.* **1969**, *8*, 744.
4. Bentley, M. D.; Douglass, I. B.; Lacadie, J. A.; Whittier, D. R. *Air Pollution Control Assoc.* **1969**, *22*, 1367.
5. Calvert, J. G.; Jr. Pitts, J. N. *Photochemistry* (Wiley, New York, **1996**).
6. Thompson, S. D.; Carroll, D. G.; Watson, F.; O'Donnell, M.; McGlynn, S. P. *J. Chem. Phys.* **1966**, *45*, 1367.
7. Rao, P. M.; Knight, A. R. *Can. J. Chem.* **1968**, *46*, 2462.
8. Wayne, R. P. *Chemistry of Atmospheres* (Clarendon, Oxford, **1991**).
9. Andreae, M. O.; Raemdonck, H. *Science* **1983**, *221*, 744.
10. Yin, F.; Grosjean, D.; Seinfeld, J. H. *J. Geophys. Res.* **1986**, *91*, 14417.
11. Bulter, J. J.; Baer, T.; Evans, S.A. *J. Am. Chem. Soc.* **1983**, *105*, 3451.

12. Ma, Z.–X.; Liao, C.–L.; Ng, C. Y.; Cheung, Y.–S.; Li, W.–K.; Baer, T. *J. Chem. Phys.* **1994**, *100*, 4870.
13. Chiang, S.–Y.; Ma, C.–I.; Shr, D.– J. *J. Chem. Phys.* **1999**, *110*, 9056.
14. Curtiss, L. A.; Raghavachari, K.; Redfern, P. C.; Rassolov V.; Pople, J. A. *J. Chem. Phys.* **1998**, *109*, 7764.
15. Frisch, M. J.; Trucks, G. W.; Schlegel, H. B.; Scuseria, G. E.; Robb, M. A.; Cheeseman, J. R.; Zakrzewski, V. G.; Montgogery, J. A.; Jr.; Stratmann, R.E.; Burant, J. C.; Dapprich, S.; Millam, J. M.; Daniels, A. D.; Kudin, K. N.; Strain, M. C.; Farkas, O.; Tomasi, J.; Barone, V.; Cossi, M.; Cammi, R.; Mennucci, B.; Pomelli, C.; Adamo, C.; Clifford, S.; Ochterski, J.; Petersson, G. A.; Ayala, P. Y.; Cui, Q.; Morokuma, K.; Malick, D. K.; Rabuck, A. D.; Raghavachari, K.; Foresman, J. B.; Cioslowski, J.; Ortiz, J. V.; Baboul, A. G.; Stefanov, B. B.; Liu, G.; Liashenko, A.; Piskorz, P.; Komaromi, I.; Gomperts, R.; Martin, R. L.; Fox, D. J.; Keith, T.; Al-Laham, M. A.; Peng, C. Y.; Nanayakkara, A.; Gonzalez, C.; Challacombe, M.; Gill, P. M. W.; Johnson, B.; Chen, W.; Wong, M. W.; Andres, J. L.; Gonzalez, C.; Head-Gordon, M.; Replogle, E. S.; Pople, J. A. *GAUSSIAN 98*, Revision A.7; Gaussian, Inc., Pittsburgh PA, 1998.

Chapter 5

A Gaussian–3 Study of the Photodissociation Channels of Propylene Sulfide

Abstract

We have carried out the Gaussian–3 (G3) calculations to examine the photodissociation of propylene sulfide at 193 nm. Based on the good agreements between the G3 and experimental results obtained by our collaborators, three dissociation channels involving transition structures have been established. Besides, two dissociation channels leading to the dissociation of sulfur atom are also observed. Furthermore, our collaborators have found some additional dissociation processes, also leading to the neutral fragments, C_3H_6 and S (^{1}D) or S (^{3}P), and having exceedingly high experimental reaction barriers. These reactions are not likely to take place at the ground state of propylene sulfide. These high experimental reaction barriers are in very good accord with our calculated excitation energies of propylene sulfide.

5.1 Introduction

Sulfur-containing hydrocarbons are important intermediates in combustion and atmospheric chemistry. These species may play an important role in the atmospheric sulfur cycle and could contribute to acid rain and atmospheric aerosols.[1–7] Photodissociation of the sulfur compounds is an interesting topic from both theoretical and experimental perspectives. Using synchrotron radiation, our collaborators at Ernest Orlando Lawrence Berkeley National Laboratory in Berkeley, California, have obtained eight pairs of neutral photodissociation products of thiirane (C_2H_4S) at the 193 nm region.[8] In order to interpret the results observed in these experiments, high theoretical methods have been employed to establish these dissociation channels.[8]

Recently, the same collaborators have studied the photodissociation of propylene sulfide (C_3H_6S) by using the synchrotron radiation again. They found that the observed neutral products to be similar to the dissociations of thiirane. In this work, we use the Gaussian–3 (G3)[9] method to examine the structures and energetics

of the neutral photodissociation products of propylene sulfide. Based on the good agreements between the experimental reaction barriers and the G3 energies, three dissociation channels involving transition structures have been established:

$$C_3H_6S \rightarrow CH_3 + C_2H_3S \quad (1)$$

$$C_3H_6S \rightarrow HS + C_3H_5 \quad (2)$$

$$C_3H_6S \rightarrow H_2S + C_3H_4 \quad (3)$$

Also, two dissociation channels leading to the dissociation of sulfur atom are observed:

$$C_3H_6S \rightarrow C_3H_6 + S\ (^1D) \quad (4)$$

$$C_3H_6S \rightarrow C_3H_6 + S\ (^3P) \quad (5)$$

Besides the aforementioned dissociation channels, our collaborators have found some additional channels, involving exceedingly high experimental barriers, but also leading to the neutral fragments C_3H_6 and S (^1D) or S (^3P). The dissociation processes involving high energy barriers are believed to take place at the excited states. In order to examine these channels, the energy profiles for the ground and excited states of propylene sulfide have been constructed. From these energy profiles, it is hoped that the dissociation mechanisms of propylene sulfide can be understood.

5.2 Methods of Calculations

All calculations were carried out on DEC 500au, XP900, and XP1000 workstations using the Gaussian 98[10] packages of program. The computational model we employed was the aforementioned G3 level of theory. For the dissociation involved in the excited states, the excitation energy (relative to the ground state) is calculated by the time–dependent (TD) DFT method.[11] In this method, the geometry is optimized at the B3LYP/6–31G(d) level.

5.3 Results and Discussion

The structural formulas of all the neutral stable species involved in this work, along with their symmetry point groups, are shown in Figure 1. The calculated G3 energies and standard heats of formation (ΔH°_f) at 0 K and 298 K of various species involved in the dissociations of propylene sulfide (**1**) are summarized in Table 1.

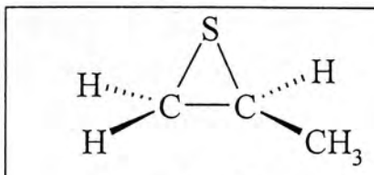

1, C_1

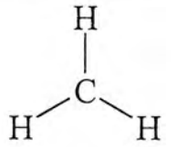

2, D_{3h}

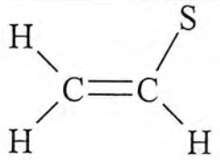

3, C_s

4, $C_{\infty v}$

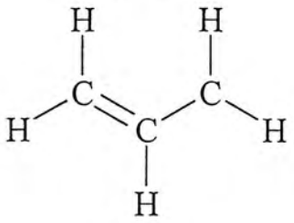

5, C_{2v}

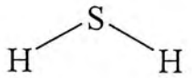

6, C_{2v}

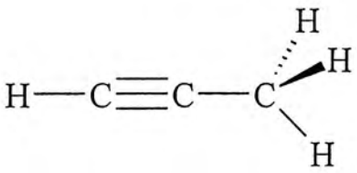

7, C_{3v}

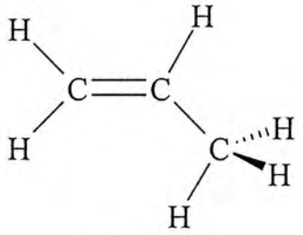

8, C_s

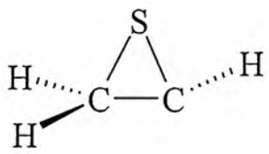

9, C_1

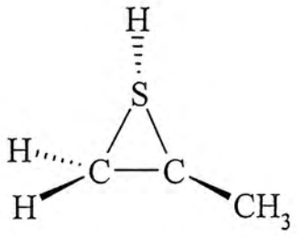

10, C_1

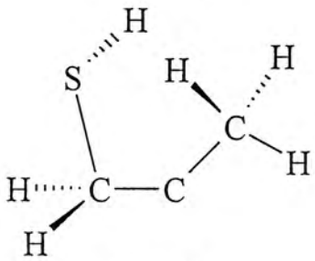

11, C_1

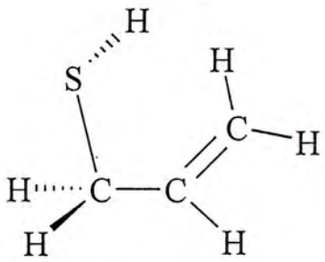

12, C_1

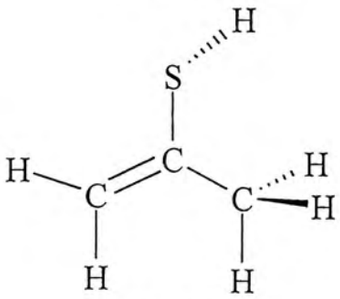

13, C_1

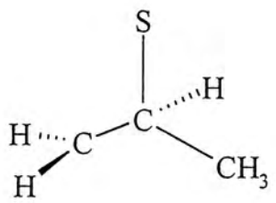

14, C_1

Figure 1. Structural formula of the stable species involved in the dissociation of propylene sulfide, along with their symmetry point groups.

Table 1: G3 Total Energies[a] (E_0), Enthalpies (H_{298}), and Standard Heats of Formation at 0 K (ΔH°_{f0}) and 298 K (ΔH°_{f298}) of the Species Involved in the Dissociation of Propylene Sulfide (C_3H_6S)

species	E_0 (hartree)	H_{298} (hartree)	ΔH°_{f0} (kcal mol^{-1})	ΔH°_{f298} (kcal mol^{-1})
C_3H_6S (**1**)	-515.83519	-515.82960	16.3	12.4
CH_3 (**2**)	-39.79144	-39.78733	35.8	35.2
CH_2CHS (**3**)	-475.93261	-475.92810	50.3	48.9
HS (**4**)	-398.59510	-398.59180	33.8	34.0
CH_2CHCH_2 (**5**)	-117.14132	-117.13657	44.5	41.9
H_2S (**6**)	-399.23786	-399.23407	-3.5	-4.1
CH_3CCH (**7**)	-116.55517	-116.54984	46.3	45.1
CH_3CHCH_2 (**8**)	-117.77961	-117.77453	9.9	6.6
9	-475.89880	-475.89452	71.5	69.9
10	-515.73390	-515.72786	79.9	76.2
11	-515.72318	-515.71627	86.6	83.5
12	-515.82914	-515.82287	20.1	16.6
13	-515.83695	-515.83057	15.2	11.8
14	-515.74878	-515.74219	70.5	67.2
TS_a	-515.68626	-515.67821	109.8	107.4
TS_b	-475.88502	-475.88091	80.2	78.5
TS_c	-515.72872	-515.72275	83.1	79.4
TS_d	-515.72037	-515.71401	88.4	84.9
TS_e	-515.71412	-515.70792	92.3	88.7
TS_f	-515.73004	-515.72418	82.3	78.5
TS_g	-515.71332	-515.70626	92.8	89.8
TS_h	-515.73729	-515.73112	77.7	74.2

With the aid of these results, it is possible to establish the dissociation channels of propylene sulfide.

5.3.1 The dissociation channels involving transition structures. In this section, we consider the dissociation mechanisms of propylene sulfide, which involve TSs.

$$C_3H_6S\ (\mathbf{1}) \rightarrow CH_3\ (\mathbf{2}) + C_2H_3S\ (\mathbf{3}) \qquad (1)$$

The potential energy surface for the above dissociation is shown in Figure 2. It is seen that the reaction starts with **1** undergoing methyl group dissociation to form CH_3 (**2**) and *c*-CH_2CHS (**9**). Then, rearrangement of **9** leads to the formation of CH_2CHS (**3**). The G3 overall barrier for this reaction is found to be 99.6 kcal mol^{-1}, which is lower than the experimental value of 111 kcal mol^{-1}. Bearing in mind that the experimental barrier is measured from the exit barrier plus the heats of reaction and it represents an upper bound, the G3 barrier as well as the proposed dissociation

pathway are hence acceptable. On the other hand, kinetic shift may give rise to the discrepancy between the calculated and experimental reaction barriers.

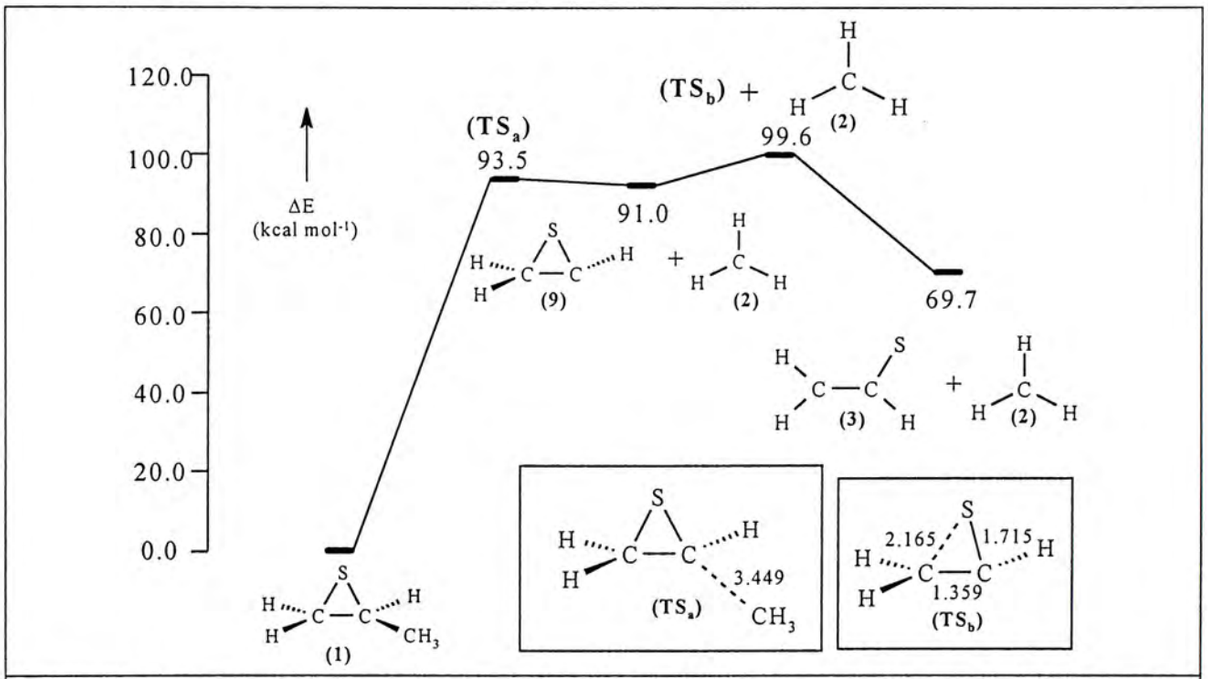

Figure 2. Potential energy surface showing the possible mechanism for dissociation $C_3H_6S \rightarrow CH_3 + C_2H_3S$.

$$C_3H_6S\ (\mathbf{1}) \rightarrow HS\ (\mathbf{4}) + C_3H_5\ (\mathbf{5}) \qquad (2)$$

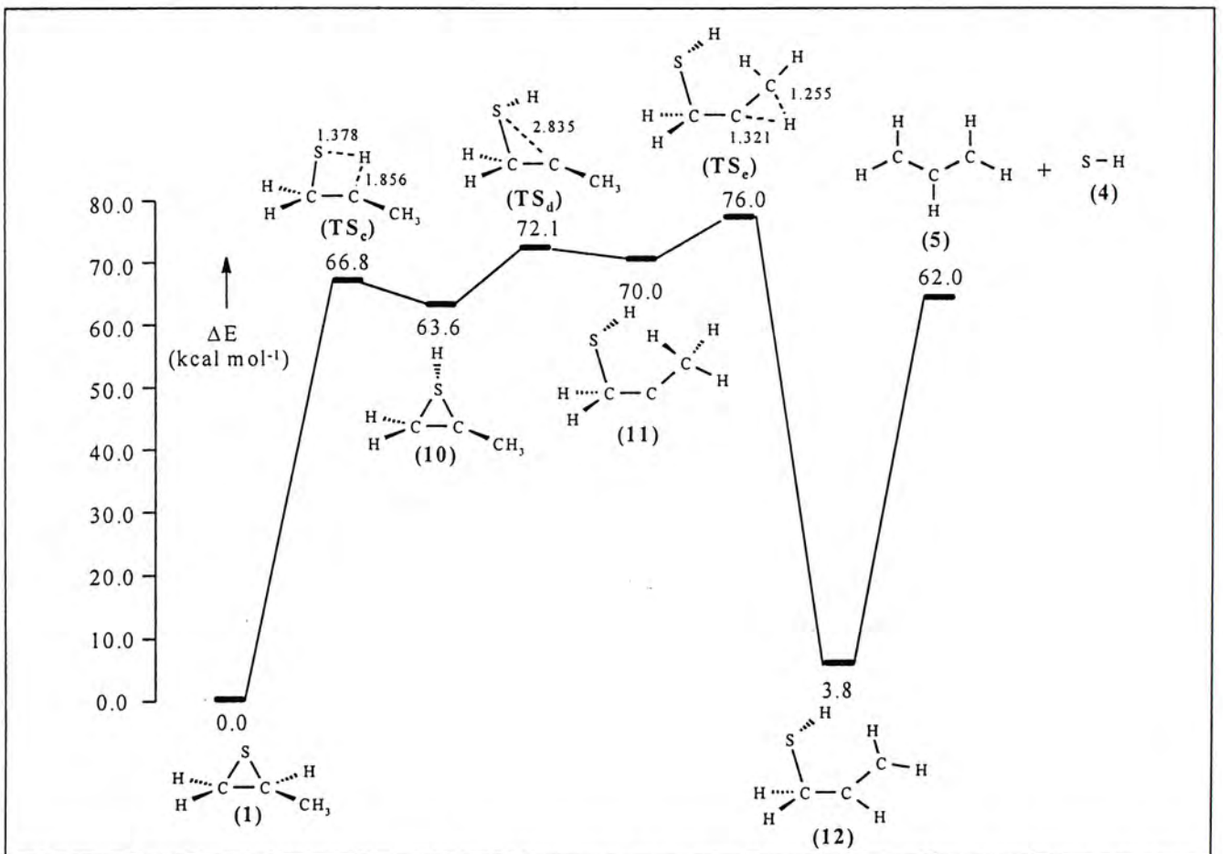

Figure 3. Potential energy surface showing the possible mechanism for dissociation $C_3H_6S \rightarrow HS + C_3H_5$.

The energy profile for this reaction is given in Figure 3. Here, **1** first undergoes hydrogen shift to form intermediate **10**, which then undergoes ring opening by breaking a S–C bond to form **11**. Then **11** undergoes another hydrogen shift to form intermediate **12**. Finally, cleavage of S–C bond in **12** produces HS (**4**) and C_3H_5 (**5**). The overall G3 barrier for this dissociation is 76.0 kcal mol^{-1} which is in a very good agreement with experimental result of 74.5 kcal mol^{-1}.

$$C_3H_6S\ (\mathbf{1}) \rightarrow H_2S\ (\mathbf{6}) + C_3H_4\ (\mathbf{7}) \qquad (3)$$

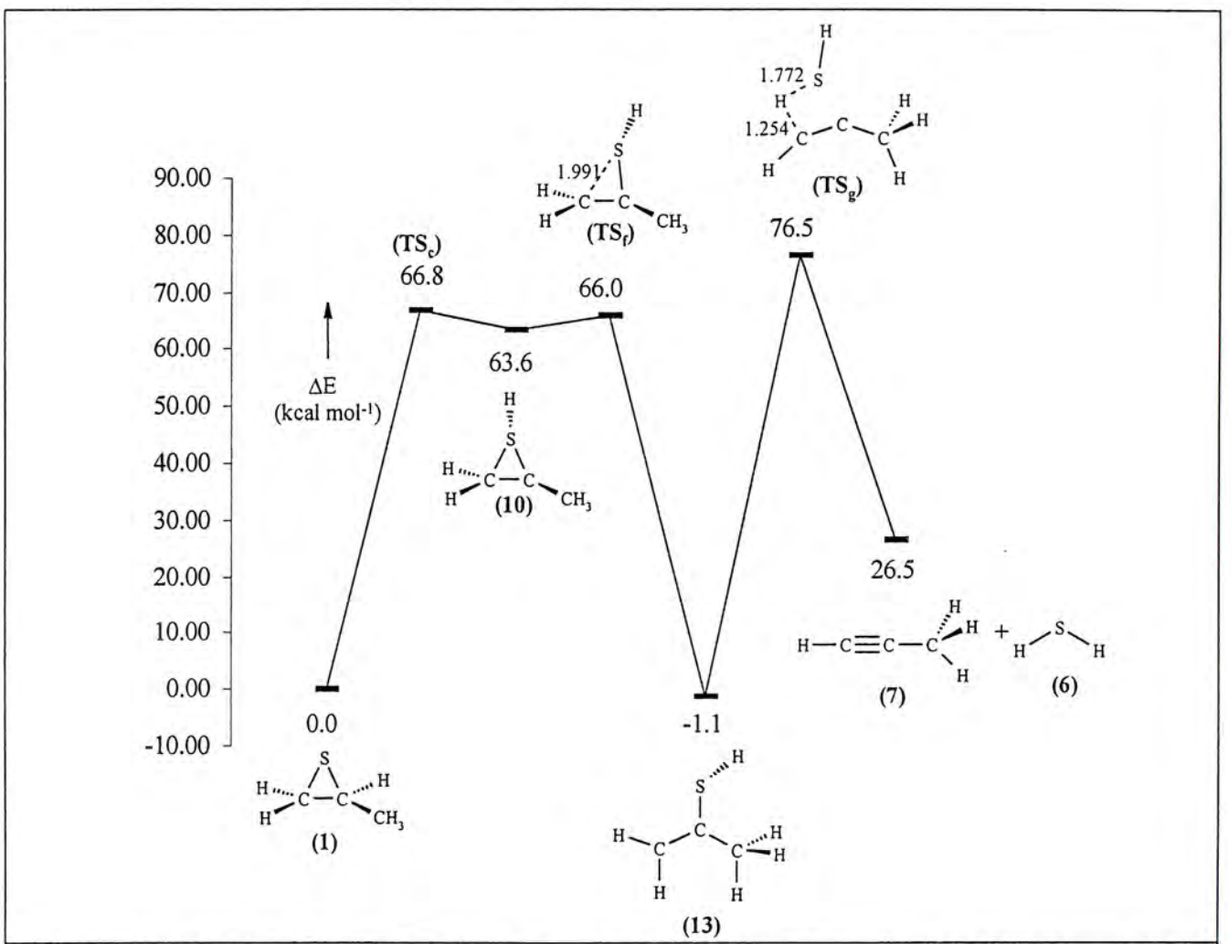

Figure 4. Potential energy surface showing the possible mechanism for dissociation $C_3H_6S \rightarrow H_2S + C_3H_4$.

The energy profile for this reaction is shown in Figure 4. It is seen that **1** first undergoes hydrogen shift via $\mathbf{TS_c}$ to form intermediate **10**, which then undergoes ring opening via $\mathbf{TS_f}$ to form **11**. Finally, the dissociation of H_2S (**6**) from **11** via $\mathbf{TS_g}$ produces C_3H_4 (**7**). The G3 overall barrier for this reaction is 76.5 kcal mol^{-1} which is much higher than the experimental value of 44 kcal mol^{-1}. Such a large difference between experimental (35 kcal mol^{-1}) and G3 (81.4 kcal mol^{-1}) barriers[8] was also obtained for the dissociation C_2H_4S (thiirane) $\rightarrow H_2S$ + HCCH. It is believed that the energy of a highly strained species ($\mathbf{TS_g}$ in this instance) is not likely to be available

to translation as the system relaxes in the exit channel. Hence the experimental barrier is an underestimation of the true value.

5.3.2 The dissociations of sulfur atom. Our collaborators have observed some of the dissociation channels leading to the product of S (^{1}D) and S (^{3}P). Besides, they also found some additional channels, involving exceedingly high experimental barriers, but also leading to the neutral fragments C_3H_6 and S (^{1}D) or S (^{3}P). We believe these dissociations involving exceedingly high experimental barriers take place in excited states. In order to examine these channels, the energy profiles for the ground and excited states of propylene sulfide have been constructed using the TD–DFT method.

Dissociation of singlet sulfur atom. There are three experimental energy barriers for the dissociations of singlet sulfur atom: 98, 110, and 126 kcal mol^{-1}.

$$C_3H_6S\ (\mathbf{1}) \rightarrow C_3H_6\ (\mathbf{8}) + S\ (^1D) \qquad (4)$$

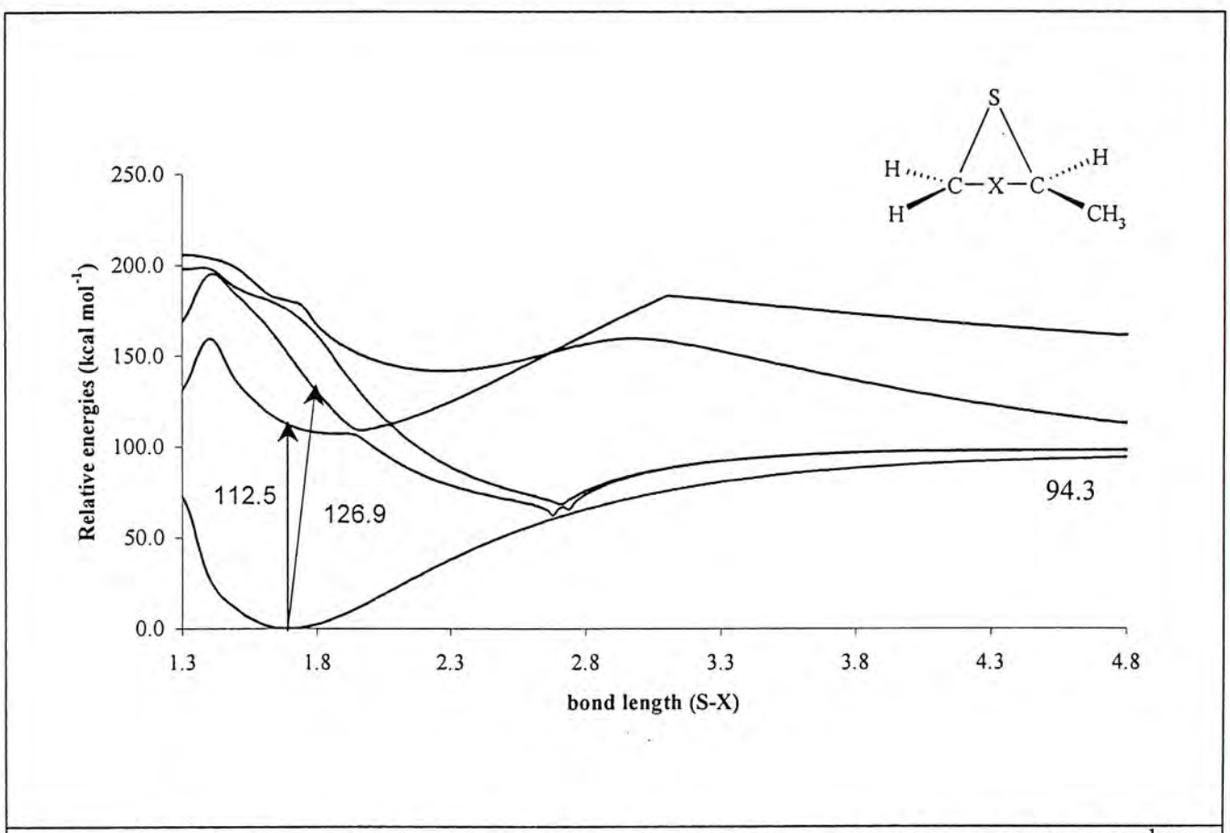

Figure 5. Singlet potential energy profiles for dissociation $C_3H_6S \rightarrow C_3H_6 + S\ (^1D)$.

The energy profiles for the ground and excited states for the dissociation of sulfur atom from propylene sulfide are shown in Figure 5. It is seen that the energy required for the dissociation of sulfur atom in the ground state is 94.3 kcal mol^{-1}, which is in fair agreement with the value (98 kcal mol^{-1}) measured by our collaborators. The

arrows shown in Figure 5 denote the electronic transitions between the ground state and the first and second excited states. The calculated first excitation energy is 112.5 kcal mol^{-1}, which is consistent with the experimental value of 110 kcal mol^{-1}. Besides, the calculated second excitation energy of 126.9 kcal mol^{-1} is also in good accord with the experimental value of 126 kcal mol^{-1}.

Dissociation of triplet sulfur atom. The experimental energy barriers for the dissociations of triplet sulfur atom are 126 and 73 kcal mol^{-1}.

$$C_3H_6S\ (\mathbf{1}) \rightarrow C_3H_6\ (\mathbf{8}) + S\ (^3P) \qquad (5)$$

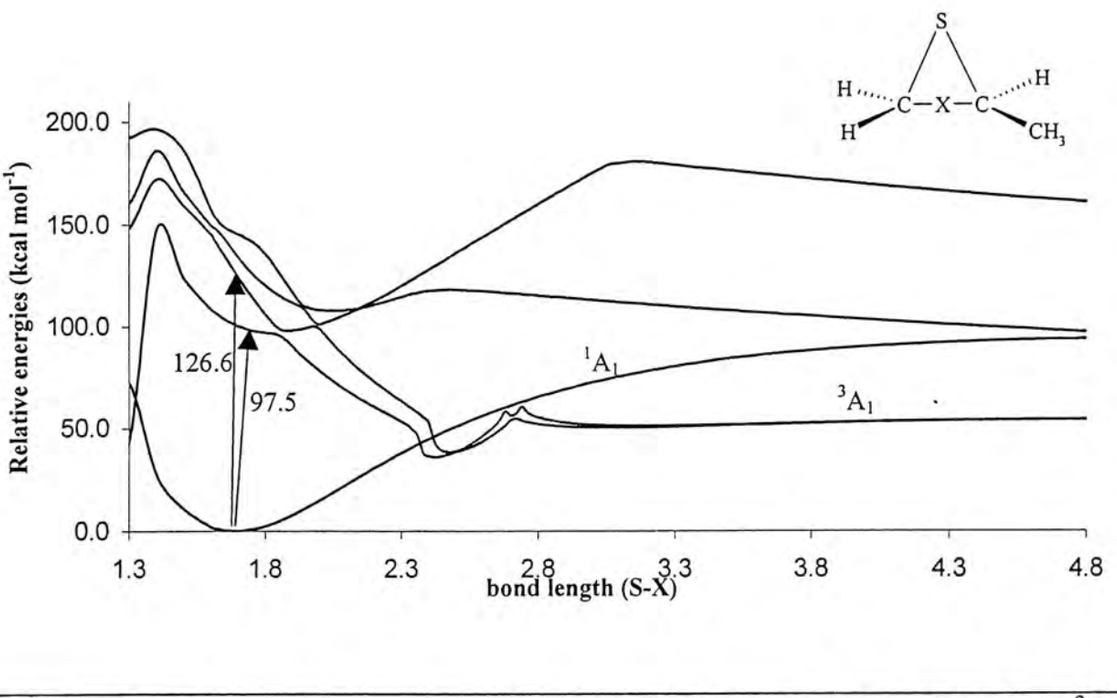

Figure 6. Triplet potential energy profiles for dissociation $C_3H_6S \rightarrow C_3H_6 + S\ (^3P)$.

The energy profiles for the dissociation of triplet sulfur atom from propylene sulfide in the excited states are shown in Figure 6. It is seen that the energies required for the first and second excitation are 97.5 and 126.6 kcal mol^{-1}, respectively. The latter value is in very good agreement with the experimental result (126 kcal mol^{-1}) reported by our collaborators. However, we find that the calculated energy required for the first excitation (97.5 kcal mol^{-1}) of triplet sulfur dissociation is different from the experimental result (73 kcal mol^{-1}).

We now consider the dissociation of triplet sulfur atom taking place in the ground state. The energy profile for this dissociation is given in Figure 7. It is seen that singlet C_3H_6S (**1**) first undergoes intersystem crossing to form triplet C_3H_6S (**14**). Then the cleavage of C–S bond leads to the formation of S (^3P) and C_3H_6 (**8**). The

energy required for this process is 61.4 kcal mol^{-1} which lower than the experimental result (73 kcal mol^{-1}). Since the experimental measurements represent the upper bound values, we believe the triplet sulfur dissociation is more likely to take place at the ground state.

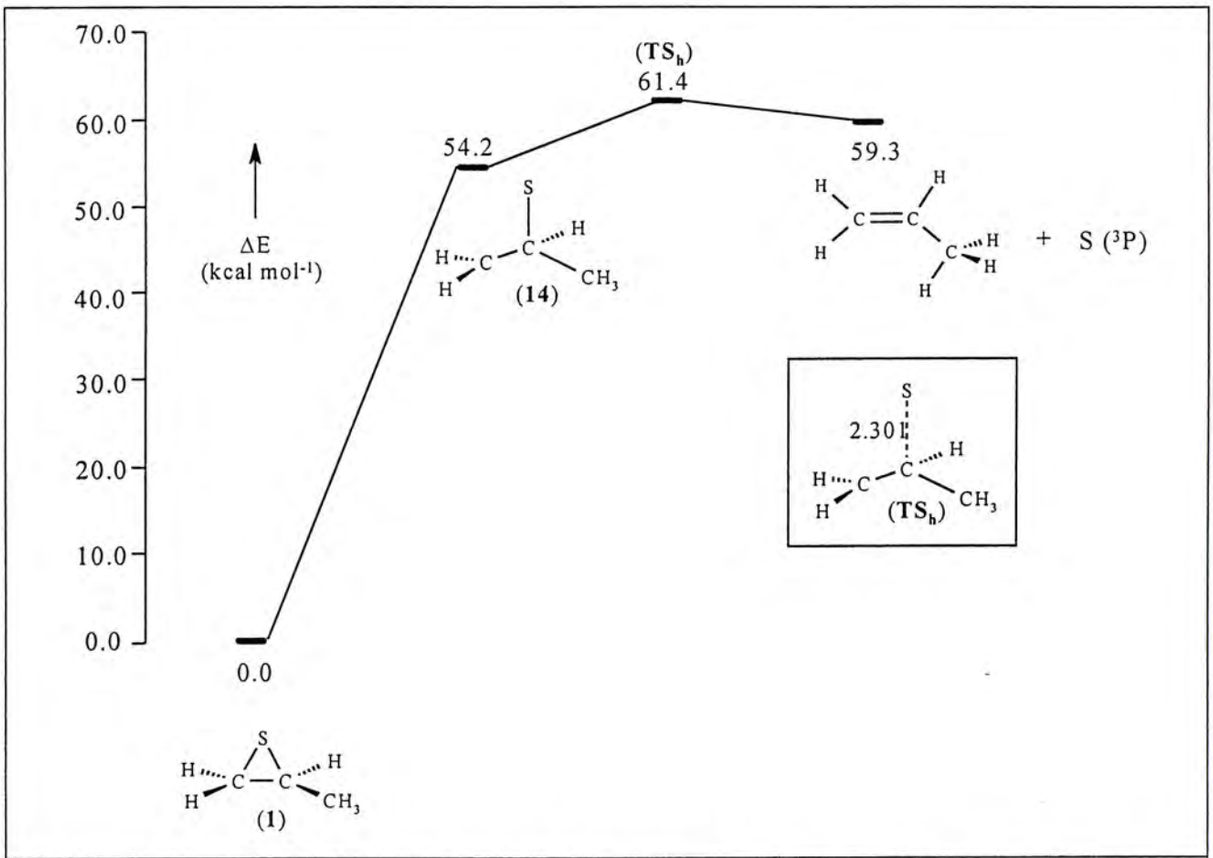

Figure 7. Potential energy surface showing the possible mechanism for dissociation $C_3H_6S \rightarrow C_3H_6S + S\ (^3P)$.

The agreements between the TD–DFT and experimental results imply that the first step for these dissociation channels should be the electronic transitions from ground state to excited state. Then, by either interconversion or intersystem crossing, the dissociations proceed at the ground state or other lower lying excited states.

5.4 Conclusions

Based on the good agreements between the G3 and experimental results, we have established the dissociation channels of propylene sulfide at the ground state. For the dissociation channels taking place at the excited states, TD–DFT method has been used to resolve the excitation energies involved in these channels.

5.5 References

1. Farquhar, J.; Bao, H.; Thiemens, M. H. *Science* **2000**, *289*, 756.
2. Farquhar, J.; Savarino, J.; Jackson, T. L.; Thimens, M. H. *Nature* **2000**, *404*, 50.
3. Kulmala, M.; Pirjola, L.; Makela, J. M. *Nature* **2000**, *44*, 66.
4. Calvert, J. G.; Pitts, J. N.; *Photochemistry* (Wiley, New York, **1996**).
5. Wayne, R. P. *Chemistry of Atmospheres* (Clarendon, Oxford, **1991**).
6. Yin, F; Grosjean, D.; Seinfeld, J. H. *J. Geophys. Res.* **1986**, *91*, 14417.
7. Andreae, M. O.; Raemdonck, H. *Science* **1983**, *221*, 744.
8. Qi, F.; Sorkhabi, O.; Suit, A. G.; Chien, S.–H.; Li, W.–K. *J. Am. Chem. Soc.* **2001**, *123*, 148.
9. Curtiss, L. A.; Raghavachari, K.; Redfern, P. C.; Rassolov V.; Pople, J. A. *J. Chem. Phys.* **1998**, *109*, 7764.
10. Frisch, M. J.; Trucks, G. W.; Schlegel, H. B.; Scuseria, G. E.; Robb, M. A.; Cheeseman, J. R.; Zakrzewski, V. G.; Montgogery, J. A.; Jr.; Stratmann, R.E.; Burant, J. C.; Dapprich, S.; Millam, J. M.; Daniels, A. D.; Kudin, K. N.; Strain, M. C.; Farkas, O.; Tomasi, J.; Barone, V.; Cossi, M.; Cammi, R.; Mennucci, B.; Pomelli, C.; Adamo, C.; Clifford, S.; Ochterski, J.; Petersson, G. A.; Ayala, P. Y.; Cui, Q.; Morokuma, K.; Malick, D. K.; Rabuck, A. D.; Raghavachari, K.; Foresman, J. B.; Cioslowski, J.; Ortiz, J. V.; Baboul, A. G.; Stefanov, B. B.; Liu, G.; Liashenko, A.; Piskorz, P.; Komaromi, I.; Gomperts, R.; Martin, R. L.; Fox, D. J.; Keith, T.; Al-Laham, M. A.; Peng, C. Y.; Nanayakkara, A.; Gonzalez, C.; Challacombe, M.; Gill, P. M. W.; Johnson, B.; Chen, W.; Wong, M. W.; Andres, J. L.; Gonzalez, C.; Head-Gordon, M.; Replogle, E. S.; Pople, J. A. *GAUSSIAN 98*, Revision A.7; Gaussian, Inc., Pittsburgh PA, 1998.
11. Stratmann, R. E.; Scuseria, G. E.; Frisch, M. J.; *J. Chem. Phys.* **1998**, *109*, 8218.

Chapter 6

Thermochemistry of Phosphorus Fluorides: A Gaussian–3 and Gaussian–3X Study

Abstract

The Gaussian–3 (G3) and Gaussian–3X (G3X) models of theory have been used to calculate the thermochemical data for phosphorus fluorides, as well as for their singly charged cations and anions. The quantities calculated include the heats of formation (ΔH_f) and bond dissociation energies (DEs) of all the species, as well as the ionization energies (IEs) and electron affinities (EAs) of all the neutrals. By comparing the well–established experimental data of PF_3 and PF_5 with the G3 and G3X results, it is found that the G3X ΔH_f values are in better agreement with the experimental values. On the other hand, the G3 and G3X methods give similar results in predicting the IE of PF_3. Based on these findings, the G3X method is used to assess the sometimes conflicting experimental data and a set of self–consistent thermochemcial data for PF_n and their ions is recommended. In addition, the alternating patterns of the ΔH_f, DE, IE, and EA values of the phosphorus fluorides and their ions are rationalized in terms of the electronic configuration around the central P atom for the species involved.

6.1 Introduction

The properties of phosphorus fluorides PF_n along with their cations and anions have been studied computationally at various level of theory.[1–10] Gutsev[1] and Tschumper[2] et al have used Hartree–Fock–Slater method and density functional theory (DFT), respectively, to investigate the structures of PF_n and PF_n^- (n = 1–6). Based on the good agreement between the experimental and theoretical structural parameters, Tschumper[2] also determined the electron affinity (EA) of PF_n and reliable results were expected. However, among the three EAs (those of PF, PF_2, and PF_5) for which experimental results are available for comparison, only the calculated EA of PF molecule is consistent with the experimental result. The adiabatic EA of PF_5 obtained from the DFT method deviated from the well–established experimental

value by 0.35 eV.[2] Recently, Gu and his co-workers[3] re-investigated the structures and energetics of PF_n and PF_n^- using the Gaussian-2 (G2)[11] and modified G2[12] models of theory in order to obtain a more reliable set of results. From this work, they obtained very good result on the geometries of PF_n and PF_n^- and, in particular, an acceptable result for the EA of PF_5. Later, Gu[4] used large basis sets and different theoretical methods to study the adiabatic EAs of PF and PF_2. They suggested that the EA of PF and PF_2 should be 0.75 eV and 0.76 eV, respectively. In addition, Gu et al[3] also reported the heats of formation (ΔH_f) of the various PF_n species at the G2 level. Although the G2 method yields excellent results for the thermodynamics properties of most of the compounds made up of first- and second-row elements, the available reliable experimental values for the ΔH_f of PF_3 and PF_5 suggest that the G2 method underestimates these quantities by approximately 5–6 kcal mol^{-1} (or 20–25 kJ mol^{-1}).

The studies on the PF_n^+ (n = 1–4) cations have not been extensive. Lugez et al[5] studied the vibrational spectra of PF_n neutrals, cations, and anions by ab inito calculations. Creve and Nguyen[6] also reported the inversion barrier height for PF_3^+. The ionization energies (IEs) of PF_n (n = 1–4) have been calculated at different theoretical levels.[7–10] On the other hand, it seems that theoretical determinations of the heats of formation (ΔH_f) and bond dissociation energies (DEs) of PF_n^+ are lacking, while experimental data for the PF_n^+ cations are widely available in the literature.[13,14] Despite the existence of fairly extensive experimental thermochemical data for the PF_n and PF_n^+ systems, there is a lack of general agreement among these measurements for many of these species. In this work, we will employ high-level calculations to arrive at a set of self-consistent thermochemical data for PF_n, PF_n^+, and PF_n^- (n = 1–6). For those quantities where no experimental data are available, it is hoped that our calculated results will serve as reliable estimates.

The Gaussian-3 (G3)[15] method proposed in 1998 by Pople and his co-workers provides an improvement in accuracy and a reduction in computational time, when compared with the G2 method.[11] Still, the G3 theory still does poorly for some of the larger non-hydrogen systems containing second-row atoms such as the hypervalent SF_6 and PF_5 molecules.[16] Very recently, a modification of the G3 theory, called Gaussian-3X (G3X)[16], has been developed. This method shows an improvement for the energetics of the non-hydrogen systems over the G3 theory: the

G3 mean absolute deviation is 2.11 kcal mol^{-1} (8.8 kJ mol^{-1}) for the 47 non–hydrogen species in the G3/99 test set[17], while the corresponding deviation for the G3X method is 1.49 kcal mol^{-1} (6.2 kJ mol^{-1}). In this work, both the G3 and G3X methods are used to calculate the thermochemical properties, including the ΔH_f, IE, EA, and DE values of phosphorus fluoride neutrals, cations, and anions. Upon comparing the experimental data with the two sets (G3 and G3X) of calculated quantities, an assessment on the relative merits of the two methods can then be made.

6.2 Methods of Calculations

All calculations were carried out on DEC 500au, COMPAQ XP900, COMPAQ XP1000 and SGI10000 workstations, as well as on an SGI Origin 2000 High Performance Server, using the Gaussian 94[18] and Gaussian 98[19] packages of programs. The computational models employed were the G3[15] and G3X[16] levels of theory. For the PF_3^- anion, and for this anion only, the structure was optimized at the MP2(Full)/6–31+G(d) level, in order to maintain a C_{2v} symmetry.

6.3 Results and Discussion

The equilibrium structures of PF_n, PF_n^+, and PF_n^- (n = 1–6) optimized at MP2(Full)/6–31G(d) level and B3LYP/6–31G(2df,p) level are displayed in Figure 1. The G3 and G3X standard heats of formation at 0 K and 298 K of these species are summarized in Tables 1–3, respectively, while the G3 and G3X IEs and EAs are listed in Table 4.

6.3.1 Comparison of the G3 and G3X methods. As mentioned previously, the experimental data for PF_3 and PF_5 in the literature are the most well–established among the phosphorus fluorides. Hence, the comparison between the calculated and the experimental results for these two molecules are most significant in order to assess the relative merits of the G3 and G3X methods. The experimental ΔH°_{f0} for PF_3 is –953±4 [13] kJ mol^{-1}, while the G3 and G3X results are –932.1 and –944.7 kJ mol^{-1}, respectively. For PF_5, the experimental, G3, and G3X results are –1584,[13] –1553.4, and –1575.8 kJ mol^{-1}, respectively. Hence in both instances the G3X methods give better results; this is expected for non–hydrogen systems.[16] On the other hand, as shown in Table 4, the G3 IE (11.47 eV) and G3X IEs (11.44 eV) for PF_3 are quite similar to each other. The experimental IEs for PF_3 found in the

literature range from 11.38±0.01 [20] to 11.57±0.01 [21] eV, and the calculated results are in very good agreement with the value reported by Lias et al,[13] 11.44 eV. Although there is no experimental EA value for PF_3 is found in the literature, G3 (–0.38 eV) and G3X (–0.42 eV) give fairly close predictions. Based on this finding, we may conclude that the G3X method is more reliable to predict the ΔH°_{f} values of the PF_n systems. However, for the IEs or EAs, both the G3 and G3X methods give similar results. This indicates that the G3 method underestimates the ΔH°_{f0} values of the neutral and singly charged species simultaneously, and these errors cancel each other when the IEs and the EAs are calculated. In the following discussion, the G3X results will thus be given more emphasis.

Table 1: G3X and G3 Total Energies[a] (E_0), Enthalpies (H_{298}), Standard Heats of Formation at 0 K (ΔH°_{f0}), and 298 K (ΔH°_{f298}) of Phosphorus Fluorides

Species	E_0 (hartree)	H_{298} (hartree)	ΔH°_{f0} (kJ mol^{-1})	ΔH°_{f298} (kJ mol^{-1})
PF	**-440.97517**	**-440.97180**	**-58.7**	**-59.4**
	–440.97115	*–440.96778*	*–54.7*	*–55.4*
			[–51±21][b]	[–52±21][b]
			(–47±42)[c]	
PF_2	**-540.84826**	**-540.84399**	**-472.1**	**-474.7**
	–540.84071	*–540.83643*	*–463.9*	*–466.5*
			[–478.6±2.1][b]	[–482±2.1][b]
			(–510±40)[c]	
			(–485±21)[d]	
PF_3	**-640.74392**	**-640.73893**	**-944.7**	**-949.6**
	–640.73273	*–640.72772*	*–932.1*	*–936.9*
			[–953±4][b]	(–958±4)[b]
				[–957.4±1.3][c]
PF_4	**-740.51785**	**-740.51197**	**-1097.8**	**-1104.6**
	–740.50333	*–740.49739*	*–1081.5*	*–1088.1*
PF_5	**-840.41552**	**-840.40911**	**-1575.8**	**-1585.3**
	–840.39674	*–840.39030*	*–1553.4*	*–1562.9*
			[–1584][b]	(–1596)[b]
				[–1593.3±1.3][c]
			(–1584±3)[d]	(–1594±3)[d]

[a]G3X results are shown in bold font, and G3 results are in italic font. Experimental values are given in brackets; those given in square brackets are recommended values. [b]From ref.13; [c]From ref. 22; [d]From ref.14.

Table 2: G3X and G3 Total Energies[a] (E_0), Enthalpies (H_{298}), Standard Heats of Formation at 0 K (ΔH°_{f0}), and 298 K (ΔH°_{f298}) of Phosphorus Fluoride Cations.

Species	E_0 (hartree)	H_{298} (hartree)	ΔH°_{f0} (kJ mol^{-1})	ΔH°_{f298} (kJ mol^{-1})
PF^+	**-440.62050**	**-440.61716**	**872.5**	**871.7**
	–440.61602	*–440.61268*	*877.7*	*876.9*
			(≤888)[b]	(≤887)[b]
			(895.7±37.7)[c]	(901.5±37.7)[c]
PF_2^+	**-540.52236**	**-540.51820**	**383.6**	**380.7**
	–540.51392	*–540.50974*	*394.1*	*391.3*
			[375][b]	[378.5][b]
			(496.1±33.5)[c]	(472.3±33.5)[c]
			(340.1±3.5)[d]	
PF_3^+	**-640.32365**	**-640.31871**	**158.7**	**153.7**
	–640.31119	*–640.30624*	*174.6*	*169.6*
			[151][b]	[146][b]
			(146.3±1.6)[d]	
PF_4^+	**-740.24273**	**-740.23716**	**-375.5**	**-383.0**
	–740.22584	*–740.22021*	*–353.0*	*–360.4*

[a]G3X results are shown in bold font, and G3 results are in italic font. Experimental values are given in brackets; those given in square brackets are recommended values. [b]From ref. 13; [c]From ref. 14; [d]From ref. 20.

Table 3: G3X and G3 Total Energies[a] (E_0), Enthalpies (H_{298}), Standard Heats of Formation at 0 K (ΔH°_{f0}), and 298 K (ΔH°_{f298}) of Phosphorus Fluoride Anions.

Species	E_0 (hartree)	H_{298} (hartree)	ΔH°_{f0} (kJ mol^{-1})	ΔH°_{f298} (kJ mol^{-1})
PF^-	**-441.00247**	**-440.99903**	**-130.3**	**-130.9**
	–440.99849	*–440.99506*	*–126.5*	*–127.0*
			(–157.6±69)[b]	(–164.0±69)[b]
PF_2^-	**-540.87747**	**-540.87300**	**-548.8**	**-550.8**
	–540.87035	*–540.86590*	*–541.7*	*–543.8*
			(–630.0±69)[b]	(–639.2±69)[b]
PF_3^-	**-640.72852**	**-640.72271**	**-904.3**	**-907.0**
	–640.71879	*–640.71277*	*–895.5*	*–897.7*
PF_4^-	**-740.63087**	**-740.62465**	**-1394.5**	**-1400.4**
	–740.61770	*–740.61156*	*–1381.8*	*–1387.9*
PF_5^-	**-840.44863**	**-840.44179**	**-1662.7**	**-1671.1**
	–840.43221	*–840.42543*	*–1646.5*	*–1655.1*
PF_6^-	**-940.37411**	**-940.36707**	**-2213.6**	**-2225.7**
	–940.35379	*–940.34668*	*–2192.3*	*–2204.2*
				[–2200±42][c]
				(-2171±14)[d]
				(-2264±35)[e]

[a]G3X results are shown in bold font, and G3 results are in italic font. Experimental values are given in brackets; those given in square brackets are recommended values. [b]From ref. 14; [c]From ref. 13; [d]From ref. 29; [e]From ref. 30.

Table 4: G3X and G3 IEs[a] and EAs of Phosphorus Fluorides.

Species	IE (eV)	EA (eV)
PF	***9.65***	**0.74**
	9.66	*0.74*
	[9.60±0.01][b]	(1.1±0.5)[g]
	(9.74±0.01)[c]	(<3.4)[h]
PF_2	**8.87**	**0.79**
	8.89	*0.81*
	[8.85±0.01][c]	(1.5±0.5)[g]
	(~8.73)[d]	(≥1.6±0.5)[i]
		(~1.4)[j]
PF_3	**11.44**	**-0.42**
	11.47	*-0.38*
	[11.44][c]	
	(11.57±0.01)[e]	
	(11.38±0.01)[f]	
PF_4	**7.49**	**3.08**
	7.55	*3.11*
PF_5	–	**0.90**
		0.96
		(0.75±0.15)[k]

[a]G3X energies are shown in bold font, and G3 energies are in italic font.
[b]From ref. 23; [c]From ref. 13; [d]From ref. 32; [e]From ref. 21; [f]From ref. 20; [g]From ref. 14; [h]From ref. 24; [i]From ref. 25; [j]From ref. 26; [k]From ref. 28.

6.3.2 Assessments of the experimental results. In this section, with the help of the G3X results, we will assess the (sometimes) widely scattered experimental results for various species in order to obtain a set of self-consistent thermochemical data for the PF_n molecules and their ions.

Energetics of PF, PF^+, and PF^-. The two experimental values reported for $\Delta H^\circ_{f0}(PF)$ are –51±21 [13] and –47±42 [22] kJ mol^{-1}. The former value is closer to the G3X result of –58.4 kJ mol^{-1} and is hence recommended, although the value of –47±42 kJ mol^{-1} is also consistent with the G3X prediction. The experimental values for $\Delta H^\circ_{f0}(PF^+)$ are ≤ 888 [13] and 895.7±37.7 [14] kJ mol^{-1}; both are in agreement with our G3X result, 872.5 kJ mol^{-1}. As shown in Table 4, there are two experimental IEs (9.74±0.01 [13] and 9.60±0.01 [23] eV) for PF. While both are consistent with the G3X value, 9.65 eV, the one reported by Butcher et al[23] (9.60±0.01 eV) is in better agreement and hence is our recommended value. The experimental ΔH°_{f0} for PF^- is –157.6±69[13] kJ mol^{-1} and it is consistent with our G3X value of –130.3 kJ mol^{-1}. Considering that the experimental uncertainty for this quantity is so exceedingly large, it is believed that the G3X result gives a more reliable estimate. The two EAs for PF found in the

literature are 1.1±0.5[14] and < 3.4[24] eV, with the latter giving only an upper bound. The G3X result is calculated to be 0.74 eV, which is consistent with the result reported by Chase et al,[14] 1.1±0.5 eV. A recent very high level calculation by Gu et al reports that the EA of PF should be 0.75 eV,[4] in excellent agreement with the G3X result.

Energetics of PF_2, PF_2^+, and PF_2^-. The experimental values for $\Delta H^\circ_{f0}(PF_2)$ range from –478.6±2.1 [13] to –510±40 [22] kJ mol^{-1}. Among these data, the value of –478.6±2.1 kJ mol^{-1} reported in Lias' compendium[13] is in very good agreement with our G3X result, –472.1 kJ mol^{-1}. Thus this is our recommended value. But, taking into account the experimental uncertainties, the value of –485±21[14] kJ mol^{-1} is also consistent with our calculation. For cation PF_2^+, there are three experimental ΔH°_{f0} values, as shown in Table 2. Among them, the value reported by Lias,[13] 375 kJ mol^{-1}, is closest to the G3X result, 383.6 kJ mol^{-1}, and hence is recommended. Also, the measured IE of PF_2, 8.85±0.01 eV,[23] is consistent with the G3X value of 8.87 eV. The experimental EAs of PF_2 are 1.5±0.5 [14], > 1.6±0.5 [25], and ~1.4 [26] eV. There is a big difference between our G3X result (0.79 eV) and the experimental *estimates*. Besides, the experimental $\Delta H^\circ_{f0}(PF_2^-)$ value of –630.0±69[14] kJ mol^{-1} is not consistent with our G3X result of –548.8 kJ mol^{-1}. However, it is noted that the experimental $\Delta H^\circ_{f0}(PF_2^-)$ was calculated from $EA(PF_2)$ = 1.5±0.5 eV and the experimental EA of PF_2 was determined by the following assumption:[14] The EA values are found to be oscillating between the even– and odd–electron molecules in S–F systems, with the odd–electron molecules having a higher EA value. Chase et al[14] thus assumed that the same trend should be found in the P–F systems and the $EA(PF_2)$ should be higher than the EA(PF), which is 1.1±0.5 eV. So, they adopted the $EA(PF_2)$ value of 1.5±0.5 eV. As this is not a direct experimental measurement, the accuracy of the experimental $\Delta H^\circ_{f0}(PF_2^-)$ and $EA(PF_2)$ are in doubt. In addition, Gu et al[4] suggested that the $EA(PF_2)$ should be 0.76 eV, in excellent accord with the G3X result. They have also pointed out that there are problems regarding the assumptions in arriving at the experimental $EA(PF_2)$ values of > 1.6±0.5 and ~1.4 eV.

Energetics of PF_3, PF_3^+, and PF_3^-. As mentioned before, there is a very good agreement between experimental and the G3X results for the quantities of $\Delta H^\circ_{f0}(PF_3)$

and IE(PF_3). Hence no further discussion is required here for PF_3. The experimental $\Delta H^\circ_{f0}(PF_3^+)$ values are 146.3±1.6 [20] and 151 [13] kJ mol^{-1}, both of which are consistent with the G3X value of 158.7 kJ mol^{-1}. Thus our recommended value for $\Delta H^\circ_{f0}(PF_3^+)$ is 151 kJ mol^{-1}. The G3X $\Delta H^\circ_{f0}(PF_3^-)$ and EA(PF_3) are calculated to be –904.3 kJ mol^{-1} and –0.42 eV, respectively. These results indicate that PF_3^- is unstable and will lose an electron spontaneously. Indeed, so far no EA for PF_3 has been reported in the literature.

Energetics of PF_4, PF_4^+, and PF_4^-. There are no experimental thermochemical data for PF_4, as well as for its cation and anion. Our calculated G3X results show that $\Delta H^\circ_{f0}(PF_4)$ and $\Delta H^\circ_{f0}(PF_4^+)$ are –1097.8 and –375.5 kJ mol^{-1}, respectively. Hence, the G3X IE(PF_4) is determined to be 7.49 eV. On the other hand, at the G3X level, $\Delta H^\circ_{f0}(PF_4^-)$ and EA(PF_4) are –1394.5 kJ mol^{-1} and 3.08 eV, respectively. Although experimental data are not available for PF_4 and its ions, the excellent agreement between the experimental and G3X values in the previous discussion supports our results.

Energetics of PF_5 and PF_5^-. The discussion on $\Delta H^\circ_{f0}(PF_5)$ has been given in the previous section. The equilibrium structures for PF_5^+ has not been found because the cation tends to dissociate to PF_4^+ + F at the MP2(Full)/6–31G(d) and B3LYP/6–31G(2df,p) levels. Indeed, no experimental adiabatic IE(PF_5) is found in the literature, while vertical IE for PF_5 has been reported.[27] On the other hand, the structure of PF_5^- has been determined. The G3X $\Delta H^\circ_{f0}(PF_5^-)$ is calculated to be –1662.7 kJ mol^{-1}, while the G3X EA(PF_5) is 0.90 eV. The experimental EA(PF_5)[28] of 0.75±0.15 eV shows a large uncertainty. Taking into account of this uncertainty, our G3X EA is in fair agreement with the experimental value. There is no available experimental value for $\Delta H^\circ_{f0}(PF_5^-)$. By using the experimental ΔH°_{f0} and EA values of PF_5, the deduced experimental $\Delta H^\circ_{f0}(PF_5^-)$ ranges from –1656 kJ mol^{-1} to –1666.8 kJ mol^{-1}. Such a range is consistent with the G3X result of –1662.7 kJ mol^{-1}.

Energetics of PF_6^-. Experimental results show that $\Delta H^\circ_{f298}(PF_6^-)$ should be between –2171±14 [29] and –2264±35 [30] kJ mol^{-1}. In our calculation, G3X $\Delta H^\circ_{f298}(PF_6^-)$ is found to be –2225.7 kJ mol^{-1}, which is closer to the experimental value of –2200±42 [13] kJ mol^{-1}. Thus this is our recommended value. However, all the other reported data may be viewed as acceptable, when their large uncertainties are taken into

account. In this work, no equilibrium structure has been identified for PF_6, in agreement with the finding of Schaefer et al.[2]

Bond dissociation energies of PF_n, PF_n^+, and PF_n^-. The G3 and G3X bond dissociation energies (DEs) of PF_n, PF_n^+, and PF_n^- are summarized in Table 5. Only the experimental DEs of P–F, FP–F and F_2P–F are available in the literature; they are included in the table for comparison. It is seen that both the G3 and G3X results are in good agreement with the experimental data, with DE(F_2P–F) being the only exception. It should be noted that the experimental DE(F_2P–F) was estimated from the atomization energy of PF_3, multiplied by a factor of 1.1.[14] This estimation is obviously a crude approximation and may not be able to arrive at a very accurate value for DE(F_2P–F). The bond dissociation of F_2P–F is the energy required for the reaction $PF_3 \rightarrow PF_2 + F$. When we apply the experimental $\Delta H^\circ_{f0}(PF_3) = -952.8$ kJ mol^{-1}, $\Delta H^\circ_{f0}(PF_2) = -485.3$ kJ mol^{-1}, and $\Delta H^\circ_{f0}(F) = 77.4$ kJ mol^{-1} from ref. 14 to the above reaction, the heat of reaction (DE of F_2P–F) is calculated to be 544.9 kJ mol^{-1}. This value is consistent with our G3X result of 550.1 kJ mol^{-1}.

Table 5: G3X and G3 Bond Dissociation Energies (in kJ mol^{-1}) at 0 K for Phosphorus Fluorides and Their Ions. [a,b]

Bond	Neutral	Cation	Anion
P–F	**451.7**	**530.0**	**453.0**
	447.7	*524.9*	*447.9*
	(443.9±19.2)[b]		
FP–F	**490.8**	**566.3**	**495.8**
	486.6	*561.0*	*492.7*
	(510.4±41.8)[b]		
F_2P–F	**550.1**	**302.3**	**432.9**
	545.6	*296.8*	*431.2*
	(518.8±8.4)[b]		
F_3P–F	**230.5**	**611.6**	**567.6**
	226.8	*605.0*	*563.7*
F_4P–F	**555.3**		**345.5**
	549.3		*342.1*
F_5P–F			**628.4**
			623.2

[a]G3X energies are shown in bold font, and G3 energies are in italic font.
[b]Experimental values, taken from ref. 14, are given in brackets.

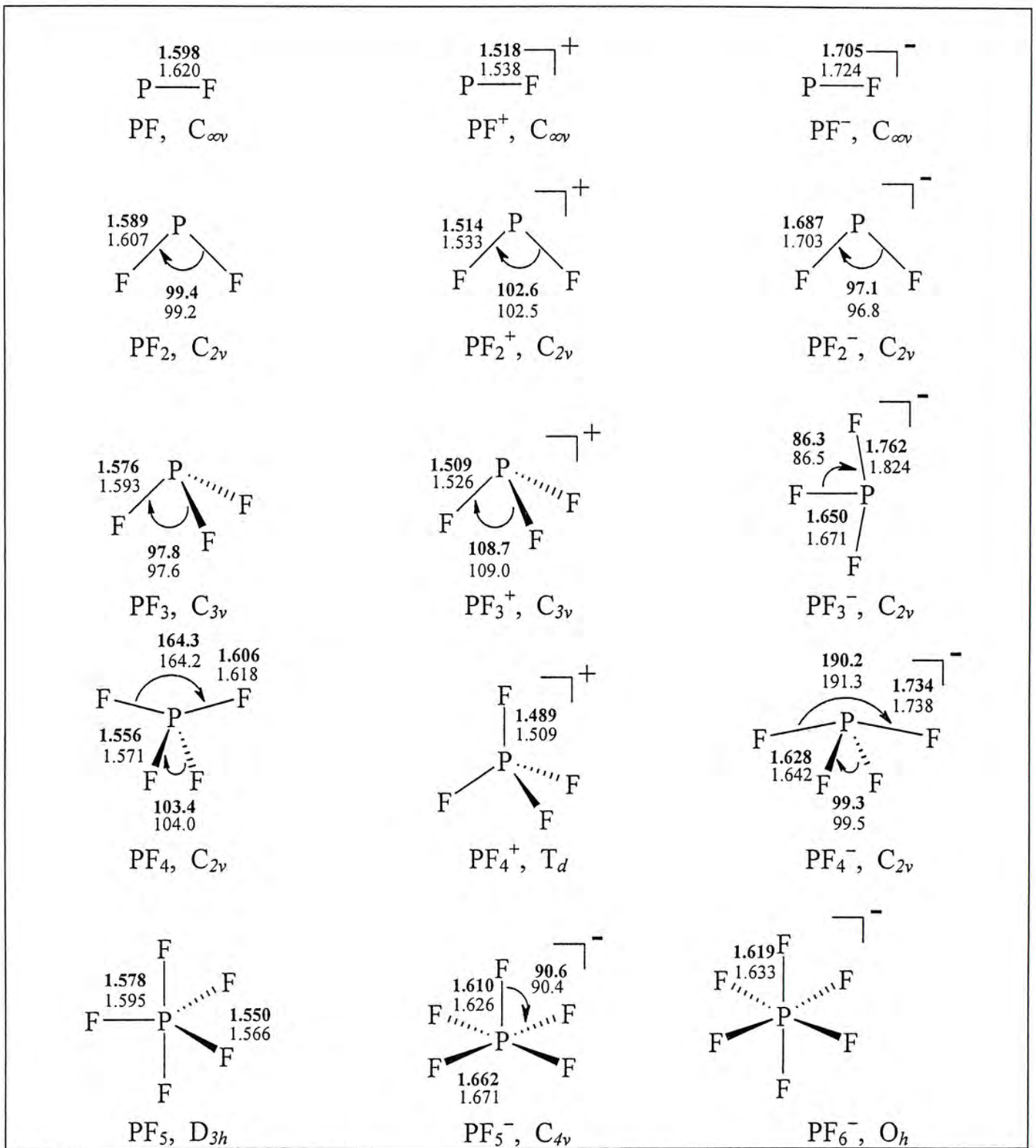

Figure 1. Theoretical equilibrium structures of phosphorus fluorides and their singly charged cations and anions optimized at the levels of MP2(Full)/6–31G(d) (normal font) and B3LYP/6–31G(2df,p) (bold font). The structural parameters for PF_3^- shown in normal font are optimized at the MP2(Full)/ 6–31+G(d) level (see text).

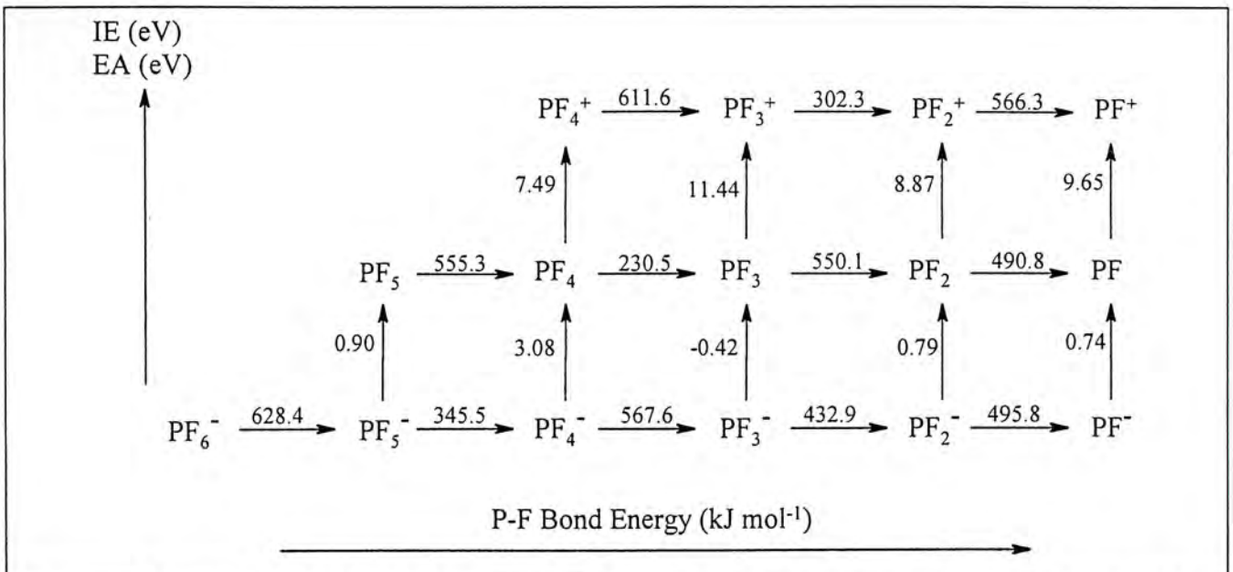

Figure 2. Summary of the G3X thermochemical data of the phosphorus fluorides and their ions, illustrating the alternating patterns of the data.

Summary of the thermochemical data. The G3X IEs, EAs, and DEs of PF_n, PF_n^+, and PF_n^- are summarized in Figure 2. Examining these results, it is seen that there is an alternating pattern for these three sets of data. Take the DEs as an example. The larger DE values correspond to the P–F bond energies (in kJ mol^{-1}) for PF_2^+ (566.3), PF_4^+ (611.6), PF_3 (550.1), PF_5 (555.3), PF_2^- (495.8), PF_4^- (567.6), and PF_6^- (628.4). In all of these cases, the dissociation involves the transformation from a higher and more stable species to a lower and less stable species plus a fluorine atom. Each of the stable species has a closed–shell configuration with six, eight, ten, or twelve valence electrons around the central atom, whereas the unstable species do not. Analogously, a smaller DE corresponds to the transformation from a higher and less stable species to a lower and more stable species plus a fluorine atom: PF_3^+ (302.3), PF_2 (490.8), PF_4 (230.5), PF_3^- (432.9), and PF_5^- (345.5), where the DEs given in brackets are in kJ mol^{-1}. Referring to the other data summarized in Figure 2, IE is a measure of the transition energy from the neutral to its cation, whereas EA measures the transition from an anion to its corresponding neutral. The processes $PF \rightarrow PF^+ + e^-$ and $PF_3 \rightarrow PF_3^+ + e^-$ correspond to ionization from a stable neutral to a less stable cation, and thus the IEs of PF (9.65 eV) and PF_3 (11.44 eV) have large values. The smaller IEs for PF_2 (8.87 eV) and PF_4 (7.49 eV) are due to ionization from a less stable neutral to a more stable cation. Similarly, the electron detachment processes $PF_2^- \rightarrow PF_2 + e^-$ and $PF_4^- \rightarrow PF_4 + e^-$ involve the formation of a less stable species

from a more stable one. Therefore, we expect the EAs for PF_2 (0.79 eV) and PF_4 (3.08 eV) to be larger than those for PF (0.74 eV) and PF_3 (–0.42 eV), which correspond to detachment processes from a less stable anion to a more stable neutral. The alternating patterns for the IEs, EAs, and DEs of phosphorus fluorides and their ions discussed here have also been observed for the corresponding data of sulfur fluorides and their ions.[31]

6.4 Conclusion

We have applied the G3 and G3X methods to study the thermochemistry of phosphorus fluorides PF_n, as well as for their singly charged cations and anions. Based on these results, we have obtained the ΔH°_{f0} values and the DEs of all the species, and the IEs and EAs of all the neutrals. When we compare the G3 and G3X ΔH°_{f0} results with the experimental data for PF_3 and PF_5, it is found that G3X is more reliable method for this type for non–hydrogen systems. For the IEs or EAs of PF_n, both the G3 and G3X method give similar results and these results are in good agreement with the available literature values. Based on the excellent agreement between the G3X and available experimental result, a set of self–consistent experimental thermochemical data for PF_n, PF_n^+, and PF_n^- is obtained. The experimental bond dissociation energies are only available for P–F, FP–F, and F_2P–F. The first two are consistent with our G3X results. It is believed that the discrepancy between the experimental and G3X DE(F_2P–F) values originates from the assumption made in arriving at the experimental result. The excellent agreement between the known experimental values and the G3X results lends support to our predictions for the missing thermochemical data of phosphorus fluorides. The general trends of the thermochemical data of the phosphorus fluorides and their ions may be rationalized in terms of the electronic configurations of the species involved.

6.5 References

1. Gutsev, G. L. *J. Chem. Phys.* **1993**, *98*, 444.
2. Tschumper, G. S.; Fremann, J. T.; Schaefer III, H. F. *J. Chem. Phys.* **1996**, *104*, 3673.
3. Gu, J.; Leszczynski, J. *J. Phys. Chem. A* **1999**, *103*, 7856.

4. Gu, J.; Chen, K.; Xie, Y.; Schaefer III, H. F.; Morris, R. A.; Viggiano, A. A. *J. Chem. Phys.* **1998**, *108*, 1050.
5. Lugez, C. L.; Irikura, K. K.; Jacox, M. E.; *J. Chem. Phys.* **1998**, *108*, 8381.
6. Creve, C.; Nguyen, M. T. *Chem. Phys. Lett.* **1997**, *273*, 199.
7. Latifzaldeh, L. Balasubramanian, K. *Chem. Phys. Lett.* **1994**, *228*, 463.
8. Chau, F. T.; Dyke, J. M.; Lee, E. P. F.; Ridha, A.; Wang, D. C. *Chem. Phys.* **1997**, *224*, 157.
9. Creve, S.; Nguyen, M. T. *J. Phys. Chem. A* **1998**, *102*, 6549.
10. Tuckett, R. P.; Knowles, P. J. *Chem. Phys. Lett.* **1996**, *261*, 486.
11. Curtiss, L. A.; Rahavachari, K.; Trucks, G. W.; Pople, J. A. *J. Chem. Phys.* **1991**, *94*, 7221.
12. Curtiss, L. A.; Raghavachari, K.; Pople, J. A. *J. Chem. Phys.* **1993**, *98*, 1293.
13. Lias, S. G.; Bartmess, J. E.; Liebman, J. F.; Holmes, J. L.; Levin, R. D.; Mallard, W. G. *J. Phys. Chem. Ref. Data* **1988**, *17* (Suppl.1).
14. *JANAF Themochemical Tables*, 3rd ed.; Plenum: New York, 1985.
15. Curtiss, L. A.; Raghavachari, K.; Redfern, P. C.; Rassolov, V.; Pople, J. A. *J. Chem. Phys.* **1998**, *109*, 7764.
16. Curtiss, L. A.; Redfern, P. C.; Raghavachari, K.; Pople, J. A. *J. Chem. Phys.* **2001**, *114*, 108.
17. Curtiss, L. A.; Raghavachari, K.; Redfern, P. C.; Pople, J. A. *J. Chem. Phys.* **2000**, *112*, 7374.
18. Frisch, M. J.; Trucks, G. W.; Schlegel, H. B.; Gill, P. M. W.; Johnson, B. J.; Robb, M. A.; Cheeseman, J. R.; Keith, T. A.; Petersson, G. A.; Montgomery, J. A.; Raghavachari, K.; Al-Laham, M. A.; Zarkrewski, V. G.; Ortiz, J. V.; Foresman, J. B.; Cioslowski, J.; Stefanov, B. B.; Nanayakkara, A.; Challacombe, M.; Peng, C. Y.; Ayala, P. Y.; Chen, W.; Wong, M. W.; Andres, J. L.; Replogle, E. S.; Gomperts, R.; Martin, R. L.; Fox, D. J.; Binkley, J. S.; Defrees, D. J.; Baker, J.; Stewart, J. J. P.; Head-Gordon, M.; Gonzalez, C.; Pople, J. A. *GAUSSIAN* 94, Revision D4; Gaussian, Inc., Pittsburgh, PA, 1995.
19. Frisch, M. J.; Trucks, G. W.; Schlegel, H. B.; Scuseria, G. E.; Robb, M. A.; Cheeseman, J. R.; Zakrzewski, V. G.; Montgogery, J. A.; Jr.; Stratmann, R.E.; Burant, J. C.; Dapprich, S.; Millam, J. M.; Daniels, A. D.; Kudin, K. N.; Strain, M. C.; Farkas, O.; Tomasi, J.; Barone, V.; Cossi, M.; Cammi, R.; Mennucci, B.; Pomelli, C.; Adamo, C.; Clifford, S.; Ochterski, J.; Petersson, G. A.; Ayala, P.

Y.; Cui, Q.; Morokuma, K.; Malick, D. K.; Rabuck, A. D.; Raghavachari, K.; Foresman, J. B.; Cioslowski, J.; Ortiz, J. V.; Baboul, A. G.; Stefanov, B. B.; Liu, G.; Liashenko, A.; Piskorz, P.; Komaromi, I.; Gomperts, R.; Martin, R. L.; Fox, D. J.; Keith, T.; Al-Laham, M. A.; Peng, C. Y.; Nanayakkara, A.; Gonzalez, C.; Challacombe, M.; Gill, P. M. W.; Johnson, B.; Chen, W.; Wong, M. W.; Andres, J. L.; Gonzalez, C.; Head-Gordon, M.; Replogle, E. S.; Pople, J. A. *GAUSSIAN 98*, Revision A.7; Gaussian, Inc., Pittsburgh PA, 1998.

20. Ruede, R.; Troxler, H.; Beglinger, C.; Jungen, M. *Chem. Phys. Lett.* **1993**, *203*, 477.
21. Maier, J. P.; Turner, D. W. *J. Chem. Soc. Faraday Trans. II* **1972**, *68*, 711.
22. Gurvich, L. V.; Veyts, I. V.; Alcock, C. B., Eds. *Thermodynamic Properties of Individual Substances*, 4th ed. New York: Hemisphere **1989**.
23. Butcher, V.; Dyke, J. M.; Lewis, A. E.; Morris, A.; Ridha, A. *J. Chem. Soc. Faraday Trans. II* **1988**, *84*, 299.
24. Karachevtsev, G. V. *Russ. J. Phys. Chem.* **1978**, *52*, 1581.
25. Thynne, J. C. J. *Dyn. Mass Spectrom.* **1972**, *3*, 67.
26. Harland, P. W.; Rankin, W. H. and Thynne, J. C. J. *Int. J. Mass Spectrom. Ion. Phys.* **1974**, *13*, 395.
27. Goodman, J. W.; Dewar, M. J. R.; Schweiger, J. R.; Cowley, A. H. *Chem. Phys. Lett.* **1973**, *21*, 474.
28. Miller, T. M.; Miller, A. E. S.; Viggiano, A. A.; Morris, R. A.; Paulson, J. F. *J. Chem. Phys.* **1994**, *100*, 7200.
29. Aleshina, V. E.; Borshchevskii, Y.; Korobov, V. M. ; Sidorov, L. N. *Russ. J. Phys. Chem.*, **1996**, *70*, 1085.
30. Mallouk, T. E.; Rosenthal, G. L.; Muller, G.; Brusasco, R.; Bartlett, N. *Inorg. Chem.*, **1984**, *23*, 3167.
31. Cheung, Y.–S.; Chen, Y. –J.; Ng, C.Y.; Chiu, S. –W.; Li, W. –K. *J. Am. Chem. Soc.* **1995**, *117*, 9725.
32. Howe, J. D.; Ashfold, M. N.R.; Hudgens, J. W.; Johnson, R. D., III *J. Chem. Phys.* **1994**, *101*, 3549.

Chapter 7
Conclusion

Since conclusions have been made in each Chapter, we will not comment on the chemical systems studied in this work. On the other hand, different models of theory, modified Gaussian–2 (G2++) and Gaussian–3 (G3) models, as well as their variants, have been employed to study the structures and energetics of several interesting systems. We will now remark on the relative merits of these models.

In this thesis, we have employed the G3 method to study the dissociative photoionization of dimethyl disulfide and photodissociation of propylene sulfide. Combining with the experimental results, good to excellent agreements between the G3 results and experimental values are observed in most cases. In addition, we have used both G2++ and G3 models to study the decompositions of alkoxide anions. It is worth mentioning that G2++ yields a better result than G3 for these anionic systems, although the G2++ method is more time demanding. It shows that the use of diffuse functions is important in studying the anionic systems. Furthermore, both the G3 and G3X methods have been used to study the thermochemistry of phosphorus fluorides. We found that G3X gives more accurate results than G3 in the heats of formation calculations of hypervalent molecules. However, the G3X method is again more computationally expensive than the G3 method.

Since most of the calculated results obtained in this work are in good agreement with the available experimental data, and, based on the previous successes for the G2 and G3 methods, the unexpected large discrepancies between experimental and calculated results for some quantities reported in this thesis may not be due to the failure of the theoretical model. Rather, these discrepancies suggest that the experimental results may be inaccurate and deserve re–examination.

Appendix A

The Gaussian–2 and Gaussian–3 Theoretical Models

The mathematical details of the Gaussian–2 (G2) and Gaussian–3 (G3) methodologies as well as the variant of the G3 method, G3(MP2) and G3X, are presented below.

A.1 The G3 Theory

The G3 energies are the approximation of the energy calculated at the ab initio QCISD(T)/G3large level. It involves geometry optimization at the MP2(Full)/6–31G(d) level. Also, vibrational frequency calculations at the MP2(Full)/6–31G(d) level for the zero–point vibrational energy (ZPVE), thermal corrections, and a semi–empirical higher–level correction (HLC) are required. Based on the optimized geometry, several single–point energy calculations are performed, and the G3 energy are given as follow.

The G3 energy:

$$E(G3) = E_{base} + \Delta E(QCI) + \Delta E(+) + \Delta E(2df) + \Delta E(G3large) + \Delta E(SO) + 0.9661 \times ZPVE_{MP2} + HLC_{G3}, \quad (1)$$

where E_{base} = E[MP4SDTQ/6–31G(d)],

$\Delta E(QCI)$ = E[QCISD(T)/6–31G(d) – MP4SDTQ/6–31G(d)],

$\Delta E(+)$ = E[MP4SDTQ/6–31+G(d) – MP4SDTQ/6–31G(d)],

$\Delta E(2df)$ = E[MP4SDTQ/6–31G(2df,p) – MP4SDTQ/6–31G(d)],

$\Delta E(G3large)$ = E[MP2(full)/G3large – MP2/6–31G(2df,p) – MP2/6–31+G(d) + MP2/6–31G(d)],

$ZPVE_{MP2}$ = ZPVE at MP2(Full)/6–31G(d),

$HLC_{G3} = -6.386\times10^{-3}n_\beta - 2.977\times10^{-3}(n_\alpha - n_\beta)$ and

$-6.219\times10^{-3}n_\beta - 1.185\times10^{-3}(n_\alpha - n_\beta)$

for molecular and atomic species, respectively. Here $n_\alpha \geq n_\beta$ and n_α and n_β are the numbers of α and β valence electrons, respectively.

$\Delta E(SO)$ is spin–orbit correction for atomic species, and is taken from experiment or accurate theoretical calculations in the case where no experimental data are available.

A.2 The G3(MP2) Theory

In the G3(MP2) procedure, the basis–set–extension corrections is obtained at MP2 level, instead of the MP4 level in G3, thus eliminating the MP4 calculations:

The G3(MP2) energy:

$$E(G3(MP2)) = E[QCISD(T)/6\text{–}31G(d)] + \Delta E_{MP2} + \Delta E(SO) + 0.9661 \times ZPVE_{MP2} + HLC_{G3MP2}, \quad (2)$$

where $\Delta E_{MP2} = E[MP2/G3MP2large - MP2/6\text{–}31G(d)]$,

$HLC_{G3MP2} = -9.729\times10^{-3}n_\beta - 4.471\times10^{-3}(n_\alpha - n_\beta)$ and

$-9.345\times10^{-3}n_\beta - 2.021\times10^{-3}(n_\alpha - n_\beta)$ for molecular and atomic species, respectively.

A.3 The G3X Theory

The G3X method involves geometry optimization and vibrational frequency calculations at the B3LYP/6–31G(2df,p). In the energy calculations, apart from the five single–points in the G3 model, one more single–point calculation, HF/G3Xlarge, is required.

The G3X energy:

$$E(G3X) = E_{base} + \Delta E(QCI) + \Delta E(+) + \Delta E(2df) + \Delta E(G3Xlarge) + \Delta E(SO) + 0.9854 \times ZPVE_{B3LYP} + HLC_{G3X}, \quad (3)$$

where $\Delta E(G3Xlarge) = E[MP2(full)/G3large - MP2/6\text{–}31G(2df,p) - MP2/6\text{–}31+G(d) + MP2/6\text{–}31G(d) + HF/G3Xlarge - HF/G3large]$,

$ZPVE_{B3LYP}$ = ZPVE at B3LYP/6–31G(2df,p),

$HLC_{G3X} = -6.783\times10^{-3}n_\beta - 3.083\times10^{-3}(n_\alpha - n_\beta)$ and

$-6.877\times10^{-3}n_\beta - 1.152\times10^{-3}(n_\alpha - n_\beta)$ for molecular and atomic species, respectively.

A.4 The G2++ Theories

G2++ is a modified G2 method. It involves geometry optimization and vibrational frequency calculations at the MP2(Full)/6–31++G(d) level. The details of G2++ energies are given as follow.

The G2++ energy:

$$E(G2++) = E_{base} + \Delta E(QCI) + \Delta E(+) + \Delta E(2df) + \Delta + 0.893 \times ZPVE_{MP2(+)} + HLC_{G2++}, \quad (4)$$

where E_{base} = E[MP4SDTQ/6–311G(d,p)],

$\Delta E(QCI)$ = E[QCISD(T)/6–311G(d,p) – MP4SDTQ/6–311G(d,p)],

$\Delta E(+)$ = E[MP4SDTQ/6–311++G(d,p) – MP4SDTQ/6–311G(d,p)],

$\Delta E(2df)$ = E[MP4SDTQ/6–311G(2df,p) – MP4SDTQ/6–311G(d,p)],

Δ = E[MP2/6–311++G(3df,2p) – MP2/6–311G(2df,p) – MP2/6–311++G(d,p) + MP2/6–311G(d,p)],

$ZPVE_{MP2(+)}$ = ZPVE at MP2(Full)/6–31++G(d),

$HLC_{G2++} = -5.03 \times 10^{-3} n_\beta - 0.18 \times 10^{-3} n_\alpha n_\beta$.

Appendix B

Calculation of Enthalpy at 298 K, H_{298}

The theoretical energies obtained with the Gaussian–n methods refer to isolated molecules at 0 K with stationary nuclei, while thermochemical measurements are carried out with vibrating molecules at finite temperature, usually 298 K. Hence, comparison of theoretical results with experimental data normally requires zero–point vibrational energy and thermal corrections. From statistical mechanics, and assuming ideal gas behavior, the difference between the enthalpy at finite temperature (H_T) and the energy at 0 K (E_0) is given by

$$H_T - E_0 = E_T^{trans} + E_T^{rot} + E_T^{vib} + RT$$

where $E_T^{trans} = \frac{3}{2}RT$,

$E_T^{rot} = \frac{3}{2}RT$ (for a non–linear molecule)

$E_T^{rot} = RT$ (for a linear molecule) or 0 (for an atom)

$E_T^{vib} = E_T^{vib} - E_0^{vib}$

$= \sum_i^{3n-6} \frac{h\nu_i}{\exp(h\nu_i / kT) - 1}$, where ν_i's are scaled harmonic frequencies.